Title

Fractionation of yttrium and holmium during basaltic soil weathering

Authors

Thompson, Aaron
Amistadi, Mary Kay
Chadwick, Oliver A
et al.

Publication Date

2013-10-01

DOI

10.1016/j.gca.2013.06.003

Peer reviewed

Available online at www.sciencedirect.com

SciVerse ScienceDirect

Geochimica et Cosmochimica Acta 119 (2013) 18–30

Geochimica et Cosmochimica Acta

www.elsevier.com/locate/gca

Fractionation of yttrium and holmium during basaltic soil weathering

Aaron Thompson [a,*], Mary Kay Amistadi [b], Oliver A. Chadwick [c], Jon Chorover [b]

[a] Department of Crop and Soil Sciences, University of Georgia, Athens, GA 30602, USA
[b] Department of Soil, Water & Environmental Science, University of Arizona, Tucson, AZ 85721, USA
[c] Department of Geography, University of California, Santa Barbara, CA 93106, USA

Received 30 April 2012; accepted in revised form 2 June 2013; Available online 14 June 2013

Abstract

The anomalously low affinity of yttrium (Y) for iron (Fe) (oxyhydr)oxides relative to lanthanides with similar ionic radius (e.g., Ho) has been demonstrated in experiments with isolated Fe minerals and in a variety of marine systems that contain high concentrations of solid phase Fe. However, it has not previously been demonstrated to occur during soil genesis, despite the common observation that many soils become enriched in Fe over time. We hypothesized that Y would become progressively depleted in soils relative to Ho with increased weathering. Since, trivalent Y has an anomalously low Misono softness relative to other trivalent ions included in the rare earth element and yttrium group (REY^{3+}), we also investigated whether soil REY fractionation reflects variation in Misono softness. To test this, we measured trends in total REY concentrations for Hawaiian soils derived from basaltic parent materials aged 0.3–4100 ky, and measured REYs released from the same samples during short-time (3 h) dissolution experiments conducted as part of a previous investigation linking dissolution with surface charge properties (Chorover et al., 2004). The chondrite-normalized Y/Ho ratios in the parent Hawaiian basalt (^{Chond}[Y/Ho] = 0.998) and continental dust (^{Chond}[Y/Ho] = 0.994) inputs are remarkably similar, and thus we can interpret deviations from ^{Chond}[Y/Ho] ~ 1.0 to result from soil biogeochemical processes and not source mixing. Between 0.3 and 20 ky, the ^{Chond}[Y/Ho] ratio of the subsurface soils decreased from $0.96 \pm 0.07(2\sigma)$ to 0.71 ± 0.05, and then remained unchanged across the rest of the weathering sequence. In contrast, the ^{Chond}[Y/Ho] ratio of the surface soils decreased from 0.99 ± 0.07 to 0.76 ± 0.05 at 150 ky and then, most likely due to continued dust inputs, increased to 1.04 ± 0.07 in the oldest soils. Analysis of the short-time dissolution experiments revealed preferential release of Y relative to Ho (and also La relative Pr) at intermediate pH where aqueous REY concentrations are governed by proton competition for adsorption sites. Proton-competition-control over REY release is bounded at high pH by the onset of colloidal dispersion—represented by the point of minimum dissolution (p.m.d.) of Al—and at low pH by the soil's point of zero net charge (p.z.n.c.) and/or when proton-promoted dissolution of REY-containing solids, including Fe-(oxyhydr)oxides, control REY release. Results of our dissolution experiments suggest that complexation of REYs by dissolved organic matter (DOM) does not drive Y–Ho fractionation during pedogenesis, but rather may suppress it. Synthesis of these field and laboratory experiments suggests the Y/Ho ratio decreases early in soil development (<20 ky) when weathering rates are high and competitive proton adsorption affects REY fractionation. Given that Fe-(oxyhydr)oxide sorbents exhibit greater affinity for Ho relative to Y, their prevalent neo-formation during incipient pedogenesis likely plays a central role in Y–Ho fractionation in these soils. Persistence of low ^{Chond}[Y/Ho] ratios in the subsurface soils even at 4100 ky suggests Y–Ho fractionation continues, albeit at a slower rate, as weathering proceeds.

* Corresponding author. Tel.: +1 706 410 1293.
E-mail address: AaronT@uga.edu (A. Thompson).

0016-7037/$ - see front matter © 2013 Elsevier Ltd. All rights reserved.
http://dx.doi.org/10.1016/j.gca.2013.06.003

1. INTRODUCTION

Small predictable variations in chemical properties with increasing atomic number make the lanthanide series (elements of atomic number 57 through 71, known as the "rare earth elements") useful probes of biogeochemical weathering processes. The coherent chemical behavior of the lanthanides derives from the stable arrangement of the outer electron shell (5*sp*) across the series. Chemical variations resulting from the gradual filling of the inner 4*f* electron shell are effectively shielded by the outer 5*sp* shell such that the dominant changes in REE geochemical behavior can be ascribed to systematic variation in ionic radius with the REEs behaving as hard Lewis acids (Pearson, 1968). Because yttrium (Y) has a similar outer electron shell structure it is often included as a pseudo-lanthanide with an ionic radius nearly identical to holmium (Ho) and consequently similar chemical behavior (Bau and Dulski, 1995; Richens, 1997). However, the electron cloud of lanthanides with empty (La^{3+}, Y^{3+}), half-filled (Gd^{3+}) or filled (Lu^{3+}) 4*f* electron shells are less likely to become polarized during chemical reaction and hence will form less covalent metal-ligand bonds with Lewis bases than the rest of the lanthanide series, leading to potential anomalies in the otherwise coherent REY behavior. This effect is reflected, for example, in slightly lower metal-ligand stability for La, Gd, Lu and Y with most common organic acids (Peppard et al., 1969; Byrne and Lee, 1993). It is also associated with the "tetrad effect" that has been demonstrated for pure chemical systems (Peppard et al., 1969), but whose detection in natural environments remains controversial (Kawabe et al., 1991; Mclennan, 1994; Ohta and Kawabe, 2000; Takahashi et al., 2002). Following Pearson (1968), the behavior of La, Gd, Lu and Y suggests they can be interpreted as "harder" Lewis acids than the remainder of the lanthanide series. While some measures of Lewis acid hardness (Yang and Parr, 1985; Kinraide, 2009) do not distinguish these metals from the rest of the lanthanides, anomalies are predicted by the Misono softness parameter, '*Y*', which for the REYs (Fig. 1) is determined according to (Misono et al., 1967; Sposito, 1994):

$$Y = 10 \bullet \frac{I_Z R}{Z^{0.5} I_{Z+1}} \quad (1)$$

where I_Z is the ionization potential, R is the ionic radius and Z is the ion's formal charge. Herein, we refer specifically to "Misono softness" to avoid potential confusion with other hardness scales.

Yttrium displays the lowest Misono softness of the series, and thus we expect anomalous Y behavior to be more pronounced than anomalous behavior La, Gd and Lu. Indeed, Y–Ho fractionations are apparent during inner-sphere complexation with Fe-(oxyhydr)oxide—and to a lesser extent Mn-oxide—surfaces (Ohta et al., 2009a), where Y exhibits anomalously low sorbent affinity (Koeppenkastrop and De Carlo, 1992; De Carlo et al., 1997; Bau, 1999; Ohta and Kawabe, 2001; Quinn et al., 2004), leading to solid phase depletions of Y relative to Ho. Bau (1999) suggests that while this effect is most pronounced for Y, it is also distinguished for La and weakly evident for Gd and Lu when Fe-(oxyhydr)oxides are the sorbent.

Prior field observations of Y–Ho fractionation derive largely from marine systems, where the supra-chondritic seawater $^{[Chond]}Y/Ho$ ratio of 1.4–2.5 and longer seawater residence times for Y than Ho (Nozaki et al., 1997), are ascribed to greater Ho affinity for marine particle surfaces (Bau et al., 1995, 1997). This lower sorbent affinity for Y relative to Ho, respectively, is clearly evident in marine ferromanganese (Fe–Mn) crusts (Bau et al., 1996; Bau and Koschinsky, 2009) that are common features of redox-stratified ocean basins. In these basins, one finds aqueous Y/Ho ratios are higher in oxic than anoxic zones (e.g., Bau et al., 1997), consistent with preferential accumulation of Ho on oxidized Fe–Mn crusts. Selective extractions suggest that such preference is more pronounced for Fe relative to Mn oxides (Bau and Koschinsky, 2009), but Y depletion is evident in both solids.

In soils, prior studies of lanthanoid (re)distribution have emphasized redox-generated Ce and Eu anomalies and smooth, radius-dependent fractionation to (a) identify soil parent materials (Öhlander et al., 1996; Aide and Pavick, 2002), (b) infer soil redox conditions (Braun et al., 1990), and (c) investigate patterns of trace element mobility (Nesbitt, 1979; Braun et al., 1993; Öhlander et al., 1996; Braun

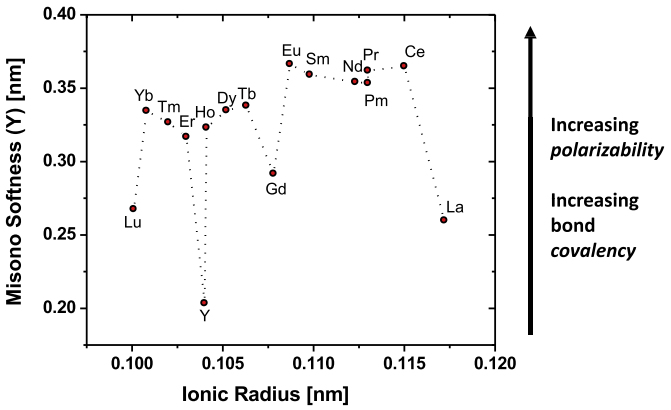

Fig. 1. Lewis acid softness of the lanthanoids expressed based on the Misono softness parameter Y (Misono et al., 1967), calculated from Eq. (1) with constants available in the Handbook of Chemistry and Physics (CRC, 2011).

et al., 1998; Minarik et al., 1998; Land et al., 1999). Attention to Y–Ho fractionation in soils is noticeably absent (Huang and Gong, 2001; Aide and Smith-Aide, 2003; Laveuf et al., 2008; Mourier et al., 2008; Zhang et al., 2008; Fernandez-Caliani et al., 2009; Laveuf and Cornu, 2009; Sako et al., 2009; Tematio et al., 2009; Laveuf et al., 2012). Perhaps this is because soils exhibit much higher solid-phase heterogeneity than marine systems (Tyler, 2004). Still, anomalous ^{Chond}Y/Ho ratios are evident when examining solution data from continental rivers (Leybourne and Johannesson, 2008), suggesting Y–Ho fractionation in terrestrial systems is likely common and may be detectable in soils. Indeed, careful inspection of existing datasets reveals elevated Y/Ho ratios in partial soil dissolutions relative to the whole soil digests (Minarik et al., 1998; Leybourne and Johannesson, 2008) and lower Y/Ho ratios in the most weathered samples in some laterite profiles (Sanematsu et al., 2011). In addition, Y–Ho fractionation between solid and aqueous phases in low temperature biogeochemical systems can be observed by inspecting data collected during Y and Ho sorption to bacterial cells (Takahashi et al., 2005) or organic acid mediated mineral dissolution (Goyne et al., 2010).

We hypothesized that Misono softness affects REY fractionation over the course of soil development from parent rock. To test this, we employed a Hawaiian chronosequence (the "long substrate age gradient" or "LSAG") of Fe-rich soils developed on basaltic lava flows ranging in age from 0.3 to 4100 ky (Vitousek et al., 1997). The Y anomaly is of particular interest because it probes a large shift in Misono softness (0.20 nm, Fig. 1) and the Y/Ho ratios of Hawaiian basalt (^{Chond}[Y/Ho] = 0.998) and Asian Dust (^{Chond}[Y/Ho] = 0.994), which is accreted at an average rate of 125 mg cm^{-2} ky^{-1} (Kurtz et al., 2001), are both within 1% of the Chondritic values (Nance and Taylor, 1976; Gladney and Roelandts, 1988).

Prior laboratory studies, including our own, have shown that conjunctive measurement of soil dissolution and quantification of soil particle surface charge can be used to distinguish proton-promoted, ligand-promoted, and nanoparticle dispersive soil dissolution mechanisms, in part through measuring their dependence on primary geochemical variables such as pH and redox potential (Chorover and Sposito, 1995a,b,c; Thompson et al., 2006a,b). The short-time-scales (e.g., <24 h) employed in such dissolution experiments model episodic infusions of rainfall into soil. In the current work, we applied this experimental design to evaluate whether contemporaneous mechanisms controlling Misono-dependent REY fractionation occur differently in proton-promoted, ligand-promoted or nano-particle dispersion dissolution regimes. We present a quantitative description of REY partitioning as a function of pH-dependent surface charge using a set of data that were collected concurrently with a study designed to investigate the evolution of surface charge and major element dissolution behavior across a chronosequence of soils (Chorover et al., 2004). In addition to observing systematic variation in the Y anomaly across the soil dissolution pH range, our study also revealed anomalous behavior for La (as ^{Chond}La/Pr), which has the second lowest Misono softness of the REY (0.25 nm, Fig. 1) and, like Y, exhibits anomalously low affinity for Fe minerals (Bau, 1999). Since Hawaiian soils are rich in organic matter (OM) and nano-crystalline Fe and Al-(oxyhydr)oxides (Chorover et al., 2004), we postulated that the dissolution-dispersion behavior of these major soil chemical constituents might modulate or overprint the impacts of Y–Ho and La–Pr sorptive fractionation. Therefore, we also report data on the concurrent experimental dissolution of organic carbon, Fe, and Al.

2. MATERIALS AND METHODS

2.1. LSAG soil collection and characterization

Soil samples were collected from six sites along the LSAG, a well-characterized basaltic chronosequence on the islands of Hawaii, Molokai, and Kauai (Vitousek et al., 1997). Site locations, additional information on soil and ecosystem properties, and reconstruction of the long-term geomorphological/climatic history of the sites as related to their use as a "true chronosequence" are given elsewhere (Crews et al., 1995; Vitousek et al., 1997; Chorover et al., 1999; Hotchkiss et al., 2000; Chorover et al., 2004; Vitousek, 2004). One of the principal conclusions of these and related studies is that the LSAG covers such a long time span that variation in state factor parameters other than time, often problematic in shorter sequences, exerts minimal impact on LSAG pedogenesis. The time sequence of mineral-organic weathering-product composition and transformation has been well characterized in prior work (Torn et al., 1997; Chorover et al., 1999, 2004; Mikutta et al., 2009) and are briefly summarized here (Table 1). Soils of the LSAG are dominated by primary silicates, volcanic glass and mineral-adsorbed organic matter in early weathering stage [Site 1 (Ola'a, 0.3 ky): Thaptic Udivitrand]; meta-stable short-range-ordered Fe and Al/Si minerals (ferrihydrite, nano-goethite, allophane) with co-precipitated organic matter at intermediate stage [Sites 2–4 (Laupahoehoe, 20 ky; Kohala, 150 ky; Pololu, 350 ky): Aquic Hydrudand], and well-crystallized Fe and Al oxides (goethite, hematite, gibbsite) and kaolinite with adsorbed organic matter at advanced stage [Site 5 (Kolekole, 1,400 ky): Aquic Hapludand] and [Site 6 (Kokee, 4,100 ky): Plinthic Kandiudox] (Chorover et al., 2004; Mikutta et al., 2009). Each soil contains organic (O) horizons overlying organic-rich mineral horizons (A), subsoil B horizons (Bw), and partially weathered parent material (Cr). Buried horizons (resulting from periodic eruptions) are evident in the two youngest soils, but at depths greater than those studied here. We collected samples from 10 to 20 cm and 50 to 70 cm depths (Chorover et al., 1999, 2004), which corresponded to A and Bw or Bg horizons, respectively. Hawaiian rainforest soils are minimally bioturbated (Ziegler et al., 2005; Marin-Spiotta et al., 2011) and thus surface horizons that accumulate aeolian material are not physically mixed with underlying horizons. Samples collected from pit faces were composited in the field and transferred into Ziploc bags, double bagged, and then transported to the laboratory in coolers maintained at low temperature by addition of ice packs. Samples were stored in plastic Ziplock bags at

Table 1
Summary of soil Characteristics[a].

Soil	Org. C[b] g kg^{-1}	Total Fe[b] g kg^{-1}	SRO[e] Fe[b] g kg^{-1}	SSA[c] m^2 g^{-1}	[Cor]SSA[c] m^2 g^{-1}	Native pH[b]	pH of p.z.n.c.[b]	Clay mineral composition[d]
Surface soils								
Olaa 0.3 ky	96(10)[4]	80(5)	16(1)	2.3	2.4	6.04(4)	2.0(2)	P, F, a
Laupahoehoe 20 ky	339(5)	150(9)	52(2)	54.4	84.4	3.59(2)	1.8(3)	F, A, m, q
Kohala 150 ky	390(14)	23(2)	11(1)	28.8	46	3.98(6)	1.9(2)	A, F, v, hiv, q
Amalu 350 ky	136(6)	33(2)	2(0)	19	45.3	3.70(3)	0.9(5)	A, F, v, hiv, k, q
Molokai 1400 ky	125(2)	129(7)	18(0)	20.2	27.4	3.82(6)	2.1(2)	K, Gi, F, he, q
Kauai 4100 ky	51(1)	314(17)	2(0)	47.6	51.8	3.80(6)	1.2(4)	K, Gi, Go, he
Subsurface soils								
Olaa 0.3 ky	6(1)	88 (4)	5(0)	9.3	9.8	6.60(8)	1.4(3)	P, F, a
Laupahoehoe 20 ky	116(15)	150(10)	102(5)	62.9	81.4	4.69(1)	3.8(2)	F, A, m, q
Kohala 150 ky	32(4)	38(2)	5(0)	55	72.4	4.23(2)	3.8(2)	A, F, hiv, q
Amalu 350 ky	104(7)	99(5)	39(8)	65.2	77.9	4.03(6)	5.3(1)	A, F, v, hiv, k, q
Molokai 1400 ky	19(7)	80(4)	8(1)	64.8	67.4	4.27(4)	1.9(2)	K, Gi, f, he, q, m
Kauai 4100 ky	14(4)	288(17)	1(0)	70.9	72.7	4.11(2)	4.6(2)	K, Gi, Go, he, m

[a] Additional information is provided in the Electronic Annex and in Chorover et al. (2004) and Mikutta et al. (2009).
[b] Data compiled from Chorover et al. (2004): native pH measured in DI water; mineral composition based on XRD, abbreviations–upper case letters indicate major constituents, lower case letters indicate minor constituents; P = plagioclase; A = short-range-ordered Al gels or aluminosilicates (e.g., allophane); F = ferrihydrite; Q = quartz; V = vermiculite; HIV = hydroxyl-interlayered vermiculite; K = kaolin minerals (kaolinite and/or halloysite); Gi = gibbsite; He = hematite; Go = goethite; M = magnetite.
[c] These values from Mikutta et al. (2009) pertain to a different set of samples collected from the same sites except that a 400 ky site (Pololu) replaces the 350 ky site. SSA^{cor} is the specific surface area after removal of organic matter. See Mikutta et al. (2009) for details.
[d] Errors in parentheses are in concise form indicating the error in the last digit [e.g., 7.14(12) is equivalent to 7.14 ± 0.12].
[e] Short-range-ordered Fe, determined by the acid ammonium oxalate method.

4 °C without drying or other modification. Prior to measurement or experiments, the soil surface ion exchange sites were saturated with LiCl in order to eliminate differences in exchange site occupancy and electrolyte composition within and among the soils, i.e., by creating 'homo-ionic' soil pastes (for details see Chorover et al., 2004). For measurement of total elemental concentrations, the soil pastes were oven dried and ground to a fine powder and subjected to Li-metaborate fusion (Hossner, 1996) and analysis via ICP-MS by Actlabs, Ancaster, ON, Canada.

2.2. REY release as a function of pH and surface charge

We previously conducted short-time, pH-dependent, batch dissolution experiments on surface and subsurface LSAG soils (Chorover et al., 2004) and report here REY element concentrations measured during these experiments that have not been published previously. In designing these experiments, we sought to link variation in surface charge with soil dissolution behavior based on a foundation laid in a series of seminal papers by Stumm and co-workers (Furrer and Stumm, 1986; Zinder et al., 1986; Wieland et al., 1988; Stumm and Wollast, 1990) where they developed mechanistic, predictive relations between surface charge/speciation (including adsorbed proton or ligand charge) and rates of polyvalent metal dissolution for Al and Fe oxyhydroxides and kaolinite (Stumm and Wollast, 1990). The approach was later applied to multi-component kaolinitic soils suspended in homo-ionic (LiCl-saturated) form in "indifferent" (LiCl) background electrolyte (Chorover and Sposito, 1995a,b,c). Short-time dissolution experiments performed conjunctively with ion (H^+, OH^-, Li^+, Cl^-) adsorption measurements using a batch titration approach in a simplified electrolyte medium enable correlation of soil dissolution rate with distinct components of surface charge. Here, we measure how REY release varies across the pH (and hence surface charge) range for elements of different Misono softness, and explore how the pH-dependent trends in fractionation vary systematically with the pedogenic time-scale sequence represented by the LSAG.

The experimental protocol was as described in Chorover et al., (2004). Briefly, dissolution experiments were conducted at 298 K, and 0.01 M ionic strength over a range in aqueous *proton concentration*, measured as $-\log[H^+]$ (hereafter referred to as "pH") with target values ranging from ~pH 2 to 9 in a constant 10.0 mM ionic strength background electrolyte solution composed of Li^+, Cl^-, H^+, and OH^-. The pH values were measured using an Orion-Ross 8102 combination electrode calibrated by Gran titration under N_2 (g) purge in the same solutions (ionic strength = 10 mM composed of the ions Li^+, Cl^-, H^+, and OH^-; Chorover and Sposito, 1995c). Duplicate subsamples of LiCl-saturated soil paste equivalent to 410 mg of dry soil were equilibrated (1:100 soil:solution ratio) in solutions of LiCl/HCl or LiCl/LiOH (total suspension mass of 41.0 g) to achieve target values for pH while maintaining an ionic strength of 0.01 M. Replicated titration "blanks" containing equivalent amounts of acid/base were prepared without soil. Tubes were mixed on an end-over-end shaker (7 rpm) for 3 h and then centrifuged at 27,000*g* (relative centrifugal force, RCF, see Wilson and Walker, 2010) for 20 min. Supernatant solutions were aspirated by Pasteur pipette into acid-washed, 60 mL HDPE bottles. Data collected on a subset of samples indicated that the pH values

stabilized to within 0.5 pH units within the first 20 min of reaction in suspension, and they remained stable to within 0.1 pH units of the final pH (reported) between 2 and 3 h.

Using Stokes law and assuming a particle density of 2.73 g cm^{-3} (Thompson et al., 2006a), we calculate particles less than 45 nm in equivalent spherical diameter remain suspended in supernatant solutions following the centrifugation step. Hence, suspensions run for ICP-MS analysis (below) can contain nanoparticles and macromolecules in addition to "true" solutes. While this precludes distinguishing nanoparticles from solutes directly—as might be achieved, e.g., by including an ultrafiltration or ultracentrifugation step—our motivation was to include by analytical design all mobile species released during soil weathering. Future researchers might benefit from including an ultrafiltration step to better refine the mass balance as reflected in other studies that have included such separations (Thompson et al., 2006a).

Elemental analysis of the supernatants was accomplished by inductively coupled plasma mass spectrometry (ICP-MS, high-resolution Finnigan Element magnetic sector at the Penn State Geosciences Dept.). Measured isotopes included: ^{56}Fe, ^{28}Si, ^{27}Al, ^{89}Y, ^{139}La, ^{140}Ce, ^{141}Pr, ^{145}Nd, ^{147}Sm, ^{151}Eu, ^{157}Gd, ^{159}Tb, ^{163}Dy, ^{165}Ho, ^{167}Er, ^{169}Tm, ^{172}Yb, ^{175}Lu. Rhodium (Rh) was included as an internal standard for Fe, Si and Al and Indium (In) was used for Y and the lanthanides based on similarities in first ionization potential (as recommended by the manufacturer). Other methods, such as the innovative use of a virtual internal standard (VIS) value by interpolating between ^{133}Cs and ^{187}Re (Schijf and Marshall, 2011), may offer improved precision in future work. Finally, note that we refer to organic carbon in these supernatants as DOC for simplicity and consistency with Chorover et al. (2004), despite evidence that some of the carbon is nanoparticulate and macromolecular (see Section 4, Discussion).

2.3. Notation and calculations

Throughout the text element concentrations and ratios are denoted as follows: ^{Chond}[M], ^{Chond}[R], where [M] is the element and [R] the ratio of interest, the preceding superscripted value, if present, denotes normalization of measured mass concentrations to standard Chondrite-Cl (Anders and Grevesse, 1989). After normalization, anomalous behavior of Y or La is evaluated as suggested by Bau (1997) as $^{[Chond]}$[Y/Ho] and $^{[Chond]}$[La/Pr].

3. RESULTS

3.1. Y–Ho trends along the LSAG

Total soil REY patterns for our selected soil horizons (Fig. EA-1 of the electronic annex) are similar to those presented by Kurtz et al. (2001), with the exception that our plots include Y placed adjacent to Ho as suggested by Bau (1999). REYs in Hawaiian soils derive from either the parent basalt material or from accumulated dust originating in Asia. However, the Y/Ho ratio of Hawaiian basalt and Asian Dust are both within 1% of the Chondritic values (Fig. 2). For both the surface and subsurface soils at the youngest (0.3 ky) site, ^{Chond}[Y/Ho] ratios are very similar to those for Hawaiian basalt. At 20 ky, the surface ^{Chond}[Y/Ho] ratio decreases and then gradually increases back to its chondritic ratio by the 4100 ky site, presumably due to contributions of Asian dust. In contrast, the subsurface soil ^{Chond}[Y/Ho] ratios decrease within 20 ky to ~70% of their chondritic value and then continue to decrease across the age sequence

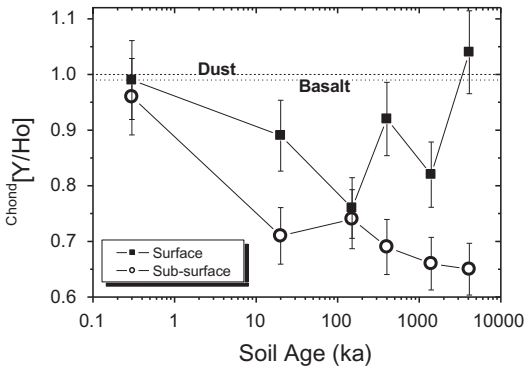

Fig. 2. Chondrite-normalized Y/Ho ratios for the surface and subsurface transect of the LSAG. The dotted and dashed lines are the values for Asian dust (Nance and Taylor, 1976) and Hawaiian basalt (Gladney and Roelandts, 1988), respectively. Errors bars are 2σ external error based on 4 measurements of a one soil during multiple analytical sessions.

3.2. Y–Ho and La–Pr fractionation during soil dissolution

Element dissolution patterns for soils across the chronosequence generally exhibit a parabolic dependence on pH with a pH (point) of minimum dissolution (p.m.d.) corresponding with either the intrinsic solubility of soil solids or the flocculation/dispersion behavior of organo-mineral nanoparticles (Figs. EA-2 and EA-3 of the electronic annex, also see Chorover et al. (2004)). Such behavior is similar to that observed previously for a range of kaolinitic tropical forest soils (Chorover and Sposito, 1995b). REYs exhibit different pH-dependent dissolution patterns for the surface versus subsurface soils. In the surface soils, the REY p.m.d. corresponds with those for DOC and Fe (represented by dashed line at lower pH in Fig. EA-2 of the electronic annex);whereas in the subsurface soils the REY p.m.d. corresponds with that for Al (dashed line at higher pH in Fig. 3 and Fig. EA-3 of the electronic annex). In all cases, the p.m.d. values for REYs and other elements were lower in the surface than in the subsurface soils. The masses of REEs released to solution during batch dissolution experiments were also generally higher in the subsurface soils, particularly at low pH (Figs. EA-2 and EA-3 of the electronic annex). To aid in the discussion of REY behavior, the p.m.d. values for Al, DOC, Fe, and the REY have been extracted from Figs. EA-2 and EA-3 of the electronic annex and are depicted by the dashed lines on Figs.3–5.

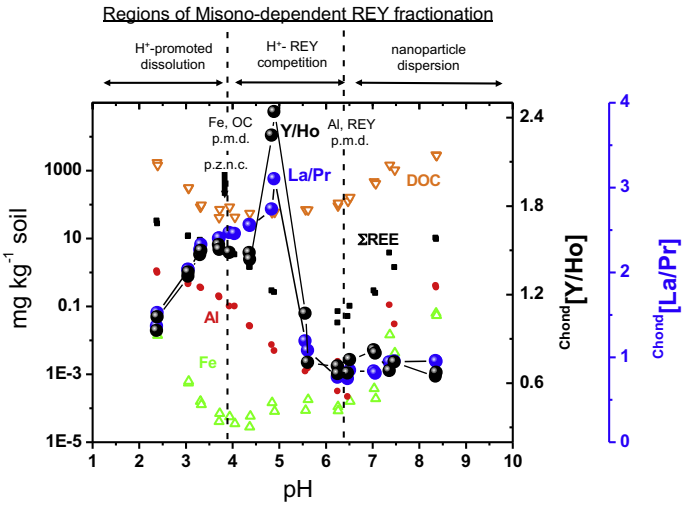

Fig. 3. Concentration of Fe (green open triangles), Al (red filled circles), ΣREE (black filled squares), and organic carbon (DOC, orange upside down open triangles) following 3-h dissolution of the 150 ky subsurface soil at the indicated pH. Chondrite normalized Y/Ho and La/Pr ratios (large black and blue spheres, respectively) are plotted on the two right *Y*-axis. The right vertical dashed line corresponds with the point of minimum dissolution (p.m.d.) for Al and ΣREE, while the left vertical dashed line corresponds with the p.m.d. for Fe and DOC. The downward pointing arrow indicates the p.z.n.c. All measurements on <0.045 μm solutions.(For interpretation of the references to colour in this figure legend, the reader is referred to the web version of this article.)

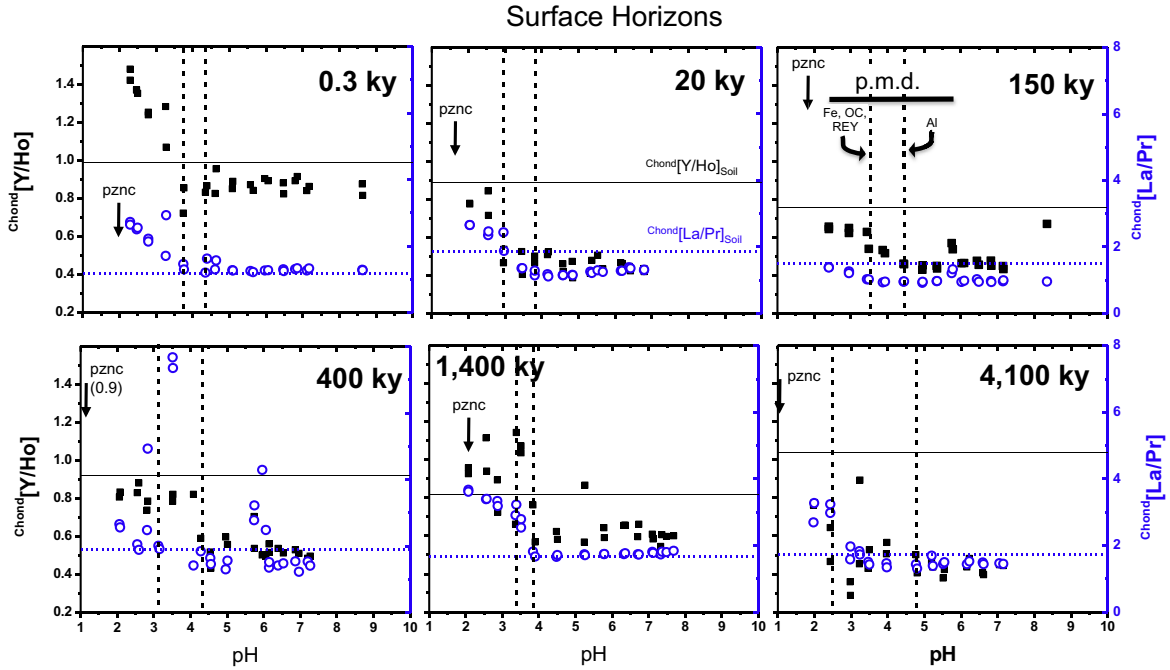

Fig. 4. Chondrite normalized Y/Ho (left axis, filled black squares) and La/Pr (right axis, open blue circles) ratios of desorbed REY's from the surface soil horizons following incubation for 3 h at the indicated pH. The points of minimum dissolution (p.m.d.) are shown as vertical dashed lines for Al (higher pH) and Fe, organic carbon, and REYs (lower pH) based on data in Fig. EA-2 of the electronic annex. The horizontal lines are the total soil dissolution values for Y/Ho (solid black line) and La/Pr (blue dashed lines). Reported pH values are those at the end of the experiment. All measurements on <0.045 μm solutions.(For interpretation of the references to colour in this figure legend, the reader is referred to the web version of this article.)

There are clear pH dependent trends in aqueous phase ratios for ^{Chond}[Y/Ho] and ^{Chond}[La/Pr] (Figs. 4 and 5). Aqueous ^{Chond}[Y/Ho] and ^{Chond}[La/Pr] exhibited similar patterns across six distinct parent material ages, each with three distinct *regions* of pH (Figs. 4 and 5) with derivation of the respective p.m.d. values exemplified in Fig. 3. Specifically, region 1 extends from the most acidic pH to the Fe and OC p.m.d. values (*ca.* pH 4); region 2 extends from

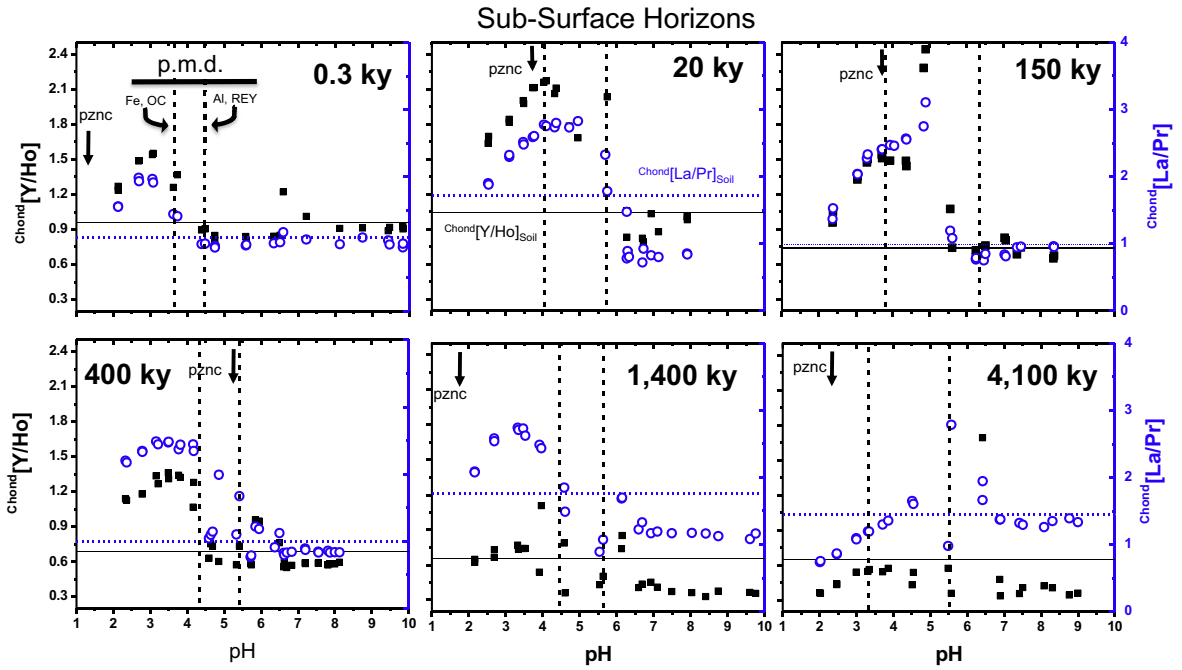

Fig. 5. Chondrite normalized Y/Ho (left axis, filled black squares) and La/Pr (right axis, open blue circles) ratios of desorbed REY's from the sub-surface soil horizons following incubation for 3 h at the indicated pH. The points of minimum dissolution (p.m.d.) are shown as vertical dashed lines for Al and REYs (higher pH) and Fe and organic carbon (lower pH) based on data in Fig. EA-3 of the electronic annex. The horizontal lines are the total soil dissolution values for Y/Ho (solid black line) and La/Pr (blue dashed lines). Reported pH values are those at the end of the experiment. All measurements on <0.045 μm solutions.(For interpretation of the references to colour in this figure legend, the reader is referred to the web version of this article.)

the Fe–OC p.m.d. values at low pH to the Al p.m.d. values at higher pH (ca. 5–6); and region 3 pertains to pH > Al p.m.d. For all subsurface soils, except the oldest, aqueous ^{Chond}[Y/Ho] or ^{Chond}[La/Pr] ratios reached a maximum within two pH units below the Al (and REY) p.m.d. Approach to this maximum was most pronounced in the younger, subsurface soils (e.g., 20–400 ky, Figs. 3 and 5), and not resolved for ^{Chond}[Y/Ho] in the two oldest soils (Fig. 5). The decrease in aqueous ^{Chond}[Y/Ho] or ^{Chond}[La/Pr] ratios at low pH for the subsurface soils coincides with the rise in Fe concentration below the Fe–OC p.m.d. (Figs. 3 and 5). For the surface soils, aqueous ^{Chond}[Y/Ho] and ^{Chond}[La/Pr] ratios continue to increase with decreasing pH to the lowest pH limits of the experiment (Fig. 4).

4. DISCUSSION

4.1. Y–Ho ratios as a tracer of Misono-dependent REY fractionation

Evaluating time-dependent changes in elemental enrichment-depletion patterns in soils along space-for-time gradients such as the LSAG can provide insight to the rates and pathways of weathered regolith formation from parent rock. We investigated here whether soil REY fractionation reflects variation in Lewis acid-base chemistry (Fig. 1) and focused our interpretation of Misono-dependent REY fractionation on Y anomalies (Y/Ho ratio) for two reasons: (1) Y has the lowest Misono softness value (0.20 nm) of trivalent REY ions (Fig. 1); and (2) the ^{Chond}[Y/Ho] ratios for dust (0.998) and basalt (0.994) are very similar (Nance and Taylor, 1976; Gladney and Roelandts, 1988). The latter feature is unlike the case for Eu, whose anomaly can be used to distinguish Hawaiian basalt from incoming continental dust (Chadwick et al., 1999; Kurtz et al., 2001; Porder et al., 2007) (Fig. EA-1). In contrast, the ^{Chond}[La/Pr], ^{Chond}[Gd/Gd*] and ^{Chond}[Lu/Yb] ratios for the Hawaiian basalt and the continental dust vary substantially and may exhibit source bias in this system (see Table EA-2). Thus, variation in soil ^{Chond}[Y/Ho] values can be considered a tracer of biogeochemical weathering stoichiometry rather than a reflection of differences in parent material. Indeed, we find between 0.3 and 20 ky of weathering, soil ^{Chond}[Y/Ho] ratio begins to decrease from its initial value of 1.0 to ca. 0.7 in the both surface and subsurface soils (Fig. 2). In the subsurface it remains at that value or below throughout the chronosequence, whereas in the surface soils after reaching a minimum of 0.7 at 150 ky, it then increases to above 1.0 at the oldest site. Using ^{Chond}[Eu/Eu*] as a measure of dust input, dust accumulation becomes evident in the surface soils by 20 ky, but never impacts the subsurface soils substantially (Fig. EA-4). Thus, data from our subsurface transects indicate that Y–Ho fractionation does indeed occur across the LSAG (Fig. 2).

4.2. Potential mechanisms generating Misono-dependent REY fractionation

Soil solid phase ^{Chond}[Y/Ho] ratios less than unity indicate the preferential loss of the yttrium during soil weathering. By examining REY release across a wide pH range in dissolution experiments we gain insight on the mechanisms of dissolution and REY loss. The batch titration approach yields concave dissolution curves for Al, Fe and DOC with points of minimum dissolution (p.m.d.) signifying a boundary between proton and ligand plus dispersion promoted dissolution at pH values below and above the p.m.d., respectively (Fig. 3) (Chorover and Sposito, 1995b; Chorover et al., 2004). The Hawaiian soils studied here are replete with nano-particulate mineral-organic complexes that contain a high mass-normalized density of reactive surface hydroxyls (Chorover et al., 2004; Mikutta et al., 2009; Thompson et al., 2011) and undergo significant dispersion as pH increases more than a unit above the soil's point of zero charge (p.z.c.) (Chorover and Sposito, 1995b; Chorover et al., 2004; Thompson et al., 2006a). Thus, ligand-promoted dissolution and nano-particulate dispersion co-occur in our experiments, and hence REY release at high pH derives from both mechanisms.

At pH values above the REY p.m.d., REY and DOC releases are strongly correlated (Fig. EA-5 of the electronic annex) and charge-induced dispersion of soluble and nanoparticulate complexes is prevalent (Chorover et al., 2004). Here, aqueous ^{Chond}[Y/Ho] and ^{Chond}[La/Pr] values reach the lowest values observed in the experiments, at or below those of the total soil (Figs. 3–5). Thus, we do not observe any preferential release of Y relative to Ho above the REY p.m.d. and therefore, we surmise ligand-promoted dissolution and/or nanoparticle dispersion are not responsible for the evolution of low solid-phase ^{Chond}[Y/Ho] ratios across the LSAG (Fig. 1). Dissociatedcarboxylic acid groups in OM become progressively more important sites for REY complexation as pH increases above *ca*. pH 4 (Markai et al., 2003; Davranche et al., 2004; Pourret et al., 2007). REY-carboxylate ligand stability is slightly lower for REYs with low Misono softness (Y and La) relative to their counterparts (Ho and Pr) (Byrne and Lee, 1993; Wood, 1993; Byrne and Li, 1995; Schijf and Byrne, 2001; Goyne et al., 2010; Christenson and Schijf, 2011), which is consistent with the low aqueous ^{Chond}[Y/Ho] and ^{Chond}[La/Pr] values we observe at higher pH. Carbonate complexation may also contribute to the non-discriminate release of Y–Ho and La–Pr at higher pH. Although carbonate concentrations (not measured) are expected to be quite low in these experimentsgiven the initial soil pH (Table 1), some REY complexation by carbonate ions is likely in the higher pH range of our experiments (Cantrell and Byrne, 1987; Ohta and Kawabe, 2000; Quinn et al., 2006b). Aqueous carbonate complexation has been shown to influence total REY partitioning to Fe oxyhydroxide phases as well as to influence Y-Ho fractionation (Quinn et al., 2006b). Ho forms stronger aqueous carbonate complexes than does Y (Liu and Byrne, 1995) and data from Quinn et al (2006b) suggest increasing aqueous carbonate concentrations—as well as increasing pH—in the presence of Fe oxyhydroxides decreases the difference between Ho and Y aqueous-solid partition coefficients (e.g.,$\log_i K^T_{Fe}$).

Preferential release of Y relative to Ho was measured over the 3 h dissolution period, but generally only at pH values below the REY p.m.d. (Figs. 3–5). Similar trends are also observed for La relative to Pr (Figs. 3–5) suggesting a common softness dependent mechanism of REY release. At pH values below the REY p.m.d., increases in aqueous REY concentrations are consistent with adsorptive competition with protons, and proton-promoted dissolution of phases hosting co-precipitated REYs. This release evidently favors low Misono softness ions Y (0.20 nm) and La (0.25 nm) relative to the more strongly sorbed Ho (0.32 nm) and Pr (0.36 nm).

Preferential Y and La release extends to the lowest pH values in our experiment in the surface soils. Organo-mineral associations decrease the soil p.z.n.c. values in the surface soils of the LSAG to ca. pH 2 (Table 1), providing sufficient negative surface charge for competitive ion re-sorption and Y–Ho and La–Pr fractionation even down to the lowest pH values in our experiments. In the subsurface soils, aqueous ^{Chond}[Y/Ho] and ^{Chond}[La/Pr] values are a concave function of pH below the REY p.m.d. with peak values between pH 3 and 5. The p.z.n.c. values of the intermediate-aged (20–400 ky) and oldest (4100 ky) subsurface soils are between pH 3.8 and 5.3 (Table 1) and this may contribute to the concave Misono-dependent REY fractionation pattern we observe as a function of dissolution pH. For instance, as the dissolution pH decreases below the soil p.z.n.c. the capacity for cation re-sorption (and REY fractionation by this mechanism) would progressively diminish and eventually become overprinted as dissolution of REY-bearing phases, especially Fe-oxides, increases at the lowest pHs (Fig. EA-3). However, a similar concave ^{Chond}[Y/Ho] and ^{Chond}[La/Pr] release pattern is evident in the 0.3 and 1400 ky subsurface soils, which exhibit p.z.n.c. values below pH 2. Chorover et al. (2004) found the surface charge density of these two soils increased more gradually with pH (e.g., 15–27 $mmol_c\ kg^{-1}$ per unit pH for the 0.3 and 1400 ky subsurface soils, respectively) than the intermediate aged soils for which surface charge density increased 50–70 $mmol_c\ kg^{-1}$ per unit pH. Perhaps, this slower increase in surface charge with increasing pH limited the amount of negatively charged sites available for sorptive fractionation until the pH increased much higher than the p.z.n.c. Alternatively, variation in the patterns of fractionation may derive from differences in the mineral composition of the soils (Chorover et al., 2004; Mikutta et al., 2009, 2010) or shifting distribution of solid phase phosphorus across the LSAG (Crews et al., 1995; Chadwick et al., 1999; Vitousek, 2004). With respect to the latter, Liu and Byrne (1997) found the solubility product of Y-phosphates and Ho-phosphates to be similar, suggesting minimal Y/Ho fractionation during phosphate mineral dissolution/precipitation. Phosphorus was not measured in our experiments, but 1:10 soil solutions from an intermediate-aged soil from Maui (Thompson et al., 2006a,b) contained at most 300 $nmol\ g^{-1}$ soil P at pH 4–5, which would equate to 3 $\mu mol\ L^{-1}$ P at the 1:100 soil:solution ratio used in the current experiments. Regardless, the data indicate preferential

release of Y relative to Ho occurs when re-adsorption of REY ions are in competition with protons (Figs. 3–5).

4.3. Solid phases implicated in Y–Ho fractionation

Because ^{Chond}[Y/Ho] dissolution values were highest at low pH when organic carbon release and particle dispersion were minimized (Figs. 3–5), we infer that Y–Ho fractionation is governed by differential affinity for soil solid phases. Mineralogy of these Hawaiian soils is a strong function of pedogenic age; primary minerals and volcanic glass predominates in young soils (<20 ky), short-range-ordered (SRO) Fe and Al oxides and aluminosilicate (allophane) mineral phases predominate in the intermediate aged soils (20–400 ky), and crystalline Fe and Al oxides and kaolinite are prevalent in the older soils (400–4100 ky) (Chorover et al., 2004; Thompson et al., 2011). While sorptive Y–Ho fractionation is well established for Fe-(oxyhydr)oxide phases (Koeppenkastrop and De Carlo, 1992, 1993; Bau, 1999; Kawabe et al., 1999; Ohta et al., 1999; Ohta and Kawabe, 2000; Quinn et al., 2004, 2006a,b; Bau and Koschinsky, 2009), fewer studies pertain to Al oxide and aluminosilicate phases. Quinn et al. (2004) examined linear free energy relationships (LFERs) between the first hydroxide stability constant ($\log_{OH}\beta_1$) for trivalent REYs and measured the REY aqueous-solid partitioning coefficient ($\log K_D$) for Al and Fe hydroxides (as well as for In and Ga hydroxides) at pH 6.1. They found excellent LFERs with Al hydroxides, good correlation for Ga and In hydroxides, but poor correlation for Fe hydroxides (2004). Thus, at the pH of the Quinn et al. (2004) experiments, Fe-hydroxide precipitates are unique among the metal-hydroxide adsorbents (Al, In, Ga, and Fe). Ohta et al. (2009a,b) used extended x-ray adsorption spectroscopy (EXAFS) to study the surface coordination of REYs on Fe and Mn surfaces. They found light REEs (including La) occur in a mixture of eight and nine-fold coordination on the goethite (α-FeOOH) surface, while heavy REEs (including Y) occur in eight-fold coordination (Ohta et al., 2009b). This is consistent with the aqueous REY water-ligand coordination numbers reported by Richens (1997). Ohta et al. (2009b) detected no differences in the surface coordination number for Y and Ho and their EXAFS results suggest the Ho–O bond length on a goethite surface to be only minimally shorter than that for Y–O. The anomalously weak bond formed between Y and Fe (oxyhydr)oxide surfaces is thus likely due to a weaker electronic bonding structure (Kawabe et al., 1991; Bau et al., 1996; Bau, 1999; Ohta et al., 2009b) consistent with the lower Misono softness of Y relative to Ho (Fig. 1).

The behavior of REYs toward Fe-bearing solids may explain the concave pattern of REY release in the subsurface soils at pH < Al p.m.d. (Figs. 3 and 5). At moderately acidic pH (region 2, Fe p.m.d. < pH > Al p.m.d.), nanoparticle dispersion and proton-promoted dissolution are both minimal. Hence, REY release here is controlled by proton-REY sorptive competition. That this condition would maximize differences in Misono-dependent REY ion selectivity for Fe (oxyhydr)oxides is supported by the fact that it coincides with the peak in aqueous ^{Chond}[Y/Ho] and ^{Chond}[La/Pr] values (Figs. 3 and 5). At lower pH (pH < p.m.d. values for Fe and DOC), Misono-dependent REY fractionation decreases as Fe and DOC dissolution increases (Fig. 3) signaling proton-promoted dissolution of a variety of solid phases, including organo-mineral solids and Fe-(oxyhydr)oxides. To the extent that Fe solid phases accumulate Ho and Pr preferentially relative to Y and La, respectively (Bau, 1999), dissolution of these phases at low pH would serve to reverse the trend of increasing aqueous ^{Chond}[Y/Ho] and ^{Chond}[La/Pr] values with decreasing solution pH. Such behavior is observed in marine basins, where seawater ^{Chond}[Y/Ho] values decrease in the deep anoxic zones in conjunction with dissolution of Fe (oxyhydr)oxides (Bau et al., 1997).

Although our data are consistent with a major role for Fe-oxyhydroxides in Misono-dependent REY fractionation across the LSAG, soils are complex systems comprising a wide range of solid phases. The as yet unresolved roles of solid organic matter (Land et al., 1999; Davranche et al., 2004; Pourret et al., 2007), aluminum oxides (Rabung et al., 2000), silicates (Coppin et al., 2002; Tertre et al., 2006), accessory REY-minerals (Braun et al., 1990, 1998; Aide and Pavick, 2002; Aubert et al., 2004; Goyne et al., 2010; Sanematsu et al., 2011), microbial cell biomass (Taunton et al., 2000; Takahashi et al., 2005) and colloid vs. aqueous release (Ingri et al., 2000; Astrom and Corin, 2003; Schijf and Zoll, 2011; Stolpe et al., 2013) in Y–Ho fractionation across the LSAG cannot be discounted without further investigation of REYs in soils, which has to this point largely overlooked Y (Huang and Gong, 2001; Hodson, 2002; Tyler, 2004; Laveuf and Cornu, 2009; Davranche et al., 2011).

4.4. Why Y–Ho fractionation is most pronounced in younger soils

We expected subsoil ^{Chond}[Y/Ho] to decrease progressively with increasing soil age. Instead, ^{Chond}[Y/Ho] values decrease dramatically in the younger soils and then remain equal within error throughout the rest of the weathering sequence (Fig. 2). Certainly, the accumulation of Asian dust with Y/Ho values similar to fresh basalt could modulate the preferential loss of Y in the older soils. Although the ^{Chond}[Eu/Eu*] ratios suggest dust accumulation in the subsurface is minimal (Fig. EA-5), at the older sites dust–associated REYs in the surface may have been translocated to depth.

However, the dramatic decrease in soil weathering rate as a function of parent rock age (Chadwick and Chorover, 2001) likely plays an important role in the attenuation of Y–Ho fractionation in older soils. Early stage weathering of volcanic glass proceeds rapidly (Shoji et al., 1993), releasing framework elements such as Fe, Al, Si and Ti—as well as primary mineral-associated trace REYs—faster than thermodynamically stable crystalline minerals can precipitate. This leads to soil solutions that are over-saturated with respect to metastable, short-range-ordered (SRO) phases (allophane, ferrihydrite, and opaline silica) that have smaller critical nuclei and whose precipitation is favored kinetically over that of more crystalline minerals (Steefel and Van

Cappellen, 1990). The *de novo* SRO phases have large specific surface areas and strongly sequester REYs through either co-precipitation or surface complexation (e.g., Bau, 1999). At this early stage in LSAG soil development, organic matter coatings are also more sparsely distributed than in older soils (Chorover et al., 2004; Mikutta et al., 2009) and thus dissolved REYs are more likely to interact directly with SRO Fe mineral surfaces than in the older soils. By 150 ky, the weathering rate along the LSAG has decreased considerably with minor subsequent decreases to 4100 ky (Chadwick and Chorover, 2001).

Thus, between 0.3 and 20 ky, a high rate of primary mineral weathering combined with negligible accumulation of Asian dust, active precipitation of SRO minerals (esp. Fe oxyhydroxides) and minimal organic matter-mineral association may converge to promote preferential loss of Y relative to Ho. This coincides with a transition in the soil mineral composition from primary volcanic phases to secondary SRO Fe, Al and aluminosilicate phases embedded in a matrix of organic matter (Chorover et al., 2004; Thompson et al., 2006a; Mikutta et al., 2009).

4.5. Implications for Y–Ho fractionation in other soils

It is presently unclear what the primary drivers of Y/Ho fractionation are in landscapes of complex mineralogy and weathering history. A recent survey of surface waters from northern Canada revealed widespread enrichments of Y relative to Ho (mean NASC normalized Y/Ho = 1.14 ± 0.25, $n = 98$, Leybourne and Johannesson, 2008). The Y/Ho ratios of Basalt (BVHO-1) and several shale composites including the North American Shale Composite (NASC) (Gromet et al., 1984) and the Post-Archean Average Australian Shale (PAAS) composite (Nance and Taylor, 1976) all fall within 3% of the average chondritic value of ~26.5 (Pack et al., 2007). Natural materials with non-chondritic Y/Ho ratios all emerge from aqueous chemical speciation or mineral sorption reactions. Common examples include seawater (^{Chond}[Y/Ho] = 1.5–2.6 (Byrne and Lee, 1993; Nozaki et al., 1997), marine sedimentary dolomite (^{Chond}[Y/Ho] = 2.4), banded iron formations (^{Chond}[Y/Ho] = 1.7) and deep-sea ferromanganese nodules (^{Chond}[Y/Ho] = 0.66) (Pack et al., 2007). These materials are less likely to be distributed across terrestrial systems and thus the parent material for most soils will likely have near-chondritic Y/Ho ratio.

Our work on these Hawaiian basaltic soils highlights proton-REY^{3+} competition reactions as a key process driving the preferential loss of Y relative to Ho during pedogenesis. The younger soils in particular also contain variable, but relatively high mass fractions of SRO Fe-(oxyhydr)oxide phases that are known to sequester preferentially Ho relative to Y, thereby giving rise to Y–Ho fractionation. Indeed, the bulk of the Y–Ho fractionation is observed to occur during the rapid initial weathering stage of the soils. The observed bias toward supra-chondritic Y/Ho ratios in stream waters (Leybourne and Johannesson, 2008) may reflect similar fractionation mechanisms as SRO Fe phases are common soil constituents and most of the Canadian soils in the Leybourne and Johannesson (2008) survey are not highly weathered. However, high DOC concentrations would be expected in most northeastern Canadian soil porewaters and this would likely modulate Y–Ho fractionation. In addition, other soil components such as Al-oxides and layer-type aluminosilicates may play an important role in pedogenic Y–Ho fractionation, but sorptive Y–Ho fractionation on these minerals has not yet been adequately evaluated.

5. CONCLUSIONS

There is growing appreciation of the utility of Y anomalies as proxies for geochemical processes, especially in interpreting marine biogeochemical systems. Here, we have demonstrated for the first time that systematic Y–Ho fractionation occurs during the weathering of basaltic soils. By 20 ky of soil weathering, ^{Chond}[Y/Ho], decreases from near chondritic values [$0.96 \pm 0.07(2\sigma)$] to $0.71 \pm 0.05(2\sigma)$ in the subsurface soils and remains equal within error for the next ~4000 ky of soil weathering. Our results suggest that pedogenic Y–Ho fractionation reaches steady state by 20 ky in Hawaiian basalt during the stage when parent material weathering rates are particularly high.

These field observations are supported by short-time dissolution experiments suggesting that preferential Y loss occurs in an intermediate pH range where aqueous REY concentrations are governed by adsorptive-competition reactions. At higher pH adsorptive fractionation is obscured by the dispersion of particle and macro-molecular organics containing REYs with Y/Ho (and La/Pr) ratios similar to the whole soil. Whereas at lower pH the availability of negatively charged REY^{3+} adsorption sites decreases and proton-promoted dissolution drives dissolution of REY-rich sorbents, such as Fe-(oxyhydr)oxides, which are ubiquitous in Hawaiian soils and particularly abundant in the intermediate aged soils (20–400 ky).

To date, Y–Ho fractionation has been ascribed predominately to partitioning between the aqueous phase and Fe and Mn oxides with most field data coming from marine environments (e.g., Koeppenkastrop and De Carlo, 1992; De Carlo et al., 1997; Bau, 1999). If a similar Y–Ho fractionation bias toward Fe and Mn-oxides exists in soils, measurements of Y/Ho ratios might be useful for constraining the role of Fe-oxides during pedogenesis or the influence of Fe-oxides across a watershed. However, our findings suggest complexation of REY's by dissolved organic matter (DOM) may modulate pedogenic Y–Ho fractionation, and complicate the interpretation in organic-rich soils. Future studies across the regolith-weathering front would be helpful in isolating age-related changes in Y–Ho fractionation. Other soil components such as Al-oxides and layered aluminosilicates must be evaluated for potential Y–Ho fractionation in order to extend the use of this ratio as a tracer of soil processes.

ACKNOWLEDGEMENTS

Funding for this work was provided by the U.S. Department of Agriculture (USDA), Soil Processes Program NRI (2003–35107–13663) and AFRI-NIFA Grants (2009-65107-05830) and U.S. Na-

tional Science Foundation Grants EAR-0724958 and EAR-1053470. We also thank associate editor Robert H. Byrne and four anonymous reviewers for their careful attention and excellent suggestions that substantially improved our manuscript.

APPENDIX A. SUPPLEMENTARY DATA

Supplementary data associated with this article can be found, in the online version, at http://dx.doi.org/10.1016/j.gca.2013.06.003.

REFERENCES

Aide M. T. and Pavick Z. (2002) Rare earth element mobilization and migration in a Wisconsin spodosol. *Soil Sci.* **167**, 680–691.

Aide M. and Smith-Aide C. (2003) Assessing soil genesis by rare-earth elemental analysis. *Soil Sci. Soc. Am. J.* **67**, 1470–1476.

Anders E. and Grevesse N. (1989) Abundances of the elements: Meteoritic and solar. *Geochim. Cosmochim. Acta* **53**, 197–213.

Astrom M. and Corin N. (2003) Distribution of rare earth elements in anionic, cationic and particulate fractions in boreal humus-rich streams affected by acid sulphate soils. *Water Res.* **37**, 273–280.

Aubert D., Probst A. and Stille P. (2004) Distribution and origin of major and trace elements (particularly REE, U and Th) into labile and residual phases in an acid soil profile (Vosges Mountains, France). *Appl. Geochem.* **19**, 899–916.

Bau M., Moller P. and Dulski P. (1997) Yttrium and lanthanides in eastern Mediterranean seawater and their fractionation during redox-cycling. *Mar. Chem.* **56**, 123–131.

Bau M. (1999) Scavenging of dissolved yttrium and rare earths by precipitating iron oxyhydroxide: Experimental evidence for Ce oxidation, Y–Ho fractionation, and lanthanide tetrad effect. *Geochim. Cosmochim. Acta* **63**, 67–77.

Bau M. and Dulski P. (1995) Comparative-study of yttrium and rare-earth element behaviors in fluorine-rich hydrothermal fluids. *Contrib. Mineral. Petrol.* **119**, 213–223.

Bau M. and Koschinsky A. (2009) Oxidative scavenging of cerium on hydrous Fe oxide: Evidence from the distribution of rare earth elements and yttrium between Fe oxides and Mn oxides in hydrogenetic ferromanganese crusts. *Geochem. J.* **43**, 37–47.

Bau M., Dulski P. and Moller P. (1995) Yttrium and holmium In south-pacific seawater: Vertical-distribution and possible fractionation mechanisms. *Chem. Erde-Geochem.* **55**, 1–16.

Bau M., Koschinsky A., Dulski P. and Hein J. R. (1996) Comparison of the partitioning behaviours of yttrium, rare earth elements, and titanium between hydrogenetic marine ferromanganese crusts and seawater. *Geochim. Cosmochim. Acta* **60**, 1709–1725.

Braun J.-J., Pagel M., Muller J.-P., Bilong P., Michard A. and Guillet B. (1990) Cerium anomalies in lateritic profiles. *Geochim. Cosmochim. Acta* **54**, 781–795.

Braun J. J., Pagel M., Herbillon A. and Rosin C. (1993) Mobilization and redistribution of REEs and thorium in a syenitic lateritic profile: A mass-balance study. *Geochim. Cosmochim. Acta* **57**, 4419–4434.

Braun J. J., Viers J., Dupre B., Polve M., Ndam J. and Muller J. P. (1998) Solid/Liquid REE fractionation in the lateritic system of Goyoum, East Cameroon: The implication for the present dynamics of the soil covers of the humid tropical regions. *Geochim. Cosmochim. Acta* **62**, 273–299.

Byrne R. H. and Lee J. H. (1993) Comparative yttrium and rare earth element chemistries in seawater. *Mar. Chem.* **44**, 121–130.

Byrne R. H. and Li B. Q. (1995) Comparative complexation behavior of the rare-earths. *Geochim. Cosmochim. Acta* **59**, 4575–4589.

Cantrell K. J. and Byrne R. H. (1987) Rare earth element complexation by carbonate and oxalate ions. *Geochim. Cosmochim. Acta* **51**, 597–605.

Chorover J. and Sposito G. (1995a) Colloid chemistry of kaolinitic tropical soils. *Soil Sci. Soc. Am. J.* **59**, 1558–1564.

Chorover J. and Sposito G. (1995b) Dissolution behavior of kaolinitic tropical soils. *Geochim. Cosmochim. Acta* **59**, 3109–3121.

Chorover J. and Sposito G. (1995c) Surface charge characteristics of kaolinitic tropical soils. *Geochim. Cosmochim. Acta* **59**, 875–884.

Chadwick O. A. and Chorover J. (2001) The chemistry of pedogenic thresholds. *Geoderma* **100**, 321–353.

Chadwick O. A., Derry L. A., Vitousek P. M., Huebert B. J. and Hedin L. O. (1999) Changing sources of nutrients during four million years of ecosystem development. *Nature* **397**, 491–497.

Chorover J., DiChiaro M. J. and Chadwick O. A. (1999) Structural charge and cesium retention in a chronosequence of tephritic soils. *Soil Sci. Soc. Am. J.* **63**, 169–177.

Chorover J., Amistadi M. K. and Chadwick O. A. (2004) Surface charge evolution of mineral-organic complexes during pedogenesis in Hawaiian basalt. *Geochim. Cosmochim. Acta* **68**, 4859–4876.

Christenson E. A. and Schijf J. (2011) Stability of YREE complexes with the trihydroxamate siderophore desferrioxamine B at seawater ionic strength. *Geochim. Cosmochim. Acta* **75**, 7047–7062.

Coppin F., Berger G., Bauer A., Castet S. and Loubet M. (2002) Sorption of lanthanides on smectite and kaolinite. *Chem. Geol.* **182**, 57–68.

CRC (2011) *CRC Handbook of Chemistry and Physics*. CRC Press, Boca Raton, FL.

Crews T. E., Kitayama K., Fownes J. H., Riley R. H., Herbert D. A., Muellerdombois D. and Vitousek P. M. (1995) Changes in soil-phosphorus fractions and ecosystem dynamics across a long chronosequence in Hawaii. *Ecology* **76**, 1407–1424.

Davranche M., Pourret O., Gruau G. and Dia A. (2004) Impact of humate complexation on the adsorption of REE onto Fe oxyhydroxide. *J. Colloid Interface Sci.* **277**, 271–279.

Davranche M., Grybos M., Gruau G., Pédrot M., Dia A. and Marsac R. (2011) Rare earth element patterns: A tool for identifying trace metal sources during wetland soil reduction. *Chem. Geol.* **284**, 127–137.

De Carlo E. H., Wen X.-Y. and Irving M. (1997) The influence of redox reactions on the uptake of dissolved Ce by suspended Fe and Mn oxide particles. *Aquat. Geochem.* **3**, 357–389.

Fernandez-Caliani J. C., Barba-Brioso C. and De la Rosa J. D. (2009) Mobility and speciation of rare earth elements in acid minesoils and geochemical implications for river waters in the southwestern Iberian margin. *Geoderma* **149**, 393–401.

Furrer G. and Stumm W. (1986) The coordination chemistry of weathering: 1. Dissolution kinetics of δ-Al_2O_3 and BeO. *Geochim. Cosmochim. Acta* **50**, 1847–1860.

Gladney E. and Roelandts I. (1988) 1987 Compilation of elemental concen- tration data from USGS BHVO-1, MAG-1, QLO-1, RGM-1, SCo-1, SDC-1, SGR-1 and STM-1. *Geostand. Newsl* **12**, 253–262.

Goyne K. W., Brantley S. L. and Chorover J. (2010) Rare earth element release from phosphate minerals in the presence of organic acids. *Chem. Geol.* **278**, 1–14.

Gromet L. P., Dymek R. F., Haskin L. A. and Korotev R. L. (1984) The North-American shale composite: Its compilation,

major and trace-element characteristics. *Geochim. Cosmochim. Acta* **48**, 2469–2482.

Hodson M. E. (2002) Experimental evidence for mobility of Zr and other trace elements in soils. *Geochim. Cosmochim. Acta* **66**, 819–828.

Hossner L. R. (1996) Dissolution for total elemental analysis. In *Methods of Soil Analysis: Part 3-Chemical Methods* (ed. D. L. Sparks). Soil Science Society of America, Madison, WI.

Hotchkiss S., Vitousek P. M., Chadwick O. A. and Price J. (2000) Climate cycles, geomorphological change, and the interpretation of soil and ecosystem development. *Ecosystems* **3**, 522–533.

Huang C. M. and Gong Z. T. (2001) Geochemical implication of rare earth elements in process of soil development. *J. Rare Earth* **19**, 57–62.

Ingri J., Widerlund A., Land M., Gustafsson O., Andersson P. and Ohlander B. (2000) Temporal variations in the fractionation of the rare earth elements in a Boreal River: The role of colloidal particles. *Chem. Geol.* **166**, 23–45.

Kawabe I., Kitahara Y. and Naito K. (1991) Non-chondritic yttrium/holmium ratio and lanthanide tetrad effect observed in pre-Cenozoic limestones. *Geochem. J.*, 309–335.

Kawabe I., Ohta A., Ishii S., Tokumura M. and Miyauchi K. (1999) REE partitioning between Fe–Mn oxyhydroxide precipitates and weakly acid NaCl solutions: Convex tetrad effect and fractionation of Y and Sc from heavy lanthanides. *Geochem. J.* **33**, 167–179.

Kinraide T. B. (2009) Improved scales for metal ion softness and toxicity. *Environ. Toxicol. Chem.* **28**, 525–533.

Koeppenkastrop D. and De Carlo E. H. (1992) Sorption of rare-earth elements from seawater onto synthetic mineral particles: An experimental approach. *Chem. Geol.* **95**, 251–263.

Koeppenkastrop D. and De Carlo E. H. (1993) Uptake of rare-earth elements from solution by metal-oxides. *Environ. Sci. Technol.* **27**, 1796–1802.

Kurtz A. C., Derry L. A. and Chadwick O. A. (2001) Accretion of asian dust to Hawaiian soils: Isotopic, elemental, and mineral mass balances. *Geochim. Cosmochim. Acta* **65**, 1971–1983.

Land M., Ohlander B., Ingri J. and Thunberg J. (1999) Solid speciation and fractionation of rare earth elements in a spodosol profile from northern Sweden as revealed by sequential extraction. *Chem. Geol.* **160**, 121–138.

Laveuf C. and Cornu S. (2009) A review on the potentiality of Rare Earth Elements to trace pedogenetic processes. *Geoderma* **154**, 1–12.

Laveuf C., Cornu S. and Juillot F. (2008) Rare earth elements as tracers of pedogenetic processes. *C. R. Geosci.* **340**, 523–532.

Laveuf C., Cornu S., Guilherme L. R. G., Guerin A. and Juillot F. (2012) The impact of redox conditions on the rare earth element signature of redoximorphic features in a soil sequence developed from limestone. *Geoderma* **170**, 25–38.

Leybourne M. I. and Johannesson K. H. (2008) Rare earth elements (REE) and yttrium in stream waters, stream sediments, and Fe–Mn oxyhydroxides: Fractionation, speciation, and controls over REE plus Y patterns in the surface environment. *Geochim. Cosmochim. Acta* **72**, 5962–5983.

Liu X. and Byrne R. H. (1995) Comparative carbonate complexation of yttrium and gadolinium at 25 °C and 0.7 mol dm^{-3} ionic strength. *Mar. Chem.* **51**, 213–221.

Liu X. and Byrne R. H. (1997) Rare earth and yttrium phosphate solubilities in aqueous solution. *Geochim. Cosmochim. Acta* **61**, 1625–1633.

Marin-Spiotta E., Chadwick O. A., Kramer M. and Carbone M. S. (2011) Carbon delivery to deep mineral horizons in Hawaiian rain forest soils. *J. Geophys. Res. Biogeosci.* **116**.

Markai S., Andrès Y., Montavon G. and Grambow B. (2003) Study of the interaction between europium (III) and *Bacillus subtilis*: Fixation sites, biosorption modeling and reversibility. *J. Colloid Interface Sci.* **262**, 351–361.

McLennan S. M. (1994) Rare-Earth element geochemistry and the tetrad effect. *Geochim. Cosmochim. Acta* **58**, 2025–2033.

Mikutta R., Schaumann G. E., Gildemeister D., Bonneville S., Kramer M. G., Chorover J., Chadwick O. A. and Guggenberger G. (2009) Biogeochemistry of mineral-organic associations across a long-term mineralogical soil gradient (0.3–4100 kyr), Hawaiian Islands. *Geochim. Cosmochim. Acta* **73**, 2034–2060.

Mikutta R., Kaiser K., Dörr N., Vollmer A., Chadwick O. A., Chorover J., Kramer M. G. and Guggenberger G. (2010) Mineralogical impact on organic nitrogen across a long-term soil chronosequence (0.3–4100 kyr). *Geochim. Cosmochim. Acta* **74**, 2142–2164.

Minarik L., Zigova A., Bendl J., Skrivan P. and St'astny M. (1998) The behaviour of rare-earth elements and Y during the rock weathering and soil formation in the Ricany granite massif, Central Bohemia. *Sci. Total Environ.* **215**, 101–111.

Misono M., Ochiai E. I., Saito Y. and Yoneda Y. (1967) A new dual parameter scale for strength of Lewis acids and bases with evaluation of their softness. *J. Inorg. Nucl. Chem.* **29**, 2685–2691.

Mourier B., Poulenard J., Chauvel C., Faivre P. and Carcaillet C. (2008) Distinguishing subalpine soil types using extractible Al and Fe fractions and REE geochemistry. *Geoderma* **145**, 107–120.

Nance W. B. and Taylor S. R. (1976) Rare earth element patterns and crustal evolution: I. Australian post-Archean sedimentary rocks. *Geochim. Cosmochim. Acta* **40**, 1539–1551.

Nesbitt H. W. (1979) Mobility and fractionation of rare-earth elements during weathering of a granodiorite. *Nature* **279**, 206–210.

Nozaki Y., Zhang J. and Amakawa H. (1997) The fractionation between Y and Ho in the marine environment. *Earth Planet. Sci. Lett.* **148**, 329–340.

Öhlander B., Land M., Ingri J. and Widerlund A. (1996) Mobility of rare earth elements during weathering of till in northern Sweden. *Appl. Geochem.* **11**, 93–99.

Ohta A., Ishii S., Sakakibara M., Mizuno A. and Kawabe I. (1999) Systematic correlation of the Ce anomaly with the Co/(Ni + Cu) ratio and Y fractionation from Ho in distinct types of Pacific deep-sea nodules. *Geochem. J.* **33**, 399–417.

Ohta A. and Kawabe I. (2000) Theoretical study of tetrad effects observed in REE distribution coefficients between marine Fe–Mn deposit and deep seawater, and in REE(III)-carbonate complexation constants. *Geochem. J.* **34**, 455–473.

Ohta A. and Kawabe I. (2001) REE(III) adsorption onto Mn dioxide (d-MnO_2) and Fe oxyhydroxide: Ce(III) oxidation by d-MnO_2. *Geochim. Cosmochim. Acta* **65**, 695–703.

Ohta A., Kagi H., Nomura M., Tsuno H. and Kawabe I. (2009a) Coordination study of rare earth elements on Fe oxyhydroxide and Mn dioxides: Part I. Influence of a multi-electron excitation on EXAFS analyses of La, Pr, Nd, and Sm. *Am. Mineral.* **94**, 467–475.

Ohta A., Kagi H., Nomura M., Tsuno H. and Kawabe I. (2009b) Coordination study of rare earth elements on Fe oxyhydroxide and Mn dioxides: Part II. Correspondence of structural change to irregular variations of partitioning coefficients and tetrad effect variations appearing in interatomic distances. *Am. Mineral.* **94**, 476–486.

Pack A., Russell S. S., Shelley J. M. G. and van Zuilen M. (2007) Geo- and cosmochemistry of the twin elements yttrium and holmium. *Geochim. Cosmochim. Acta* **71**, 4592–4608.

Pearson R. G. (1968) Hard and soft acids and bases, HSAB, part 1: Fundamental principles. *J. Chem. Educ.* **45**, 581–587.

Peppard D. F., Mason G. W. and Lewey S. (1969) A tetrad effect in the liquid–liquid extraction ordering of lanthanides(III). *J. Inorg. Nucl. Chem.* **31**, 2271–2272.

Porder S., Hilley G. E. and Chadwick O. A. (2007) Chemical weathering, mass loss, and dust inputs across a climate by time matrix in the Hawaiian Islands. *Earth Planet. Sci. Lett.* **258**, 414–427.

Pourret O., Davranche M., Gruau G. and Dia A. (2007) Rare earth elements complexation with humic acid. *Chem. Geol.* **243**, 128–141.

Quinn K. A., Byrne R. H. and Schijf J. (2004) Comparative scavenging of yttrium and the rare earth elements in seawater: Competitive influences of solution and surface chemistry. *Aquat. Geochem.* **10**, 59–80.

Quinn K. A., Byrne R. H. and Schijf J. (2006a) Sorption of yttrium and rare earth elements by amorphous ferric hydroxide: Influence of pH and ionic strength. *Mar. Chem.* **99**, 128–150.

Quinn K. A., Byrne R. H. and Schijf J. (2006b) Sorption of yttrium and rare earth elements by amorphous ferric hydroxide: Influence of solution complexation with carbonate. *Geochim. Cosmochim. Acta* **70**, 4151–4165.

Rabung T., Stumpf T., Geckeis H., Klenze R. and Kim J. I. (2000) Sorption of Am(III) and Eu(III) onto gamma-alumina: Experiment and modelling. *Radiochim. Acta* **88**, 711–716.

Richens D. T. (1997) *Group 3 Elements: Scandium, Yttrium, the Lanthanides and Actinides, The Chemistry of Aqua Ions*. John Woley & Sons Ltd., New York.

Sako A., Mills A. J. and Roychoudhury A. N. (2009) Rare earth and trace element geochemistry of termite mounds in central and northeastern Namibia: Mechanisms for micro-nutrient accumulation. *Geoderma* **153**, 217–230.

Sanematsu K., Moriyama T., Sotouky L. and Watanabe Y. (2011) Mobility of rare earth elements in basalt-derived laterite at the Bolaven plateau, Southern Laos. *Res. Geol.* **61**, 140–158.

Schijf J. and Byrne R. H. (2001) Stability constants for mono- and dioxalato-complexes of Y and the REE, potentially important species in groundwaters and surface freshwaters. *Geochim. Cosmochim. Acta* **65**, 1037–1046.

Schijf J. and Marshall K. S. (2011) YREE sorption on hydrous ferric oxide in 0.5 M NaCl solutions: A model extension. *Mar. Chem.* **123**, 32–43.

Schijf J. and Zoll A. M. (2011) When dissolved is not truly dissolved—The importance of colloids in studies of metal sorption on organic matter. *J. Colloid Interface Sci.* **361**, 137–147.

Shoji S., Nanzyo M. and Dahlgren R. A. (1993) *Volcanic Ash Soils: Genesis, Properties and Utilization*. Elsevier, New York.

Sposito G. (1994) *Chemical Equilibria and Kinetics in Soils*. Oxford University Press, New York.

Steefel C. I. and Van Cappellen P. (1990) A new kinetic approach to modeling water-rock interaction: The role of nucleation, precursors, and ostwald ripening. *Geochim. Cosmochim. Acta* **54**, 2657–2677.

Stolpe B., Guo L. and Shiller A. M. (2013) Binding and transport of rare earth elements by organic and iron-rich nanocolloids in Alaskan rivers, as revealed by field-flow fractionation and ICP-MS. *Geochim. Cosmochim. Acta* **106**, 446–462.

Stumm W. and Wollast R. (1990) Coordination chemistry of weathering: Kinetics of the surface-controlled dissolution of oxide minerals. *Rev. Geophys.* **28**, 53–69.

Takahashi Y., Yoshida H., Sato N., Hama K., Yusa Y. and Shimizu H. (2002) W- and M-type tetrad effects in REE patterns for water-rock systems in the Tono uranium deposit, central Japan. *Chem. Geol.* **184**, 311–335.

Takahashi Y., Chatellier X., Hattori K. H., Kato K. and Fortin D. (2005) Adsorption of rare earth elements onto bacterial cell walls and its implication for REE sorption onto natural microbial mats. *Chem. Geol.* **219**, 53–67.

Taunton A. E., Welch S. A. and Banfield J. F. (2000) Geomicrobiological controls on light rare earth element, Y and Ba distributions during granite weathering and soil formation. *J. Alloys Compd.* **303**, 30–36.

Tematio P., Fritsch E., Hodson M. E., Lucas Y., Bitom D. and Bilong P. (2009) Mineral and geochemical characterization of a leptic aluandic soil and a thapto aluandic-ferralsol developed on trachytes in Mount Bambouto (Cameroon volcanic line). *Geoderma* **152**, 314–323.

Tertre E., Castet S., Berger G., Loubet M. and Giffaut E. (2006) Surface chemistry of kaolinite and Na-montmorillonite in aqueous electrolyte solutions at 25 and 60 degrees C: Experimental and modeling study. *Geochim. Cosmochim. Acta* **70**, 4579–4599.

Thompson A., Chadwick O. A., Boman S. and Chorover J. (2006a) Colloid mobilization during soil iron redox oscillations. *Environ. Sci. Technol.* **40**, 5743–5749.

Thompson A., Chadwick O. A., Rancourt D. G. and Chorover J. (2006b) Iron-oxide crystallinity increases during soil redox oscillations. *Geochim. Cosmochim. Acta* **70**, 1710–1727.

Thompson A., Rancourt D. G., Chadwick O. A. and Chorover J. (2011) Iron solid-phase differentiation along a redox gradient in basaltic soils. *Geochim. Cosmochim. Acta* **75**, 119–133.

Torn M. S., Trumbore S. E., Chadwick O. A., Vitousek P. M. and Hendricks D. M. (1997) Mineral control of soil organic carbon storage and turnover. *Nature* **389**, 170–173.

Tyler G. (2004) Rare earth elements in soil and plant systems – A review. *Plant Soil* **267**, 191–206.

Vitousek P. M. (2004) *Nutrient Cycling and Limitation: Hawai'i as a Model System*. Princeton Unversity Press, Princeton.

Vitousek P. M., Chadwick O. A., Crews T. E., Fownes J. H., Hendricks D. H. and Herbert D. (1997) Soil and ecosystem development across the Hawaiian islands. *GSA Today* **7**, 1–8.

Wieland E., Wehrli B. and Stumm W. (1988) The coordination chemistry of weathering: 3. A generalization on the dissolution rates of minerals. *Geochim. Cosmochim. Acta* **52**, 1969–1981.

Wilson K. and Walker J. (2010) *Principals and Techniques of Biochemistry and Molecular Biology*. Cambridge University Press, New York.

Wood S. A. (1993) The aqueous geochemistry of the rare earth elements: Critical stability-constants for complexes with simple carboxylic-acids at 25 degrees C and 1 Bar and their application to nuclear waste management. *Eng. Geol.* **34**, 229–259.

Yang W. and Parr R. G. (1985) Hardness, softness, and the fukui function in the electronic theory of metals and catalysis. *Proc. Natl. Acad. Sci.* **82**, 6723–6726.

Zhang Q. W., Lei T. W. and Zhao J. (2008) Estimation of the detachment rate in eroding rills in flume experiments using an REE tracing method. *Geoderma* **147**, 8–15.

Ziegler K., Chadwick O. A., Brzezinski M. A. and Kelly E. F. (2005) Natural variations of [delta]30Si ratios during progressive basalt weathering, Hawaiian Islands. *Geochim. Cosmochim. Acta* **69**, 4597–4610.

Zinder B., Furrer G. and Stumm W. (1986) The coordination chemistry of weathering: 2. Dissolution of Fe(III) oxides. *Geochim. Cosmochim. Acta* **50**, 1861–1869.

Associate editor: Robert H. Byrne

Electronic Annex for

"Fractionation of yttrium and holmium during basaltic soil weathering"

Geochimica et Cosmochimica Acta

Aaron Thompson[1], Oliver A. Chadwick[3] & Jon Chorover[4]

[1]Department of Crop and Soil Sciences, University of Georgia, Athens, Georgia 30602, USA. [2]Department of Geography, University of California, Santa Barbara, California, 93106, USA. [3]Department of Soil, Water & Environmental Science, University of Arizona, Tucson, Arizona, 85721, USA.

*Corresponding author E-mail: AaronT@uga.edu

Prepared: 18 May 2013

SECTION 1: FIGURES AND TABLES

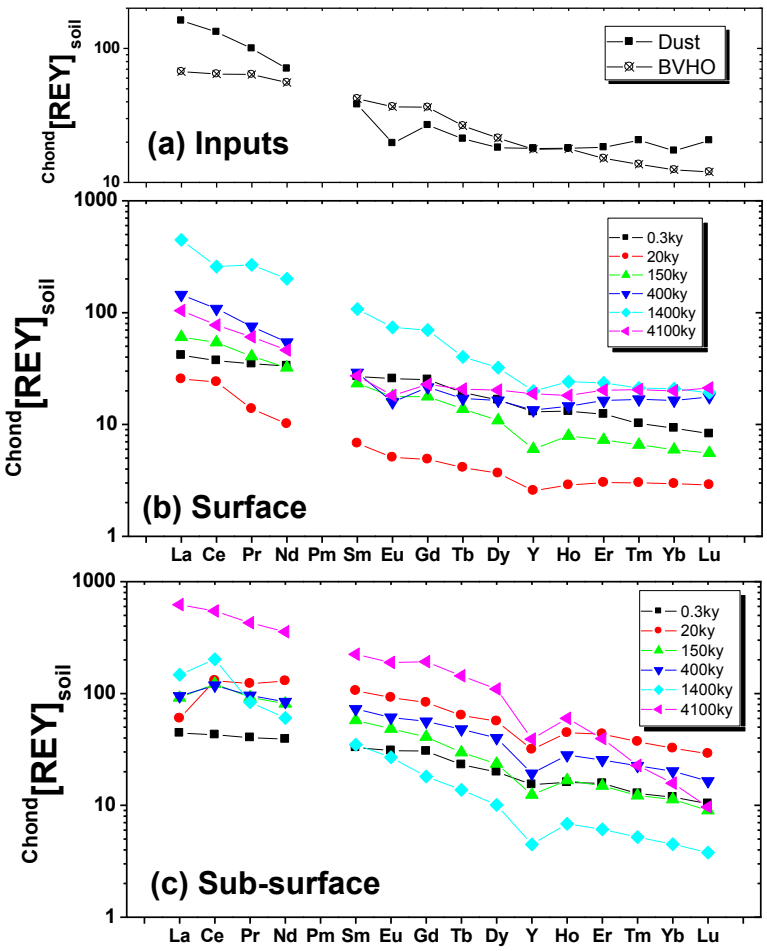

Figure EA-1: Chondrite normalized REY profiles for (a) Asian Dust and BVHO, and (b) the surface (c) and sub-surface transects across the Long Substrate Age Gradient (LSAG). Y has been inserted adjacent to Ho to facilitate comparison of these elements.

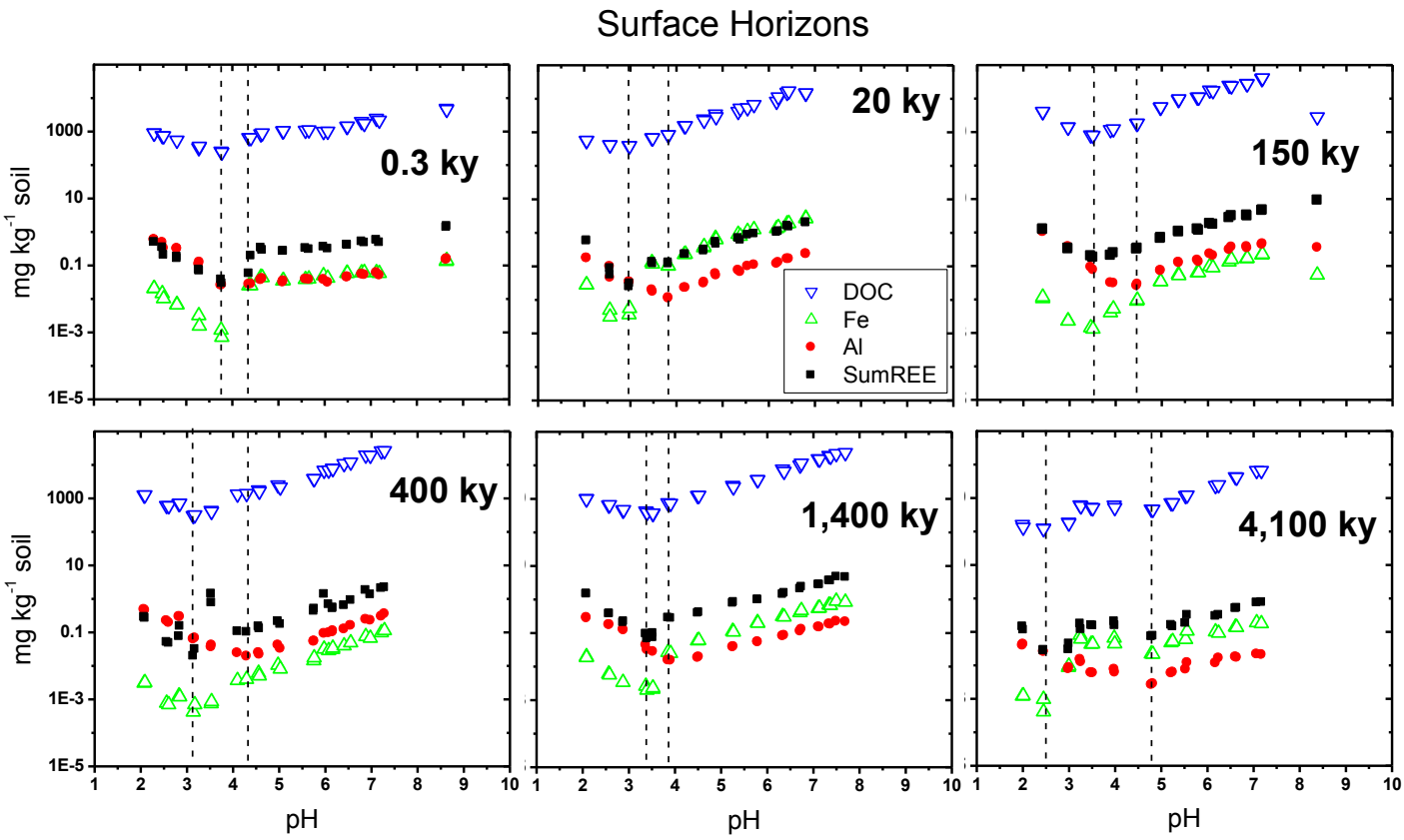

Figure EA-2: Mass of ΣREE (does not include Y) desorbed from the surface soil horizons during a 3 h incubation as a function of pH (see methods, Exp #1). The points of minimum dissolution (p.m.d.) are shown as vertical dashed lines for Al (higher pH) and Fe, organic carbon, and ΣREE (lower pH). Reported pH values are those at the end of the experiment. All measurements on < 0.045 μm solutions.

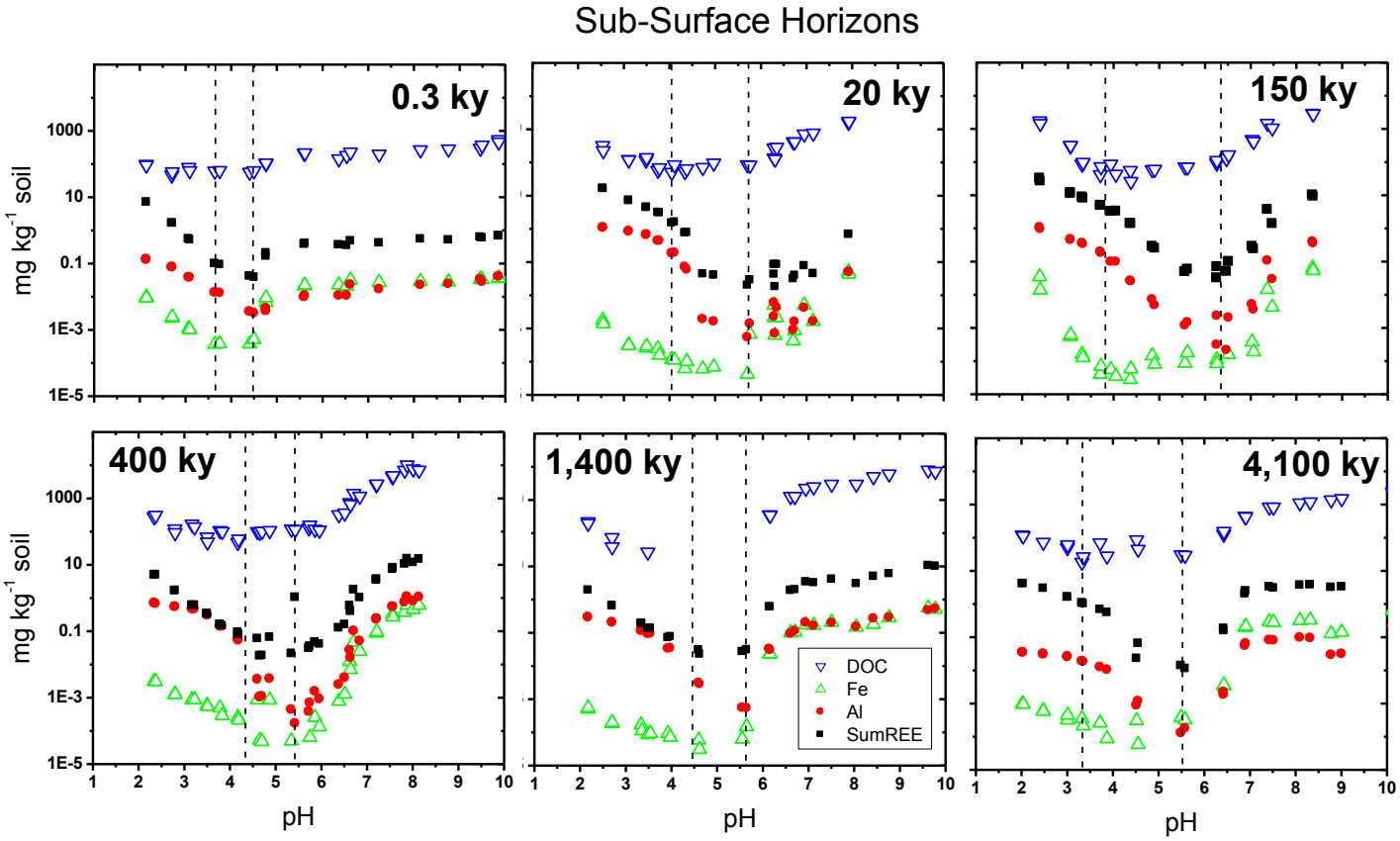

Figure EA-3: Mass of ΣREE (does not include Y) desorbed from the sub-surface soil horizons during a 3 hr incubation as a function of pH (see methods, Exp #1). The points of minimum dissolution (p.m.d.) are shown as vertical dashed lines for Al and ΣREE (higher pH) and Fe and organic carbon (lower pH). Reported pH values are those at the end of the experiment. All measurements on < 0.045 μm solutions.

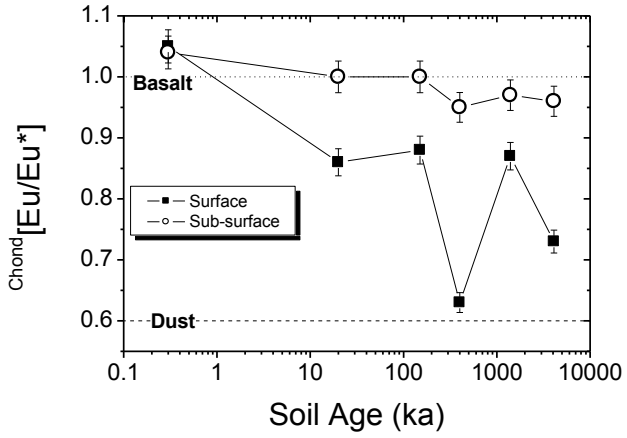

Figure EA-4: Chondrite-normalized Eu anomaly for the surface and sub-surface transect of the LSAG. The dotted and dashed lines are the values for Asian dust (Nance and Taylor, 1976) and Hawaiian basalt (USGS-BVHO-1), respectively. Errors bars are 2σ external error based on 4 measurements of a one soil during multiple analytical sessions.

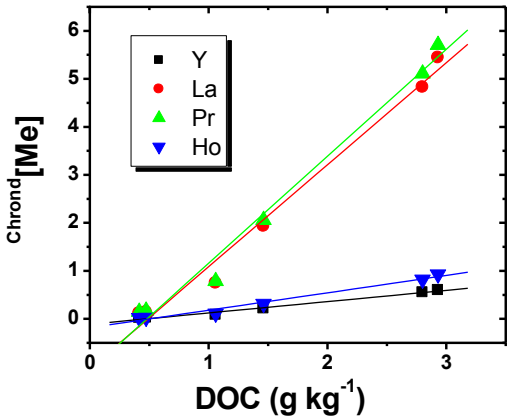

Figure EA-5: Correlation between aqueous concentrations of chrondrite normalized Y, La, Pr and Ho and DOC for the 150 ky subsurface soil at pH > Al p.m.d. (see Fig. 4). Note the slope of the regression lines is lower for Y (0.24 ± 0.01) and La (2.1 ± 0.1), than for Ho (0.36 ± 0.03) and Pr (2.2 ± 0.1), respectively. All errors are standard deviation of the linear regressions ($P < 0.0002$ in all cases). All measurements on < 0.045 μm solutions.

Table EA-1: Total elemental composition

Soil	Fe	Si	Al	Y	La	Ce	Pr	Nd	Sm	Eu	Gd	Tb	Dy	Ho	Er	Tm	Yb	Lu
SURFACE SOILS																		
OLAA 0.3 ky	7.95E+04	1.80E+05	5.50E+04	20.3	9.79	22.5	3.11	15.1	3.96	1.44	4.43	0.7	4.03	0.73	1.97	0.247	1.51	0.201
LAUPAHOEHOE 20 ky	1.50E+05	2.62E+04	1.21E+04	4	5.99	14.5	1.23	4.59	1	0.284	0.86	0.15	0.89	0.16	0.48	0.073	0.48	0.07
KOHALA 150 ky	2.28E+04	5.06E+04	3.78E+04	9.4	14.2	32.6	3.62	14.6	3.42	0.996	3.13	0.5	2.64	0.44	1.16	0.159	0.97	0.135
AMALU 350 ky	3.33E+04	1.69E+05	5.05E+04	21	33.9	65.3	6.72	24.6	4.28	0.887	3.79	0.62	3.98	0.81	2.6	0.407	2.67	0.428
MOLOKAI 1,400 ky	1.29E+05	1.27E+05	4.37E+04	31	105	156	23.8	90.8	15.8	4.14	12.3	1.46	7.83	1.34	3.74	0.513	3.39	0.468
KAUAI 4,100 ky	3.14E+05	5.23E+04	1.41E+04	29.4	24.5	46.7	5.4	20.9	4.01	1.02	4.02	0.75	4.92	1.01	3.23	0.495	3.25	0.514
SUBSURFACE SOILS																		
OLAA 0.3 ky	8.75E+04	2.26E+05	6.63E+04	24	10.4	25.8	3.6	17.7	4.83	1.73	5.37	0.84	4.83	0.89	2.5	0.309	1.93	0.252
LAUPAHOEHOE 20 ky	1.50E+05	2.83E+04	77974.6	49.3	14.1	78.6	10.9	58.6	15.6	5.16	14.6	2.32	13.7	2.47	6.91	0.898	5.27	0.705
KOHALA 150 ky	38305.2	1.18E+05	1.63E+05	19.4	21.5	73.5	8.23	36.7	8.49	2.71	7.21	1.08	5.72	0.93	2.37	0.296	1.84	0.219
AMALU 350 ky	9.93E+04	5.17E+04	1.06E+05	30.1	22.3	71.3	8.55	38.1	10.7	3.42	9.91	1.74	9.73	1.56	4.05	0.547	3.28	0.4
MOLOKAI 1,400 ky	7.97E+04	1.24E+05	1.73E+05	7	34.6	122	7.47	27.3	5.13	1.51	3.19	0.5	2.45	0.38	0.97	0.126	0.73	0.092
KAUAI 4,100 ky	2.87E+05	4.28E+04	1.02E+05	61	146	329	38.2	161	33	10.6	33.8	5.22	26.6	3.33	6.29	0.55	2.57	0.235
PARENT MATERAL STANDARDS																		
Chondrite-Cl				1.56	0.235	0.6032	0.0891	0.4524	0.1471	0.056	0.176	0.0363	0.2427	0.0556	0.1589	0.0242	0.1625	0.0243
Asian Dust				28	38	80	8.9	32	5.6	1.1	4.7	0.77	4.4	1	2.9	0.5	2.8	0.5
Hawaiian Basalt (BVHO-1)				27.6	15.8	39	5.7	25.2	6.2	2.06	6.4	0.96	5.2	0.99	2.4	0.33	2.02	0.291
HAWAII SOIL STANDARDS																		
Maui std 4-6a				18.4	31.0	58.5	6.24	22.2	3.95	0.852	3.08	0.52	3.05	0.64	2.05	0.313	2.02	0.331
Maui std 4-6b				18.6	32.1	60.6	6.51	23.3	3.89	0.874	3.09	0.53	3.16	0.65	2.11	0.329	2.07	0.345
Maui std 4-6c				17.16	27.79	50.96	5.77	20.38	3.51	0.77	2.96	0.48	2.99	0.63	2.00	0.31	1.89	0.30
Maui std 4-6d				16.76	27.51	50.26	5.66	20.35	3.44	0.76	2.91	0.47	2.93	0.63	1.97	0.32	1.87	0.30
Average (Maui 4-6)				17.7	29.6	55.1	6.0	21.6	3.7	0.8	3.0	0.5	3.0	0.6	2.0	0.3	2.0	0.3
Stdev (Maui 4-6)				0.9	2.3	5.3	0.4	1.4	0.3	0.1	0.1	0.0	0.1	0.0	0.1	0.0	0.1	0.0
% Stdev (Maui 4-6)				5%	8%	10%	7%	7%	7%	7%	3%	6%	3%	2%	3%	2%	5%	8%
Maui Std 3-2a				25.6	37.6	82.9	9.47	37.7	8.99	2.93	8.23	1.41	6.99	1.15	2.96	0.376	2.24	0.315
Maui Std 3-2b				26.3	38.9	86.0	9.74	39.0	9.36	3.05	8.76	1.45	7.18	1.17	3.07	0.380	2.24	0.321
Average (Maui 3-2)				26.0	38.2	84.5	9.6	38.3	9.2	3.0	8.5	1.4	7.1	1.2	3.0	0.4	2.2	0.3
Stdev (Maui 3-2)				0.5	1.0	2.2	0.2	0.9	0.3	0.1	0.4	0.0	0.1	0.0	0.1	0.0	0.0	0.0
% Stdev (Maui 3-2)				2%	2%	3%	2%	2%	3%	3%	4%	2%	2%	1%	3%	1%	0%	1%

All values are in mg kg^{-1} soil.

b.d., below detection

Parent Material standards from: (a) Chondrite-Cl (Anders & Grevesse, 1989); (b) Asian Dust (Nance & Taylor, 1976); (c) BVHO-1, (Gladney & Roelandts, 1988)

Table EA-2: Chondrite normalized elemental ratios

Soil	Y/Ho	La/Pr	Eu/Eu*	Gd/Gd*	Lu/Yb
SURFACE SOILS					
OLAA 0.3 ky	0.991 (±0.071)	1.194 (±0.035)	1.054 (±0.027)	1.154 (±0.083)	0.890 (±0.050)
LAUPAHOEHOE 20 ky	0.891 (±0.064)	1.846 (±0.053)	0.857 (±0.022)	0.975 (±0.070)	0.975 (±0.055)
KOHALA 150 ky	0.761 (±0.055)	1.487 (±0.043)	0.884 (±0.023)	1.052 (±0.076)	0.931 (±0.053)
AMALU 350 ky	0.924 (±0.066)	1.913 (±0.055)	0.630 (±0.016)	1.023 (±0.074)	1.072 (±0.061)
MOLOKAI 1,400 ky	0.825 (±0.059)	1.673 (±0.048)	0.867 (±0.022)	1.120 (±0.081)	0.923 (±0.052)
KAUAI 4,100 ky	1.037 (±0.074)	1.720 (±0.050)	0.726 (±0.019)	1.000 (±0.072)	1.058 (±0.060)
SUBSURFACE SOILS					
OLAA 0.3 ky	0.961 (±0.068)	1.095 (±0.032)	1.042 (±0.027)	1.158 (±0.084)	0.873 (±0.049)
LAUPAHOEHOE 20 ky	0.711 (±0.051)	0.490 (±0.014)	1.000 (±0.026)	1.066 (±0.077)	0.895 (±0.051)
KOHALA 150 ky	0.743 (±0.053)	0.990 (±0.029)	0.998 (±0.026)	1.051 (±0.076)	0.796 (±0.045)
AMALU 350 ky	0.688 (±0.049)	0.989 (±0.029)	0.946 (±0.025)	1.003 (±0.072)	0.816 (±0.046)
MOLOKAI 1,400 ky	0.657 (±0.047)	1.756 (±0.051)	0.966 (±0.025)	0.874 (±0.063)	0.843 (±0.048)
KAUAI 4,100 ky	0.653 (±0.047)	1.449 (±0.042)	0.957 (±0.025)	1.127 (±0.081)	0.611 (±0.035)
PARENT MATERIALS					
Dust	0.998	1.619	0.604	0.997	1.194
BVHO	0.994	1.051	0.995	1.150	0.963
HAWAII SOIL STANDARDS					
Maui std 4-6a	1.03	1.88	0.67	0.95	1.10
Maui std 4-6b	1.01	1.87	0.69	0.95	1.12
Maui std 4-6c	0.98	1.82	0.68	1.01	1.06
Maui std 4-6d	0.95	1.84	0.68	1.01	1.05
Average (Maui 4-6)	**0.993**	**1.855**	**0.680**	**0.979**	**1.082**
Stdev (Maui 4-6)	**0.036**	**0.027**	**0.009**	**0.035**	**0.031**
% Stdev (Maui 4-6)	**3.6%**	**1.4%**	**1.3%**	**3.6%**	**2.8%**
Maui Std 3-2a	0.792	1.504	0.974	1.015	0.939
Maui Std 3-2b	0.798	1.514	0.976	1.041	0.958
Average (Maui 3-2)	**0.795**	**1.509**	**0.975**	**1.028**	**0.948**
Stdev (Maui 3-2)	**0.004**	**0.007**	**0.001**	**0.019**	**0.013**
% Stdev (Maui 3-2)	**0.5%**	**0.5%**	**0.1%**	**1.8%**	**1.4%**

All values are in mg kg^{-1} soil.

All errors are 2 standard deviations based on multiple measurements of the % stdev for the Maui 4-6 standard (see above)

Table EA-3: 0.3 ky Olaa surface horizon

pH	DOC	Fe	Si	Al	Y	La	Ce	Pr	Nd	Sm	Eu	Gd	Tb	Dy	Ho	Er	Tm	Yb	Lu	Soln:soil
2.30	736.82	2.53E+01	2.70E+00	1.13E+03	1.59E-02	9.90E-03	1.28E-02	1.36E-03	5.23E-03	9.98E-04	2.43E-04	1.29E-03	1.83E-04	1.05E-03	2.06E-04	5.44E-04	5.33E-05	3.00E-04	4.00E-05	101.9
2.30	722.67	2.56E+01	3.24E+00	1.13E+03	1.57E-02	9.75E-03	1.28E-02	1.38E-03	5.16E-03	1.01E-03	2.43E-04	1.26E-03	1.89E-04	1.04E-03	2.12E-04	5.08E-04	5.92E-05	2.89E-04	4.00E-05	102.2
2.48	604.95	1.77E+01	4.45E+00	9.26E+02	1.04E-02	6.64E-03	8.89E-03	9.94E-04	3.79E-03	6.92E-04	1.84E-04	8.36E-04	1.15E-04	7.20E-04	1.46E-04	3.35E-04	3.55E-05	2.14E-04	2.86E-05	102.8
2.51	600.78	1.24E+01	3.56E+00	6.28E+02	6.40E-03	3.96E-03	5.13E-03	5.82E-04	2.21E-03	4.52E-04	1.05E-04	5.22E-04	7.91E-05	4.18E-04	9.09E-05	2.03E-04	2.37E-05	1.39E-04	1.71E-05	102.8
2.80	444.01	8.10E+00	7.17E+00	6.05E+02	5.53E-03	3.11E-03	4.53E-03	5.46E-04	2.14E-03	4.06E-04	1.12E-04	5.51E-04	7.29E-05	4.06E-04	8.49E-05	2.09E-04	2.37E-05	1.39E-04	1.71E-05	103.1
2.80	440.26	8.35E+00	9.25E+00	6.05E+02	4.69E-03	2.77E-03	4.16E-03	4.68E-04	1.83E-03	3.52E-04	1.05E-04	4.33E-04	6.07E-05	3.45E-04	7.28E-05	1.73E-04	1.78E-05	1.04E-04	1.71E-05	103.3
3.29	291.65	1.91E+00	1.16E+01	2.39E+02	1.69E-03	1.44E-03	1.60E-03	1.85E-04	7.83E-04	1.46E-04	4.61E-05	1.70E-04	3.03E-05	1.35E-04	3.03E-05	7.77E-05	1.18E-05	4.62E-05	5.72E-06	102.8
3.27	261.01	3.91E+00	1.25E+01	2.10E+02	2.02E-03	1.09E-03	1.92E-03	2.41E-04	9.50E-04	2.00E-04	5.92E-05	2.00E-04	3.01E-05	1.91E-04	3.03E-05	8.97E-05	1.18E-05	5.78E-05	5.72E-06	102.9
5.98	815.84	6.15E+01	4.80E+01	7.28E+01	8.56E-03	4.04E-03	8.96E-03	1.20E-03	5.11E-03	1.14E-03	3.36E-04	1.18E-03	1.83E-04	1.06E-03	1.82E-04	4.72E-04	6.51E-05	3.41E-04	4.57E-05	102.2
6.07	818.75	5.10E+01	5.96E+01	5.97E+01	7.32E-03	3.46E-03	7.81E-03	1.02E-03	4.45E-03	1.02E-03	2.96E-04	1.03E-03	1.65E-04	9.29E-04	1.58E-04	4.01E-04	5.33E-05	2.89E-04	4.00E-05	102.9
8.65	3669.97	1.74E+02	3.76E+02	2.99E+02	2.99E-02	1.72E-02	3.44E-02	5.06E-03	2.24E-02	5.31E-03	1.55E-03	5.21E-03	7.26E-04	4.15E-03	7.03E-04	1.66E-03	2.19E-04	1.17E-03	1.66E-04	103.2
8.64	3944.72	1.63E+02	4.70E+02	2.88E+02	2.87E-02	1.62E-02	3.25E-02	4.75E-03	2.12E-02	4.83E-03	1.43E-03	4.72E-03	6.65E-04	3.70E-03	6.31E-04	1.64E-03	2.01E-04	1.15E-03	1.54E-04	102.8
4.40	525.77	3.06E+01	1.62E+01	5.35E+01	5.47E-03	2.51E-03	4.91E-03	5.82E-04	2.57E-03	5.05E-04	1.65E-04	5.99E-04	9.72E-05	6.15E-04	1.21E-04	3.05E-04	3.55E-05	2.08E-04	2.29E-05	102.2
4.36	519.19	3.00E+01	2.13E+01	5.16E+01	1.57E-03	5.90E-04	1.27E-03	1.85E-04	8.67E-04	2.00E-04	6.58E-05	1.98E-04	3.03E-05	1.91E-04	3.64E-05	9.57E-05	1.18E-05	7.51E-05	1.14E-05	104.1
4.62	685.95	5.53E+01	4.46E+00	7.14E+01	8.33E-03	3.97E-03	8.01E-03	1.15E-03	4.77E-03	1.13E-03	3.03E-04	1.11E-03	1.76E-04	1.02E-03	1.94E-04	4.60E-04	5.92E-05	3.58E-04	4.57E-05	102.1
4.65	728.42	5.34E+01	6.96E+00	7.79E+01	8.44E-03	3.85E-03	7.17E-03	9.23E-04	3.58E-03	7.98E-04	2.30E-04	9.49E-04	1.46E-04	9.11E-04	1.70E-04	4.36E-04	5.33E-05	3.12E-04	4.00E-05	102.3
5.09	833.40	4.25E+01	1.48E+00	6.06E+01	6.18E-03	2.91E-03	6.58E-03	8.59E-04	3.84E-03	7.78E-04	2.70E-04	8.99E-04	1.27E-04	7.88E-04	1.39E-04	3.59E-04	4.14E-05	2.77E-04	3.43E-05	102.3
5.11	859.21	4.39E+01	1.50E+00	6.65E+01	6.46E-03	3.04E-03	6.62E-03	9.01E-04	4.01E-03	8.51E-04	2.63E-04	8.83E-04	1.34E-04	7.94E-04	1.39E-04	3.47E-04	5.33E-05	2.83E-04	4.00E-05	102.3
5.66	899.18	4.88E+01	8.20E+00	7.25E+01	7.16E-03	3.39E-03	7.41E-03	1.05E-03	4.33E-03	1.01E-03	2.83E-04	1.03E-03	1.58E-04	8.86E-04	1.64E-04	4.30E-04	5.33E-05	2.83E-04	4.00E-05	102.3
5.58	877.53	4.72E+01	9.72E+00	7.45E+01	7.42E-03	3.59E-03	8.10E-03	1.08E-03	4.92E-03	9.71E-04	3.09E-04	1.12E-03	1.64E-04	9.17E-04	1.64E-04	4.13E-04	5.33E-05	3.12E-04	4.00E-05	102.1
6.48	1138.96	7.28E+01	2.84E+01	8.53E+01	9.45E-03	4.74E-03	1.01E-02	1.37E-03	5.92E-03	1.40E-03	3.55E-04	1.36E-03	1.94E-04	1.18E-03	2.06E-04	5.32E-04	7.10E-05	3.81E-04	5.72E-05	102.4
6.49	1179.75	7.20E+01	2.86E+01	8.76E+01	9.35E-03	4.60E-03	9.98E-03	1.38E-03	5.56E-03	1.42E-03	3.75E-04	1.39E-03	2.01E-04	1.24E-03	2.18E-04	5.44E-04	7.10E-05	4.05E-04	5.14E-05	102.0
6.80	1606.03	7.41E+01	4.73E+01	1.06E+02	1.15E-02	6.06E-03	1.26E-02	1.75E-03	7.65E-03	1.73E-03	5.26E-04	1.69E-03	2.74E-04	1.38E-03	2.49E-04	7.00E-04	8.29E-05	4.91E-04	6.29E-05	102.2
6.86	1412.04	7.64E+01	4.18E+01	1.01E+02	1.10E-02	5.59E-03	1.20E-02	1.58E-03	6.84E-03	1.56E-03	4.47E-04	1.71E-03	2.31E-04	1.32E-03	2.30E-04	5.68E-04	7.70E-05	4.39E-04	5.14E-05	102.0
7.12	2001.50	7.55E+01	5.92E+01	1.16E+02	1.22E-02	6.65E-03	1.38E-02	1.97E-03	8.42E-03	1.90E-03	5.46E-04	2.04E-03	2.79E-04	1.53E-03	2.79E-04	6.82E-04	8.88E-05	4.68E-04	6.86E-05	102.3
7.19	1763.38	7.14E+01	5.41E+02	9.85E+01	1.06E-02	5.63E-03	1.19E-02	1.60E-03	7.11E-03	1.66E-03	4.54E-04	1.54E-03	2.43E-04	1.35E-03	2.36E-04	6.04E-04	7.70E-05	4.45E-04	5.14E-05	102.4
3.77	196.40	8.87E-01	4.57E+02	5.06E+01	8.10E-04	3.67E-04	7.35E-04	1.06E-04	4.09E-04	7.98E-05	2.63E-05	8.73E-05	1.20E-05	8.62E-05	1.82E-05	3.59E-05	5.92E-06	2.89E-05	b.d.	101.7
3.76	209.31	1.45E+00	4.30E+02	4.93E+01	9.11E-04	4.68E-04	9.42E-04	1.21E-04	6.03E-04	1.13E-04	2.63E-05	9.99E-05	1.80E-05	8.62E-05	2.43E-05	4.78E-05	5.92E-06	3.47E-05	b.d.	101.8

All values are in µmol L^{-1} soln, except pH (-log mol L^{-1}) and Soln:Soil, which is the mass ratio of suspension to soil.
b.d., below detection

Table EA-4: 20 ky Laupahoehoe surface horizon

pH	DOC	Fe	Si	Al	Y	La	Ce	Pr	Nd	Sm	Eu	Gd	Tb	Dy	Ho	Er	Tm	Yb	Lu	Soln:soil
2.05	443.34	3.35E+01	4.25E+00	3.32E+02	8.32E-03	9.28E-03	1.84E-02	1.31E-03	4.76E-03	1.02E-03	3.16E-04	1.12E-03	2.15E-04	1.27E-03	2.06E-04	4.30E-04	5.33E-05	2.83E-04	2.86E-05	105.7
2.05	447.76	3.35E+01	4.29E+00	3.28E+02	8.54E-03	9.52E-03	1.89E-02	1.35E-03	4.82E-03	9.64E-04	3.69E-04	1.17E-03	2.20E-04	1.27E-03	2.12E-04	4.60E-04	5.33E-05	2.77E-04	2.86E-05	105.9
2.56	331.03	5.93E+00	1.63E+00	1.85E+02	1.33E-03	1.37E-03	2.76E-03	2.20E-04	7.83E-04	1.46E-04	5.92E-05	1.56E-04	3.05E-05	1.78E-04	3.03E-05	6.58E-05	5.92E-06	4.05E-05	5.72E-06	106.0
2.56	326.70	3.73E+00	1.24E+00	8.62E+01	9.00E-04	9.29E-04	1.75E-03	1.42E-04	4.78E-04	9.98E-05	3.29E-05	1.07E-04	1.83E-05	1.05E-04	2.43E-05	3.59E-05	5.92E-06	2.89E-05	5.72E-06	105.4
2.97	309.88	4.30E+00	1.07E+00	6.41E+01	2.92E-04	3.67E-04	7.07E-04	5.68E-05	2.43E-04	5.99E-05	1.97E-05	5.71E-05	1.22E-05	6.15E-05	1.21E-05	1.79E-05	5.92E-06	1.73E-05	b.d	105.6
2.98	312.05	6.67E+00	1.25E+00	6.35E+01	3.37E-04	4.25E-04	9.42E-04	8.52E-05	3.40E-04	6.65E-05	1.97E-05	5.48E-05	1.21E-05	5.54E-05	1.21E-05	1.79E-05	5.92E-06	1.16E-05	b.d	106.0
3.47	531.10	1.57E+02	1.30E+00	3.70E+01	9.90E-04	1.22E-03	4.72E-03	3.41E-04	1.48E-03	3.46E-04	1.18E-04	2.96E-04	5.46E-05	2.71E-04	3.64E-05	9.57E-05	1.18E-05	5.78E-05	5.72E-06	105.4
3.48	536.34	1.41E+02	9.18E-01	3.26E+01	8.89E-04	1.12E-03	4.05E-03	3.12E-04	1.36E-03	3.59E-04	1.18E-04	2.71E-04	4.85E-05	2.22E-04	4.24E-05	7.77E-05	1.18E-05	5.20E-05	5.72E-06	105.3
4.19	1228.04	2.78E+02	4.81E+00	4.33E+01	1.64E-03	1.73E-03	8.17E-03	5.89E-04	2.59E-03	6.45E-04	2.50E-04	5.46E-04	8.53E-05	4.31E-04	6.06E-05	1.38E-04	1.78E-05	9.82E-05	1.14E-05	105.4
4.18	1236.37	2.69E+02	4.86E+00	4.30E+01	1.60E-03	1.83E-03	8.11E-03	5.89E-04	2.49E-03	6.92E-04	2.17E-04	5.46E-04	9.80E-05	4.55E-04	6.06E-05	1.49E-04	1.78E-05	9.82E-05	1.14E-05	105.3
4.85	2727.50	8.26E+02	1.14E+01	1.13E+02	3.42E-03	4.24E-03	1.90E-02	1.38E-03	5.78E-03	1.58E-03	5.59E-04	1.25E-03	1.94E-04	9.78E-04	1.39E-04	3.05E-04	4.14E-05	2.31E-04	2.86E-05	105.4
4.86	2263.76	7.45E+02	1.14E+01	9.98E+01	2.79E-03	3.51E-03	1.64E-02	1.16E-03	4.97E-03	1.40E-03	4.15E-04	1.18E-03	1.70E-04	8.49E-04	1.39E-04	2.99E-04	3.55E-05	2.02E-04	2.86E-05	105.7
5.54	4127.88	1.29E+03	1.68E+01	1.84E+02	5.71E-03	7.54E-03	3.03E-02	2.20E-03	9.03E-03	2.46E-03	7.96E-04	1.81E-03	3.48E-04	1.50E-03	2.18E-04	4.60E-04	5.92E-05	3.87E-04	4.00E-05	107.9
5.68	5060.36	1.45E+03	1.70E+01	1.99E+02	5.71E-03	7.57E-03	3.25E-02	2.30E-03	1.01E-02	2.61E-03	8.55E-04	2.00E-03	3.59E-04	1.67E-03	2.55E-04	5.14E-04	6.51E-05	3.35E-04	5.14E-05	109.1
3.82	669.64	1.22E+02	4.35E+00	2.09E+01	8.77E-04	9.43E-04	4.10E-03	3.12E-04	1.38E-03	3.86E-04	1.18E-04	2.94E-04	4.87E-05	2.34E-04	3.64E-05	7.77E-05	5.92E-06	5.78E-05	5.72E-06	105.4
3.82	659.40	1.25E+02	4.59E+00	2.18E+01	9.45E-04	1.18E-03	4.40E-03	3.48E-04	1.45E-03	3.39E-04	1.51E-04	3.53E-04	4.86E-05	2.65E-04	3.64E-05	7.77E-05	1.18E-05	5.78E-05	5.72E-06	105.3
4.59	1951.54	4.37E+02	8.31E+00	5.82E+01	2.02E-03	2.30E-03	1.03E-02	7.59E-04	3.07E-03	8.91E-04	2.96E-04	7.40E-04	1.09E-04	5.91E-04	8.49E-05	1.61E-04	2.37E-05	1.16E-04	1.71E-05	105.2
4.60	1774.21	4.70E+02	7.97E+00	6.33E+01	2.11E-03	2.51E-03	1.12E-02	8.23E-04	3.42E-03	1.04E-03	3.42E-04	7.77E-04	1.34E-04	6.28E-04	9.70E-05	2.09E-04	2.37E-05	1.21E-04	2.29E-05	105.3
5.34	3301.97	1.09E+03	1.56E+01	1.44E+02	4.25E-03	5.72E-03	2.46E-02	1.72E-03	7.49E-03	2.00E-03	6.71E-04	1.74E-03	2.86E-04	1.31E-03	2.00E-04	3.83E-04	5.33E-05	3.12E-04	4.57E-05	105.4
5.38	4102.91	9.50E+02	1.36E+01	1.27E+02	3.91E-03	4.96E-03	2.17E-02	1.55E-03	6.32E-03	1.73E-03	5.86E-04	1.22E-03	2.37E-04	1.13E-03	1.58E-04	3.23E-04	5.33E-05	3.47E-04	3.43E-05	105.6
6.17	6596.45	1.60E+03	1.78E+01	2.24E+02	6.29E-03	8.91E-03	3.74E-02	2.63E-03	1.09E-02	2.91E-03	9.15E-04	2.44E-03	3.77E-04	1.83E-03	2.61E-04	5.68E-04	7.70E-05	4.05E-04	5.14E-05	105.6
6.21	8891.85	1.73E+03	1.94E+01	2.46E+02	6.68E-03	9.58E-03	4.01E-02	2.83E-03	1.16E-02	3.23E-03	1.03E-03	2.52E-03	4.33E-04	2.08E-03	2.79E-04	6.16E-04	8.29E-05	4.57E-04	5.72E-05	105.3
6.40	12122.22	2.20E+03	2.09E+01	3.12E+02	8.41E-03	1.56E-02	5.85E-02	4.26E-03	1.70E-02	4.06E-03	1.41E-03	3.17E-03	5.24E-04	2.67E-03	3.64E-04	7.41E-04	9.47E-05	5.61E-04	6.29E-05	106.0
6.43	13371.08	2.27E+03	2.14E+01	3.16E+02	8.77E-03	1.31E-02	5.23E-02	3.64E-03	1.61E-02	4.03E-03	1.43E-03	3.39E-03	5.35E-04	2.71E-03	4.00E-04	7.53E-04	8.88E-05	5.66E-04	6.29E-05	105.5
6.80	11689.28	3.14E+03	3.03E+01	4.35E+02	1.20E-02	1.75E-02	7.10E-02	5.03E-03	2.16E-02	5.67E-03	2.16E-03	4.70E-03	7.15E-04	3.52E-03	5.52E-04	1.07E-03	1.36E-04	7.86E-04	9.14E-05	105.6
6.80	11347.93	3.32E+03	3.12E+01	4.45E+02	1.23E-02	1.80E-02	7.44E-02	5.22E-03	2.20E-02	5.67E-03	1.95E-03	4.67E-03	7.48E-04	3.66E-03	5.46E-04	1.11E-03	1.42E-04	7.74E-04	9.72E-05	105.2

All values are in μmol L^{-1} soln, except pH (-log mol L^{-1}) and Soln:Soil, which is the mass ratio of suspension to soil.
b.d., below detection

Table EA-5: 150 ky Kohala surface horizon

pH	DOC	Fe	Si	Al	Y	La	Ce	Pr	Nd	Sm	Eu	Gd	Tb	Dy	Ho	Er	Tm	Yb	Lu	Soln:soil
2.42	3198	1.28E+01	6.64E+00	1.96E+03	1.36E-02	1.45E-02	3.42E-02	3.95E-03	1.55E-02	3.59E-03	1.17E-03	3.51E-03	5.41E-04	2.71E-03	4.00E-04	9.15E-04	1.07E-04	5.32E-04	6.86E-05	104.8
2.42	3274	1.41E+01	7.74E+00	2.01E+03	1.42E-02	1.49E-02	3.51E-02	4.09E-03	1.64E-02	3.75E-03	1.20E-03	3.71E-03	5.42E-04	2.84E-03	4.24E-04	9.03E-04	1.01E-04	5.72E-04	6.86E-05	104.8
2.97	1116	2.74E+00	5.88E+00	7.03E+02	3.88E-03	3.73E-03	9.50E-03	1.11E-03	4.37E-03	1.05E-03	3.49E-04	9.89E-04	1.33E-04	7.26E-04	1.15E-04	2.63E-04	2.96E-05	1.73E-04	2.29E-05	103.7
2.97	1120	2.76E+00	3.96E+00	7.14E+02	3.72E-03	3.48E-03	8.91E-03	1.09E-03	4.30E-03	1.18E-03	3.42E-04	9.36E-04	1.33E-04	7.20E-04	1.15E-04	2.51E-04	2.96E-05	1.62E-04	1.71E-05	104.1
3.46	639	1.72E+00	5.35E+00	1.71E+02	2.37E-03	1.92E-03	5.40E-03	7.10E-04	2.65E-03	6.98E-04	2.11E-04	6.35E-04	9.06E-05	5.48E-04	7.28E-05	1.49E-04	1.78E-05	9.82E-05	1.14E-05	105.5
3.51	632	1.59E+00	5.66E+00	1.44E+02	2.04E-03	1.78E-03	4.82E-03	6.60E-04	2.63E-03	6.32E-04	1.97E-04	5.16E-04	7.80E-05	4.31E-04	7.28E-05	1.61E-04	1.78E-05	1.10E-04	1.14E-05	103.9
4.46	1421	1.08E+01	6.54E+00	4.78E+01	3.01E-03	2.76E-03	8.44E-03	1.12E-03	4.73E-03	1.14E-03	3.62E-04	1.07E-03	1.52E-04	7.69E-04	1.09E-04	2.45E-04	2.96E-05	1.73E-04	2.29E-05	104.9
4.47	1462	1.16E+01	7.22E+00	5.43E+01	3.41E-03	3.00E-03	9.16E-03	1.19E-03	4.94E-03	1.22E-03	3.82E-04	1.10E-03	1.70E-04	8.49E-04	1.27E-04	2.57E-04	2.96E-05	1.91E-04	2.29E-05	104.2
5.36	7471	6.84E+01	2.05E+01	2.47E+02	9.71E-03	9.29E-03	2.89E-02	3.71E-03	1.59E-02	4.11E-03	1.26E-03	3.69E-03	5.46E-04	2.80E-03	4.06E-04	8.01E-04	1.07E-04	5.66E-04	7.43E-05	103.6
5.37	7822	6.27E+01	1.86E+01	2.35E+02	9.21E-03	9.16E-03	2.78E-02	3.60E-03	1.47E-02	3.80E-03	1.26E-03	3.51E-03	5.48E-04	2.66E-03	3.88E-04	8.07E-04	9.47E-05	4.80E-04	6.29E-05	104.1
6.11	13662	1.07E+02	3.59E+01	3.90E+02	1.55E-02	1.49E-02	4.62E-02	6.13E-03	2.60E-02	6.97E-03	2.14E-03	5.62E-03	9.41E-04	4.61E-03	6.97E-04	1.32E-03	1.60E-04	8.84E-04	1.03E-04	103.6
6.04	14312	1.17E+02	3.50E+01	4.36E+02	1.59E-02	1.58E-02	4.92E-02	6.32E-03	2.70E-02	7.39E-03	2.31E-03	6.12E-03	9.68E-04	4.84E-03	6.79E-04	1.46E-03	1.66E-04	9.01E-04	1.09E-04	103.7
6.84	22421	2.01E+02	6.87E+01	7.16E+02	2.81E-02	2.81E-02	8.65E-02	1.10E-02	4.88E-02	1.29E-02	4.18E-03	1.10E-02	1.73E-03	8.71E-03	1.21E-03	2.58E-03	2.90E-04	1.54E-03	1.94E-04	103.8
6.85	21847	2.08E+02	6.61E+01	6.58E+02	2.68E-02	2.75E-02	8.09E-02	1.07E-02	4.65E-02	1.25E-02	4.01E-03	1.04E-02	1.66E-03	8.29E-03	1.19E-03	2.53E-03	2.78E-04	1.57E-03	1.77E-04	103.7
3.89	934	4.84E+00	1.56E+00	5.94E+01	2.33E-03	2.20E-03	5.32E-03	6.88E-04	3.04E-03	6.98E-04	2.17E-04	6.37E-04	9.12E-05	4.68E-04	7.88E-05	1.55E-04	1.78E-05	1.27E-04	1.71E-05	104.6
3.95	992	6.36E+00	1.49E+00	5.79E+01	2.53E-03	2.97E-03	6.39E-03	8.45E-04	3.47E-03	7.71E-04	2.43E-04	6.55E-04	1.03E-04	5.35E-04	9.09E-05	1.91E-04	1.78E-05	1.21E-04	1.71E-05	103.9
4.97	4349	4.20E+01	1.45E+01	1.36E+02	5.97E-03	5.88E-03	1.79E-02	2.36E-03	9.67E-03	2.65E-03	8.09E-04	2.02E-03	3.59E-04	1.71E-03	2.49E-04	5.44E-04	6.51E-05	3.29E-04	4.57E-05	103.7
4.98	4530	4.15E+01	1.48E+01	1.41E+02	6.28E-03	6.29E-03	1.90E-02	2.43E-03	1.01E-02	2.73E-03	8.09E-04	2.38E-03	3.46E-04	1.72E-03	2.61E-04	4.42E-04	7.10E-05	3.81E-04	5.14E-05	103.5
5.80	8700	7.73E+01	2.61E+01	2.53E+02	1.02E-02	1.04E-02	3.08E-02	3.83E-03	1.72E-02	4.51E-03	1.45E-03	3.80E-03	5.81E-04	3.03E-03	4.12E-04	9.92E-04	1.01E-04	5.49E-04	6.86E-05	104.2
5.77	8631	7.57E+01	2.76E+01	2.79E+02	1.10E-02	1.06E-02	3.36E-02	4.22E-03	1.86E-02	4.77E-03	1.54E-03	4.33E-03	6.55E-04	3.27E-03	4.67E-04	9.92E-04	1.07E-04	6.13E-04	7.43E-05	105.1
6.46	19690	1.60E+02	9.53E+01	5.81E+02	2.43E-02	2.40E-02	7.38E-02	9.36E-03	4.01E-02	1.10E-02	3.44E-03	8.84E-03	1.46E-03	7.20E-03	9.82E-04	1.99E-03	2.43E-04	1.41E-03	1.54E-04	104.1
6.51	18966	1.90E+02	6.87E+01	7.00E+02	2.67E-02	2.71E-02	8.33E-02	1.09E-02	4.67E-02	1.26E-02	3.84E-03	1.02E-02	1.66E-03	8.06E-03	1.15E-03	2.38E-03	2.72E-04	1.52E-03	1.89E-04	104.1
7.17	31121	2.58E+02	8.71E+01	8.26E+02	3.82E-02	3.92E-02	1.22E-01	1.54E-02	6.67E-02	1.77E-02	5.74E-03	1.49E-02	2.40E-03	1.19E-02	1.64E-03	3.33E-03	3.73E-04	2.21E-03	2.51E-04	104.3
7.18	33270	2.72E+02	8.39E+01	8.73E+02	3.89E-02	4.15E-02	1.25E-01	1.58E-02	6.85E-02	1.74E-02	5.75E-03	1.54E-02	2.44E-03	1.22E-02	1.73E-03	3.45E-03	3.73E-04	2.21E-03	2.51E-04	103.4

All values are in μmol L^{-1} soln, except pH (-log mol L^{-1}) and Soln:Soil, which is the mass ratio of suspension to soil.

b.d., below detection

Table EA-6: 350 ky Amalu surface horizon

pH	DOC	Fe	Si	Al	Y	La	Ce	Pr	Nd	Sm	Eu	Gd	Tb	Dy	Ho	Er	Tm	Yb	Lu	Soln:soil
2.09	1033.22	3.94E+00	2.70E+00	8.74E+02	4.72E-03	4.88E-03	7.77E-03	7.17E-04	2.50E-03	5.52E-04	1.84E-04	6.27E-04	1.17E-04	6.77E-04	1.09E-04	2.33E-04	2.37E-05	1.27E-04	1.71E-05	101.7
2.07	1026.56	3.77E+00	3.24E+00	9.26E+02	5.08E-03	5.26E-03	8.10E-03	7.45E-04	2.70E-03	6.05E-04	1.91E-04	7.04E-04	1.35E-04	7.26E-04	1.21E-04	2.45E-04	2.96E-05	1.39E-04	1.71E-05	101.9
2.56	496.21	9.53E-01	4.45E+00	4.26E+02	1.05E-03	7.34E-04	1.49E-03	1.35E-04	5.55E-04	1.33E-04	5.26E-05	1.14E-04	2.45E-05	1.35E-04	2.43E-05	4.78E-05	5.92E-06	4.62E-05	5.72E-06	102.0
2.61	490.13	8.62E-01	3.56E+00	3.73E+02	8.32E-04	6.41E-04	1.49E-03	1.28E-04	4.71E-04	1.40E-04	3.29E-05	1.21E-04	1.83E-05	1.23E-04	1.82E-05	4.78E-05	5.92E-06	2.89E-05	5.72E-06	102.0
3.14	250.94	5.21E-01	7.17E+00	1.23E+02	3.37E-04	3.02E-04	5.00E-04	5.68E-05	2.29E-04	1.06E-04	1.97E-05	4.34E-05	1.23E-05	4.92E-05	1.21E-05	2.39E-05	b.d	1.16E-05	b.d	100.9
3.17	262.68	8.64E-01	9.25E+00	1.31E+02	4.50E-04	5.40E-04	8.21E-04	1.06E-04	3.47E-04	6.65E-05	3.29E-05	9.42E-05	b.d	9.23E-05	b.d	2.99E-05	b.d	2.89E-05	b.d	101.8
4.57	1325.45	6.22E+00	1.16E+01	4.24E+01	1.43E-03	1.71E-03	3.61E-03	4.44E-04	1.55E-03	3.56E-04	1.32E-04	3.87E-04	6.10E-05	3.35E-04	6.37E-05	1.05E-04	1.48E-05	9.25E-05	1.71E-05	101.9
4.55	1453.67	7.47E+00	1.25E+01	4.72E+01	2.11E-03	2.00E-03	3.82E-03	4.61E-04	1.82E-03	6.28E-04	1.25E-04	4.13E-04	6.70E-05	3.82E-04	7.88E-05	2.15E-04	2.96E-05	1.65E-04	2.29E-05	101.8
6.16	6485.72	3.84E+01	4.80E+01	2.00E+02	6.18E-03	6.37E-03	1.47E-02	1.78E-03	6.19E-03	1.77E-03	5.26E-04	1.61E-03	2.63E-04	1.42E-03	2.12E-04	4.54E-04	6.51E-05	3.41E-04	5.14E-05	101.4
6.16	6319.21	4.23E+01	5.96E+01	2.13E+02	6.49E-03	6.86E-03	1.52E-02	1.71E-03	6.59E-03	1.66E-03	5.73E-04	1.66E-03	3.07E-04	1.47E-03	2.43E-04	5.14E-04	7.10E-05	3.76E-04	6.29E-05	101.9
7.22	21305.47	1.21E+02	3.76E+02	5.80E+02	2.12E-02	2.67E-02	5.69E-02	6.58E-03	2.49E-02	6.89E-03	2.43E-03	6.03E-03	1.18E-03	5.82E-03	8.43E-04	1.69E-03	1.54E-04	1.15E-03	1.37E-04	101.7
7.28	21455.33	1.39E+02	4.70E+02	6.84E+02	2.34E-02	2.62E-02	5.98E-02	7.02E-03	2.79E-02	6.51E-03	2.32E-03	6.50E-03	1.25E-03	6.25E-03	9.09E-04	2.06E-03	2.72E-04	1.49E-03	1.71E-04	102.6
5.02	1775.04	1.00E+01	1.62E+01	6.38E+01	1.75E-03	2.05E-03	4.85E-03	4.97E-04	2.33E-03	6.19E-04	1.51E-04	5.61E-04	8.53E-05	4.00E-04	6.06E-05	1.38E-04	1.78E-05	1.73E-04	1.14E-05	101.5
4.97	2024.81	1.29E+01	2.13E+01	7.98E+01	2.63E-03	2.52E-03	5.79E-03	7.31E-04	2.98E-03	6.52E-04	1.91E-04	5.80E-04	1.03E-04	5.11E-04	8.49E-05	1.97E-04	2.37E-05	1.33E-04	1.71E-05	102.1
2.83	319.71	8.91E-01	4.46E+00	3.20E+02	6.97E-04	7.49E-04	1.23E-03	1.14E-04	4.30E-04	7.98E-05	3.29E-05	1.01E-04	1.83E-05	1.05E-04	1.82E-05	4.19E-05	5.92E-06	2.31E-05	b.d	181.3
2.85	327.70	8.28E-01	6.96E+00	3.17E+02	7.42E-04	2.33E-03	2.44E-03	1.77E-04	5.68E-04	9.31E-05	3.29E-05	9.61E-05	2.44E-05	9.85E-05	1.82E-05	4.19E-05	5.92E-06	2.89E-05	b.d	181.7
3.52	265.84	6.94E-01	1.48E+00	5.29E+01	4.95E-04	3.47E-02	3.49E-02	1.70E-03	3.27E-03	1.60E-04	4.61E-05	1.69E-04	1.53E-05	6.15E-05	1.21E-05	4.78E-05	b.d	1.73E-05	b.d	135.1
3.53	251.44	8.06E-01	1.50E+00	6.08E+01	5.17E-04	1.78E-02	2.03E-02	9.08E-04	1.62E-03	9.98E-05	2.63E-05	1.19E-04	1.08E-05	7.38E-05	1.21E-05	2.39E-05	b.d	1.73E-05	b.d	133.7
4.09	981.60	4.06E+00	8.20E+00	4.18E+01	1.55E-03	1.27E-03	2.59E-03	3.41E-04	1.12E-03	2.86E-04	8.55E-05	2.92E-04	4.27E-05	2.46E-04	3.64E-05	1.14E-04	2.96E-05	7.51E-05	1.14E-05	113.7
4.29	1011.57	4.38E+00	9.72E+00	3.34E+01	1.11E-03	1.35E-03	2.43E-03	2.77E-04	1.10E-03	2.73E-04	8.55E-05	2.48E-04	4.27E-05	2.52E-04	3.64E-05	8.97E-05	1.18E-05	7.51E-05	1.14E-05	114.0
5.76	3097.99	2.11E+01	2.84E+01	1.04E+02	3.37E-03	1.06E-02	1.51E-02	1.23E-03	3.75E-03	9.18E-04	3.22E-04	7.93E-04	1.46E-04	7.57E-04	1.21E-04	3.65E-04	2.96E-05	2.14E-04	3.43E-05	103.7
5.75	3050.54	1.74E+01	2.86E+01	1.00E+02	3.77E-03	7.76E-03	1.21E-02	1.05E-03	5.20E-03	7.91E-04	2.83E-04	7.16E-04	1.19E-04	7.82E-04	1.03E-04	2.45E-04	2.96E-05	1.73E-04	2.86E-05	104.4
5.97	5510.78	3.84E+01	4.73E+01	1.74E+02	5.69E-03	3.44E-02	4.25E-02	3.00E-03	8.34E-03	1.62E-03	5.00E-04	1.46E-03	2.42E-04	1.35E-03	2.18E-04	4.42E-04	6.51E-05	3.47E-04	5.72E-05	103.6
6.07	5526.60	3.49E+01	4.18E+01	1.81E+02	5.46E-03	1.21E-02	1.99E-02	1.83E-03	6.28E-03	1.48E-03	5.59E-04	1.37E-03	2.82E-04	1.35E-03	2.12E-04	3.95E-04	5.33E-05	3.64E-04	4.57E-05	104.0
6.41	8575.47	4.79E+01	5.92E+01	2.33E+02	7.59E-03	7.44E-03	1.72E-02	1.99E-03	7.73E-03	2.07E-03	6.91E-04	2.02E-03	3.39E-04	1.82E-03	2.73E-04	5.56E-04	7.10E-05	4.22E-04	6.29E-05	104.6
6.55	9507.95	5.88E+01	5.41E+02	3.01E+02	8.22E-03	1.17E-02	2.51E-02	2.99E-03	1.02E-02	2.68E-03	9.21E-04	2.27E-03	4.62E-04	2.35E-03	3.09E-04	6.58E-04	7.10E-05	5.61E-04	6.29E-05	104.5
6.98	15452.50	8.08E+01	4.57E+02	4.30E+02	1.30E-02	1.50E-02	3.64E-02	4.62E-03	1.65E-02	4.56E-03	1.57E-03	4.12E-03	7.65E-04	3.85E-03	4.91E-04	1.14E-03	1.07E-04	8.15E-04	8.57E-05	104.1
6.88	15560.74	9.09E+01	4.30E+02	4.59E+02	1.52E-02	2.62E-02	5.00E-02	6.39E-03	2.13E-02	5.11E-03	1.57E-03	4.55E-03	8.01E-04	4.02E-03	5.52E-04	1.17E-03	1.18E-04	8.49E-04	1.20E-04	104.2

All values are in μmol L^{-1} soln, except pH (-log mol L^{-1}) and Soln:Soil, which is the mass ratio of suspension to soil.
b.d., below detection

Table EA-7: 1,400 ky Molokai surface horizon

pH	DOC	Fe	Si	Al	Y	La	Ce	Pr	Nd	Sm	Eu	Gd	Tb	Dy	Ho	Er	Tm	Yb	Lu	Soln:soil
2.08	827.66	2.46E+01	2.93E+00	5.62E+02	6.64E-03	3.66E-02	4.86E-02	3.75E-03	1.12E-02	1.56E-03	4.41E-04	1.42E-03	1.83E-04	8.55E-04	1.33E-04	2.45E-04	2.96E-05	1.44E-04	1.71E-05	101.7
2.08	801.85	2.31E+01	2.80E+00	5.39E+02	6.70E-03	3.59E-02	4.78E-02	3.73E-03	1.13E-02	1.46E-03	4.21E-04	1.30E-03	1.70E-04	8.74E-04	1.39E-04	2.87E-04	2.96E-05	1.39E-04	1.71E-05	101.9
2.58	542.42	6.97E+00	1.09E+00	3.45E+02	1.78E-03	9.05E-03	1.22E-02	1.00E-03	3.17E-03	4.32E-04	1.38E-04	3.57E-04	4.01E-05	2.09E-04	3.64E-05	7.77E-05	5.92E-06	3.47E-05	5.72E-06	101.7
2.57	531.51	7.45E+00	1.10E+00	3.41E+02	1.75E-03	9.03E-03	1.19E-02	1.00E-03	3.14E-03	4.79E-04	1.32E-04	3.50E-04	4.64E-05	1.91E-04	3.03E-05	6.58E-05	5.92E-06	4.62E-05	5.72E-06	102.3
3.37	352.01	3.23E+00	2.13E+00	8.44E+01	4.16E-04	2.03E-03	2.91E-03	2.63E-04	9.43E-04	1.73E-04	7.24E-05	1.03E-04	1.13E-05	7.38E-05	1.21E-05	1.79E-05	5.92E-06	1.16E-05	b.d.	101.9
3.39	321.79	2.50E+00	1.65E+00	6.15E+01	3.60E-04	1.71E-03	1.93E-03	1.99E-04	7.42E-04	7.32E-05	2.63E-05	5.70E-05	1.18E-05	3.69E-05	6.06E-06	1.20E-05	b.d.	1.16E-05	b.d.	100.9
4.49	1024.06	7.39E+01	1.07E+01	3.61E+01	1.37E-03	6.04E-03	1.25E-02	1.38E-03	5.16E-03	9.11E-04	2.37E-04	5.58E-04	5.65E-05	2.95E-04	4.24E-05	1.02E-04	1.78E-05	1.04E-04	1.14E-05	100.9
4.52	1044.04	7.47E+01	1.09E+01	3.76E+01	1.46E-03	6.76E-03	1.29E-02	1.49E-03	5.59E-03	8.45E-04	2.43E-04	5.57E-04	6.23E-05	3.08E-04	4.85E-05	8.97E-05	1.78E-05	9.25E-05	1.14E-05	101.3
5.79	3059.70	2.58E+02	2.68E+01	1.06E+02	3.63E-03	1.62E-02	3.17E-02	3.52E-03	1.22E-02	2.29E-03	5.46E-04	1.29E-03	1.67E-04	7.57E-04	1.09E-04	2.45E-04	3.55E-05	1.73E-04	3.43E-05	101.2
5.79	3044.71	2.44E+02	2.31E+01	1.05E+02	3.34E-03	1.58E-02	3.21E-02	3.42E-03	1.33E-02	2.17E-03	5.86E-04	1.35E-03	1.59E-04	7.20E-04	1.09E-04	2.57E-04	3.55E-05	1.68E-04	2.86E-05	101.1
7.69	19240.70	1.02E+03	6.91E+01	4.13E+02	1.41E-02	7.61E-02	1.49E-01	1.56E-02	5.65E-02	9.24E-03	2.57E-03	5.96E-03	7.47E-04	3.11E-03	4.55E-04	9.75E-04	1.24E-04	7.28E-04	9.14E-05	102.4
7.49	18349.85	1.11E+03	7.17E+01	4.39E+02	1.48E-02	7.81E-02	1.55E-01	1.64E-02	5.94E-02	9.88E-03	2.76E-03	6.01E-03	7.37E-04	3.28E-03	4.79E-04	1.08E-03	1.18E-04	7.74E-04	9.14E-05	101.1
2.89	380.32	7.30E+00	2.64E+01	2.35E+02	9.11E-04	5.18E-03	6.72E-03	6.10E-04	2.05E-03	2.86E-04	9.21E-05	1.92E-04	2.85E-05	1.23E-04	2.43E-05	7.17E-05	5.92E-06	2.31E-05	b.d.	103.3
2.87	375.41	4.21E+00	2.66E+01	2.49E+02	8.44E-04	4.79E-03	6.61E-03	5.39E-04	1.86E-03	2.73E-04	7.90E-05	1.85E-04	2.89E-05	1.17E-04	1.82E-05	3.59E-05	5.92E-06	2.89E-05	b.d.	101.7
3.52	304.39	2.85E+00	1.94E+00	5.41E+01	3.37E-04	2.16E-03	3.16E-03	2.91E-04	1.03E-03	8.65E-05	3.29E-05	8.58E-05	1.15E-05	4.31E-05	6.06E-06	2.39E-05	b.d.	1.16E-05	b.d.	102.3
3.52	298.56	2.66E+00	2.27E+00	5.46E+01	3.26E-04	1.48E-03	2.43E-03	2.20E-04	7.49E-04	9.98E-05	2.63E-05	7.62E-05	1.18E-05	5.54E-05	6.06E-06	1.79E-05	b.d.	1.16E-05	b.d.	100.9
5.25	2041.46	1.39E+02	2.26E+01	7.35E+01	3.03E-03	1.24E-02	2.48E-02	2.70E-03	9.98E-03	1.66E-03	4.41E-04	1.29E-03	1.20E-04	5.60E-04	1.03E-04	1.97E-04	2.96E-05	1.73E-04	2.86E-05	102.3
5.27	1835.82	1.32E+02	2.54E+01	7.57E+01	3.81E-03	1.26E-02	2.43E-02	2.80E-03	1.37E-02	1.67E-03	5.33E-04	1.34E-03	1.60E-04	6.71E-04	8.49E-05	2.09E-04	3.55E-05	1.73E-04	2.86E-05	102.2
6.33	6278.41	3.91E+02	2.57E+01	1.59E+02	5.15E-03	2.33E-02	4.68E-02	5.06E-03	1.71E-02	2.98E-03	7.77E-04	1.90E-03	2.17E-04	9.17E-04	1.52E-04	3.23E-04	5.33E-05	2.54E-04	4.00E-05	101.6
6.37	5455.83	3.78E+02	4.26E+01	1.68E+02	5.98E-03	2.62E-02	5.19E-02	5.60E-03	1.95E-02	3.19E-03	9.61E-04	2.05E-03	2.70E-04	1.17E-03	1.76E-04	4.07E-04	6.51E-05	3.64E-04	6.29E-05	100.1
6.71	8359.00	5.07E+02	3.91E+01	2.22E+02	6.74E-03	3.44E-02	6.83E-02	7.47E-03	2.55E-02	4.89E-03	1.18E-03	2.65E-03	3.83E-04	1.48E-03	2.18E-04	4.84E-04	7.10E-05	3.18E-04	5.14E-05	101.0
6.74	9149.95	5.64E+02	5.07E+01	2.44E+02	7.90E-03	3.73E-02	7.42E-02	8.18E-03	3.00E-02	4.75E-03	1.37E-03	3.35E-03	3.53E-04	1.62E-03	2.30E-04	5.32E-04	6.51E-05	3.76E-04	5.72E-05	104.8
7.11	12788.28	6.75E+02	5.10E+01	2.90E+02	8.81E-03	4.58E-02	9.11E-02	9.56E-03	3.37E-02	5.68E-03	1.49E-03	3.60E-03	4.49E-04	2.04E-03	2.79E-04	6.46E-04	8.88E-05	4.74E-04	6.86E-05	102.1
7.13	12396.97	6.92E+02	4.53E+01	2.91E+02	8.81E-03	4.60E-02	9.06E-02	9.78E-03	3.40E-02	5.68E-03	1.57E-03	3.87E-03	4.55E-04	2.10E-03	2.91E-04	6.40E-04	8.29E-05	4.62E-04	7.43E-05	101.4
7.34	15752.23	8.51E+02	6.51E+01	3.59E+02	1.18E-02	5.90E-02	1.17E-01	1.29E-02	4.61E-02	8.86E-03	2.11E-03	4.67E-03	5.88E-04	2.70E-03	4.18E-04	8.37E-04	1.07E-04	6.93E-04	8.00E-05	102.6
7.37	15252.69	8.41E+02	6.56E+01	3.55E+02	1.20E-02	5.93E-02	1.17E-01	1.23E-02	4.51E-02	7.24E-03	2.07E-03	4.53E-03	5.83E-04	2.77E-03	3.82E-04	8.49E-04	1.12E-04	6.24E-04	9.72E-05	101.2
3.90	604.03	3.09E+01	8.64E+00	2.98E+01	1.25E-03	4.60E-03	8.40E-03	1.04E-03	3.67E-03	6.19E-04	1.71E-04	3.88E-04	4.58E-05	2.65E-04	4.24E-05	7.77E-05	1.18E-05	8.09E-05	1.14E-05	101.1
3.85	628.17	3.32E+01	9.80E+00	3.00E+01	1.44E-03	4.82E-03	8.92E-03	1.00E-03	3.68E-03	6.32E-04	1.78E-04	3.84E-04	5.21E-05	2.40E-04	3.64E-05	8.97E-05	1.18E-05	7.51E-05	1.14E-05	101.2

All values are in μmol L^{-1} soln, except pH (-log mol L^{-1}) and Soln:Soil, which is the mass ratio of suspension to soil.

b.d., below detection

Table EA-8: 4,100 ky Kauai surface horizon

pH	DOC	Fe	Si	Al	Y	La	Ce	Pr	Nd	Sm	Eu	Gd	Tb	Dy	Ho	Er	Tm	Yb	Lu	Soln:soil
1.99	133.46	1.52E+00	1.55E+00	7.79E+01	7.20E-04	3.05E-03	4.83E-03	4.26E-04	1.25E-03	1.66E-04	5.26E-05	2.14E-04	3.01E-05	1.48E-04	1.82E-05	2.99E-05	5.92E-06	5.78E-06	b.d	99.8
2.01	111.15	1.56E+00	b.d.	8.32E+01	7.31E-04	2.60E-03	3.55E-03	2.98E-04	9.91E-04	1.86E-04	5.26E-05	2.14E-04	3.04E-05	1.60E-04	1.82E-05	3.59E-05	0.00E+00	5.78E-06	b.d	100.3
2.45	103.74	1.22E+00	6.85E-01	5.09E+01	2.02E-04	6.19E-04	9.35E-04	7.81E-05	2.84E-04	4.66E-05	1.32E-05	2.21E-05	5.94E-06	3.08E-05	6.06E-06	1.20E-05	0.00E+00	5.78E-06	b.d	99.6
2.45	99.41	5.11E-01	b.d.	5.00E+01	1.46E-04	6.12E-04	9.28E-04	7.10E-05	2.08E-04	3.99E-05	1.32E-05	2.26E-05	6.04E-06	3.08E-05	6.06E-06	5.98E-06	0.00E+00	b.d	b.d	100.3
2.99	155.77	1.11E+01	1.48E+00	1.54E+01	1.12E-04	4.46E-04	9.21E-04	1.06E-04	3.88E-04	7.32E-05	1.97E-05	6.13E-05	5.81E-06	4.31E-05	6.06E-06	1.20E-05	0.00E+00	5.78E-06	b.d.	99.8
3.00	146.87	1.20E+01	2.67E+00	1.68E+01	9.00E-05	7.41E-04	1.45E-03	1.42E-04	5.34E-04	7.32E-05	3.29E-05	8.62E-05	1.19E-05	4.92E-05	6.06E-06	5.98E-06	0.00E+00	5.78E-06	b.d.	100.3
4.78	381.98	2.79E+01	b.d.	5.12E+00	3.15E-04	9.43E-04	2.23E-03	2.48E-04	9.98E-04	1.93E-04	5.92E-05	1.68E-04	3.02E-05	1.48E-04	1.21E-05	2.99E-05	5.92E-06	2.31E-05	b.d	100.3
4.82	379.65	2.70E+01	7.10E-01	5.51E+00	3.82E-04	9.79E-04	2.33E-03	2.84E-04	1.01E-03	2.13E-04	6.58E-05	2.13E-04	2.39E-05	1.42E-04	1.82E-05	2.99E-05	0.00E+00	1.16E-05	b.d	100.5
5.53	968.28	7.55E+01	3.81E+00	1.50E+01	8.32E-04	2.41E-03	5.59E-03	6.32E-04	2.37E-03	5.45E-04	1.65E-04	6.48E-04	6.00E-05	2.71E-04	4.24E-05	4.78E-05	5.92E-06	4.05E-05	5.72E-06	100.0
5.56	1010.74	1.32E+02	7.23E+00	2.35E+01	1.86E-03	4.47E-03	8.99E-03	1.13E-03	4.40E-03	8.98E-04	3.36E-04	1.08E-03	1.08E-04	5.60E-04	8.49E-05	1.08E-04	1.18E-05	6.93E-05	1.14E-05	100.5
6.61	3545.08	1.76E+02	5.15E+00	3.50E+01	2.29E-03	6.86E-03	1.52E-02	1.74E-03	6.97E-03	1.44E-03	5.13E-04	1.39E-03	1.80E-04	7.51E-04	1.09E-04	1.61E-04	1.78E-05	7.51E-05	1.71E-05	99.9
6.63	3416.04	1.70E+02	4.67E+00	3.33E+01	2.11E-03	6.83E-03	1.55E-02	1.80E-03	7.19E-03	1.58E-03	5.00E-04	1.29E-03	1.74E-04	6.95E-04	1.03E-04	1.67E-04	2.37E-05	8.67E-05	1.14E-05	100.8
3.26	254.60	4.08E+01	2.29E+00	1.31E+01	5.62E-04	1.01E-03	1.83E-03	2.20E-04	8.32E-04	1.60E-04	5.26E-05	1.29E-04	2.42E-05	8.62E-05	1.21E-05	2.99E-05	5.92E-06	1.16E-05	b.d	189.6
3.24	267.75	5.28E+01	2.47E+00	1.53E+01	4.27E-04	1.45E-03	2.75E-03	2.98E-04	1.28E-03	2.13E-04	5.92E-05	1.65E-04	2.99E-05	1.17E-04	1.82E-05	2.99E-05	5.92E-06	1.16E-05	b.d	191.0
3.51	321.37	4.18E+01	3.51E+00	8.83E+00	6.64E-04	1.58E-03	3.47E-03	4.19E-04	1.71E-03	2.93E-04	1.05E-04	3.14E-04	3.57E-05	1.66E-04	2.43E-05	4.19E-05	5.92E-06	2.89E-05	5.72E-06	132.0
3.48	327.45	4.09E+01	2.16E+00	8.83E+00	5.40E-04	1.70E-03	3.45E-03	4.26E-04	1.68E-03	3.13E-04	1.05E-04	3.20E-04	4.20E-05	1.97E-04	2.43E-05	3.59E-05	5.92E-06	1.73E-05	5.72E-06	132.8
3.99	392.47	5.09E+01	3.24E+00	1.11E+01	8.89E-04	1.94E-03	4.18E-03	5.46E-04	2.20E-03	3.46E-04	1.18E-04	3.67E-04	4.13E-05	2.22E-04	3.03E-05	5.38E-05	5.92E-06	3.47E-05	5.72E-06	108.7
3.98	454.50	7.44E+01	3.96E+00	1.35E+01	1.11E-03	2.73E-03	5.20E-03	7.03E-04	2.71E-03	5.19E-04	1.58E-04	4.04E-04	6.59E-05	2.77E-04	4.24E-05	9.57E-05	1.18E-05	4.05E-05	5.72E-06	110.7
5.21	592.04	6.01E+01	3.17E+00	1.15E+01	8.66E-04	2.42E-03	4.75E-03	5.39E-04	2.29E-03	3.79E-04	1.32E-04	3.67E-04	4.75E-05	1.97E-04	3.64E-05	5.38E-05	5.92E-06	3.47E-05	5.72E-06	100.0
5.25	593.04	6.49E+01	3.40E+00	1.22E+01	6.86E-04	1.88E-03	4.28E-03	5.11E-04	2.06E-03	4.86E-04	1.25E-04	3.55E-04	5.41E-05	2.34E-04	3.03E-05	5.38E-05	5.92E-06	3.47E-05	5.72E-06	100.0
6.18	1951.54	1.26E+02	3.36E+00	2.29E+01	1.37E-03	3.95E-03	9.04E-03	1.04E-03	4.05E-03	9.04E-04	2.57E-04	6.94E-04	1.08E-04	4.43E-04	6.06E-05	1.14E-04	1.18E-05	5.20E-05	5.72E-06	99.9
6.24	2039.80	1.15E+02	5.08E+00	3.20E+01	1.66E-03	4.33E-03	9.83E-03	1.07E-03	4.22E-03	8.65E-04	2.57E-04	8.62E-04	1.08E-04	4.62E-04	6.67E-05	1.20E-04	1.18E-05	5.20E-05	1.14E-05	100.5
7.17	5445.01	2.22E+02	5.07E+00	4.07E+01	3.21E-03	1.02E-02	2.39E-02	2.66E-03	1.02E-02	2.22E-03	6.51E-04	1.96E-03	2.58E-04	1.22E-03	1.39E-04	2.45E-04	2.96E-05	1.91E-04	2.29E-05	100.0
7.07	5544.08	2.38E+02	5.61E+00	4.29E+01	3.24E-03	9.98E-03	2.34E-02	2.58E-03	1.04E-02	2.23E-03	6.78E-04	1.87E-03	2.76E-04	1.21E-03	1.39E-04	2.15E-04	3.55E-05	1.44E-04	2.29E-05	99.3

All values are in μmol L^{-1} soln, except pH (-log mol L^{-1}) and Soln:Soil, which is the mass ratio of suspension to soil.

b.d., below detection

Table EA-9: 0.3 ky Olaa subsurface horizon

pH	DOC	Fe	Si	Al	Y	La	Ce	Pr	Nd	Sm	Eu	Gd	Tb	Dy	Ho	Er	Tm	Yb	Lu	Soln:soil
2.14	79.93	1.22E+01	1.43E+02	2.62E+02	2.40E-01	9.83E-02	1.80E-01	2.37E-02	9.66E-02	1.89E-02	3.66E-03	2.16E-02	3.45E-03	1.99E-02	3.64E-03	9.14E-03	1.02E-03	5.34E-03	6.74E-04	100.9
2.14	76.18	1.14E+01	1.37E+02	2.52E+02	2.38E-01	9.72E-02	1.81E-01	2.35E-02	9.70E-02	1.88E-02	3.66E-03	2.11E-02	3.33E-03	1.99E-02	3.72E-03	9.12E-03	1.02E-03	5.29E-03	6.63E-04	101.6
2.71	47.21	3.05E+00	1.36E+02	1.50E+02	6.00E-02	2.70E-02	4.25E-02	5.23E-03	2.05E-02	3.75E-03	7.37E-04	4.74E-03	7.01E-04	4.14E-03	7.76E-04	1.93E-03	2.07E-04	1.04E-03	1.31E-04	101.6
2.70	38.21	2.82E+00	1.28E+02	1.50E+02	6.04E-02	2.77E-02	4.30E-02	5.23E-03	2.08E-02	3.79E-03	7.37E-04	4.76E-03	7.06E-04	4.23E-03	7.82E-04	1.93E-03	2.07E-04	1.05E-03	1.37E-04	101.1
3.64	50.20	4.57E-01	0.00E+00	2.59E+01	3.17E-03	1.31E-03	2.32E-03	3.41E-04	1.52E-03	3.26E-04	7.24E-05	3.38E-04	4.09E-05	2.58E-04	4.85E-05	1.26E-04	1.18E-05	8.67E-05	1.14E-05	101.0
3.75	52.20	4.77E-01	0.00E+00	2.54E+01	3.01E-03	1.20E-03	2.16E-03	3.19E-04	1.43E-03	2.99E-04	6.58E-05	3.20E-04	4.11E-05	2.34E-04	4.24E-05	1.20E-04	1.18E-05	7.51E-05	1.14E-05	100.6
6.36	113.98	2.76E+01	5.10E+01	2.04E+01	7.94E-03	2.97E-03	1.05E-02	1.11E-03	5.02E-03	1.20E-03	3.36E-04	1.07E-03	1.73E-04	1.01E-03	1.82E-04	4.72E-04	5.92E-05	3.47E-04	4.57E-05	103.6
6.53	148.61	2.62E+01	5.00E+01	2.10E+01	7.75E-03	2.97E-03	1.03E-02	1.09E-03	4.86E-03	1.20E-03	3.36E-04	1.02E-03	1.67E-04	1.00E-03	1.76E-04	4.60E-04	5.92E-05	3.47E-04	4.57E-05	101.2
10.15	663.97	5.63E+01	1.40E+02	1.06E+02	2.29E-02	7.28E-03	1.83E-02	2.73E-03	1.29E-02	3.13E-03	9.54E-04	3.24E-03	4.93E-04	2.71E-03	4.91E-04	1.32E-03	1.66E-04	9.53E-04	1.31E-04	101.0
10.15	661.56	6.18E+01	1.55E+02	1.13E+02	2.42E-02	7.62E-03	1.97E-02	2.94E-03	1.33E-02	3.33E-03	9.74E-04	3.43E-03	5.05E-04	2.90E-03	5.09E-04	1.36E-03	1.66E-04	1.01E-03	1.31E-04	101.2
10.88	1266.34	7.21E+01	2.14E+02	1.71E+02	3.44E-02	1.03E-02	2.24E-02	3.95E-03	1.87E-02	4.37E-03	1.36E-03	4.55E-03	7.08E-04	3.87E-03	6.79E-04	1.88E-03	2.31E-04	1.40E-03	1.83E-04	101.0
10.90	1263.01	6.92E+01	2.10E+02	1.73E+02	3.40E-02	1.08E-02	2.16E-02	4.05E-03	1.85E-02	4.66E-03	1.35E-03	4.67E-03	6.77E-04	3.80E-03	7.34E-04	1.79E-03	2.25E-04	1.33E-03	1.77E-04	100.7
3.07	65.61	1.40E+00	1.21E+02	7.54E+01	1.99E-02	9.36E-03	1.43E-02	1.78E-03	7.01E-03	1.32E-03	2.63E-04	1.57E-03	2.25E-04	1.32E-03	2.49E-04	5.98E-04	6.51E-05	3.35E-04	4.57E-05	100.2
3.09	51.54	1.27E+00	1.14E+02	7.38E+01	1.86E-02	8.55E-03	1.33E-02	1.67E-03	6.60E-03	1.24E-03	2.43E-04	1.49E-03	2.19E-04	1.24E-03	2.30E-04	5.86E-04	6.51E-05	3.18E-04	4.00E-05	101.1
4.50	51.95	6.48E-01	6.57E+01	6.30E+00	1.14E-03	3.60E-04	9.14E-04	1.35E-04	6.38E-04	1.53E-04	3.29E-05	1.35E-04	1.76E-05	1.11E-04	2.43E-05	5.38E-05	5.92E-06	4.62E-05	5.72E-06	100.2
4.40	46.54	4.73E-01	6.50E+01	6.99E+00	1.12E-03	3.96E-04	9.63E-04	1.49E-04	7.21E-04	1.60E-04	3.29E-05	1.54E-04	1.74E-05	1.17E-04	2.43E-05	5.98E-05	5.92E-06	4.05E-05	5.72E-06	100.3
4.76	83.92	8.42E+00	4.75E+01	7.15E+00	3.73E-03	1.39E-03	4.72E-03	5.39E-04	2.45E-03	5.99E-04	1.38E-04	5.15E-04	8.03E-05	4.74E-04	8.49E-05	2.15E-04	2.96E-05	1.68E-04	2.29E-05	101.0
4.76	88.67	1.17E+01	5.21E+01	8.84E+00	4.58E-03	1.68E-03	5.98E-03	6.67E-04	3.02E-03	7.58E-04	1.78E-04	6.51E-04	1.04E-04	5.85E-04	1.09E-04	2.75E-04	3.55E-05	2.02E-04	2.86E-05	100.3
5.61	179.34	2.82E+01	6.61E+01	2.12E+01	8.64E-03	3.26E-03	1.22E-02	1.24E-03	5.70E-03	1.39E-03	3.75E-04	1.19E-03	2.02E-04	1.15E-03	2.06E-04	5.20E-04	6.51E-05	3.93E-04	5.72E-05	100.1
5.60	171.84	2.66E+01	6.11E+01	1.90E+01	8.18E-03	3.07E-03	1.13E-02	1.18E-03	5.37E-03	1.29E-03	3.42E-04	1.13E-03	1.84E-04	1.07E-03	1.88E-04	4.84E-04	6.51E-05	3.76E-04	5.14E-05	101.0
8.76	233.12	3.47E+01	6.89E+01	4.71E+01	1.26E-02	4.64E-03	1.47E-02	1.59E-03	7.20E-03	1.78E-03	5.07E-04	1.48E-03	2.52E-04	1.49E-03	2.67E-04	6.64E-04	8.88E-05	5.14E-04	6.86E-05	101.1
8.14	220.80	3.67E+01	9.58E+01	4.39E+01	1.37E-02	4.56E-03	1.54E-02	1.72E-03	7.70E-03	1.95E-03	5.53E-04	1.97E-03	2.89E-04	1.69E-03	2.91E-04	7.47E-04	9.47E-05	5.84E-04	7.43E-05	100.2
9.49	306.89	4.15E+01	1.04E+02	5.51E+01	1.64E-02	5.21E-03	1.48E-02	1.97E-03	8.88E-03	2.23E-03	6.45E-04	2.28E-03	3.43E-04	1.93E-03	3.46E-04	8.79E-04	1.12E-04	6.70E-04	9.14E-05	100.4
9.46	245.28	4.18E+01	6.17E+01	6.54E+01	1.62E-02	5.78E-03	1.59E-02	2.07E-03	9.24E-03	2.40E-03	6.05E-04	2.24E-03	3.71E-04	2.10E-03	3.52E-04	9.09E-04	1.24E-04	7.69E-04	9.72E-05	100.7
9.85	448.51	4.42E+01	7.44E+01	7.85E+01	1.83E-02	5.97E-03	1.59E-02	2.36E-03	1.02E-02	2.59E-03	7.30E-04	2.89E-03	3.77E-04	2.37E-03	3.82E-04	1.03E-03	1.36E-04	8.09E-04	1.09E-04	101.0
9.85	372.24	4.59E+01	7.33E+01	7.78E+01	1.82E-02	6.00E-03	1.59E-02	2.25E-03	1.06E-02	2.48E-03	7.57E-04	2.79E-03	4.08E-04	2.30E-03	3.88E-04	1.12E-03	1.42E-04	8.15E-04	1.03E-04	101.5
7.24	164.43	3.37E+01	5.94E+01	3.30E+01	1.05E-02	3.77E-03	1.27E-02	1.33E-03	5.68E-03	1.35E-03	3.75E-04	1.10E-03	1.95E-04	1.14E-03	2.00E-04	5.14E-04	6.51E-05	3.70E-04	5.14E-05	100.4
6.61	187.00	3.97E+01	8.20E+01	4.50E+01	1.31E-02	4.68E-03	1.46E-02	1.50E-03	6.31E-03	1.52E-03	3.95E-04	1.29E-03	2.11E-04	1.24E-03	2.06E-04	5.56E-04	5.92E-05	3.99E-04	4.57E-05	101.0

All values are in μmol L^{-1} soln, except pH (-log mol L^{-1}) and Soln:Soil, which is the mass ratio of suspension to soil.
b.d., below detection

Table EA-10: 20 ky Laupahoehoe subsurface horizon

pH	DOC	Fe	Si	Al	Y	La	Ce	Pr	Nd	Sm	Eu	Gd	Tb	Dy	Ho	Er	Tm	Yb	Lu	Soln:soil
2.55	139.62	1.29E+00	3.09E+01	1.59E+03	3.26E-01	1.36E-01	2.99E-01	5.53E-02	2.24E-01	3.55E-02	1.20E-02	3.66E-02	5.07E-03	2.78E-02	5.21E-03	1.23E-02	1.33E-03	6.29E-03	8.92E-04	133.9
2.54	199.57	1.66E+00	3.14E+01	1.59E+03	3.23E-01	1.37E-01	3.01E-01	5.51E-02	2.26E-01	3.59E-02	1.21E-02	3.64E-02	5.14E-03	2.82E-02	5.35E-03	1.24E-02	1.31E-03	6.48E-03	9.20E-04	134.0
3.50	83.84	2.69E-01	1.52E+01	9.63E+02	9.03E-02	4.50E-02	8.11E-02	1.39E-02	5.47E-02	8.12E-03	2.67E-03	9.30E-03	1.20E-03	6.51E-03	1.24E-03	2.83E-03	2.96E-04	1.33E-03	1.89E-04	136.9
3.49	72.52	2.44E-01	1.56E+01	9.68E+02	9.06E-02	4.54E-02	8.07E-02	1.38E-02	5.53E-02	8.17E-03	2.75E-03	9.32E-03	1.21E-03	6.44E-03	1.22E-03	2.79E-03	2.90E-04	1.34E-03	1.89E-04	133.9
4.05	31.05	1.09E-01	6.87E+00	2.73E+02	3.10E-02	1.70E-02	2.79E-02	4.68E-03	1.83E-02	2.57E-03	8.69E-04	2.99E-03	3.71E-04	2.03E-03	3.88E-04	8.79E-04	8.88E-05	4.10E-04	5.72E-05	133.8
4.11	52.54	1.05E-01	7.01E+00	2.77E+02	3.21E-02	1.79E-02	2.94E-02	4.97E-03	1.93E-02	2.78E-03	9.21E-04	3.19E-03	3.94E-04	2.15E-03	4.00E-04	8.97E-04	9.47E-05	4.33E-04	5.72E-05	134.1
4.73	43.54	5.66E-02	4.64E+00	2.79E+00	7.99E-04	4.82E-04	7.85E-04	1.35E-04	5.55E-04	9.31E-05	2.63E-05	7.23E-05	1.08E-05	5.54E-05	1.21E-05	2.99E-05	5.92E-06	1.73E-05	b.d.	134.3
4.97	58.36	6.52E-02	4.95E+00	2.37E+00	7.54E-04	4.46E-04	7.21E-04	1.21E-04	5.06E-04	7.98E-05	2.63E-05	7.47E-05	1.10E-05	5.54E-05	1.21E-05	2.99E-05	5.92E-06	1.16E-05	b.d.	135.2
6.35	177.50	1.99E+00	4.69E+00	6.27E+00	1.41E-03	2.66E-04	1.21E-03	2.55E-04	1.36E-03	2.99E-04	1.05E-04	2.89E-04	4.23E-05	2.40E-04	5.46E-05	1.02E-04	1.18E-05	8.09E-05	1.14E-05	133.9
6.29	168.10	4.78E+00	5.99E+00	8.78E+00	1.42E-03	4.10E-04	1.57E-03	2.13E-04	1.10E-03	2.79E-04	8.55E-05	2.28E-04	3.61E-05	1.91E-04	3.64E-05	9.57E-05	1.18E-05	8.09E-05	1.14E-05	133.9
6.95	444.34	4.71E+00	7.34E-01	6.10E+00	1.38E-03	2.45E-04	1.12E-03	2.27E-04	1.20E-03	3.06E-04	9.54E-05	2.61E-04	3.94E-05	2.12E-04	3.64E-05	9.86E-05	1.18E-05	7.80E-05	1.14E-05	133.9
7.15	470.07	1.53E+00	9.73E-01	2.38E+00	6.86E-04	1.37E-04	6.28E-04	1.31E-04	7.52E-04	1.76E-04	5.92E-05	1.58E-04	2.11E-05	1.17E-04	2.12E-05	5.38E-05	5.92E-06	3.76E-05	5.72E-06	134.1
3.11	74.68	2.97E-01	2.11E+01	1.21E+03	1.41E-01	6.76E-02	1.28E-01	2.25E-02	8.96E-02	1.37E-02	4.57E-03	1.41E-02	2.04E-03	1.10E-02	2.07E-03	4.84E-03	5.03E-04	2.35E-03	3.31E-04	135.1
3.11	72.43	2.86E-01	1.95E+01	1.23E+03	1.44E-01	7.03E-02	1.33E-01	2.31E-02	9.22E-02	1.42E-02	4.74E-03	1.47E-02	2.06E-03	1.14E-02	2.15E-03	4.96E-03	5.21E-04	2.38E-03	3.49E-04	135.4
3.78	41.96	1.45E-01	1.18E+01	6.32E+02	6.15E-02	3.27E-02	5.61E-02	9.59E-03	3.76E-02	5.33E-03	1.80E-03	6.06E-03	7.78E-04	4.21E-03	7.88E-04	1.83E-03	1.89E-04	8.44E-04	1.20E-04	136.2
3.75	35.22	2.28E-01	1.14E+01	6.31E+02	6.30E-02	3.30E-02	5.70E-02	9.74E-03	3.80E-02	5.47E-03	1.82E-03	6.20E-03	7.58E-04	4.34E-03	8.06E-04	1.85E-03	1.89E-04	8.38E-04	1.20E-04	135.9
4.38	39.38	9.38E-02	7.05E+00	8.62E+01	1.51E-02	8.86E-03	1.45E-02	2.42E-03	9.32E-03	1.30E-03	4.28E-04	1.52E-03	1.82E-04	1.00E-03	1.94E-04	4.30E-04	4.14E-05	1.96E-04	2.86E-05	135.1
4.34	32.55	5.79E-02	7.09E+00	1.03E+02	1.43E-02	8.48E-03	1.40E-02	2.37E-03	9.34E-03	1.30E-03	4.34E-04	1.46E-03	1.82E-04	9.78E-04	1.88E-04	4.19E-04	4.14E-05	1.91E-04	2.86E-05	135.3
5.76	50.37	6.30E-01	3.68E+00	2.00E+00	9.11E-04	1.66E-04	3.71E-04	7.10E-05	2.50E-04	2.26E-04	3.29E-05	1.51E-04	2.43E-05	7.38E-05	1.21E-05	1.20E-05	3.55E-05	1.16E-05	5.72E-06	135.1
5.71	51.95	3.90E-02	2.91E+00	7.82E-01	6.41E-04	8.64E-05	1.21E-04	2.84E-05	1.94E-04	2.93E-04	2.63E-05	1.11E-04	2.45E-05	1.85E-05	6.06E-06	4.19E-05	2.96E-05	5.78E-06	b.d.	135.2
6.29	83.84	1.99E+00	4.44E+00	3.32E+00	7.42E-04	1.22E-04	5.78E-04	1.21E-04	6.52E-04	1.73E-04	5.26E-05	1.50E-04	2.38E-05	1.29E-04	2.43E-05	5.98E-05	5.92E-06	4.62E-05	5.72E-06	135.2
6.31	76.43	5.83E-01	4.16E+00	1.02E+00	2.92E-04	5.76E-05	2.57E-04	4.97E-05	2.70E-04	7.32E-05	2.63E-05	6.26E-05	5.72E-06	4.92E-05	1.21E-05	2.39E-05	0.00E+00	1.73E-05	b.d.	135.2
6.71	255.68	3.95E-01	4.60E+00	1.29E+00	5.51E-04	8.64E-05	4.21E-04	9.23E-05	5.06E-04	1.13E-04	3.95E-05	1.03E-04	1.19E-05	9.23E-05	1.82E-05	3.59E-05	5.92E-06	3.47E-05	5.72E-06	135.0
6.74	251.52	8.00E-01	5.28E+00	2.29E+00	7.09E-04	1.37E-04	5.71E-04	1.14E-04	5.96E-04	1.46E-04	4.61E-05	1.22E-04	1.81E-05	1.11E-04	2.43E-05	4.78E-05	5.92E-06	4.62E-05	5.72E-06	135.1
7.93	1081.51	4.09E+01	1.45E+01	7.09E+01	1.14E-02	2.11E-03	1.21E-02	1.93E-03	9.66E-03	2.37E-03	7.70E-04	2.09E-03	2.97E-04	1.80E-03	3.15E-04	8.19E-04	1.01E-04	6.36E-04	9.14E-05	134.1
7.92	995.75	4.80E+01	1.48E+01	7.39E+01	1.15E-02	2.08E-03	1.26E-02	1.87E-03	9.37E-03	2.22E-03	7.57E-04	2.15E-03	3.16E-04	1.77E-03	3.09E-04	8.13E-04	9.47E-05	6.07E-04	8.57E-05	134.2

All values are in μmol L^{-1} soln, except pH (-log mol L^{-1}) and Soln:Soil, which is the mass ratio of suspension to soil.
b.d., below detection

Table EA-11: 150 ky Kohala subsurface horizon

pH	DOC	Fe	Si	Al	Y	La	Ce	Pr	Nd	Sm	Eu	Gd	Tb	Dy	Ho	Er	Tm	Yb	Lu	Soln:soil
2.39	4.99	1.48E+00	b.d.	1.24E+00	2.84E+02	2.63E-02	4.32E-03	3.37E+00	3.50E-01	3.61E-01	9.21E-01	8.88E-02	3.16E-01	5.07E-02	1.59E-02	4.28E-02	6.68E-03	3.77E-02	6.43E-03	99.4
2.38	5.63	1.46E+00	b.d.	1.57E+00	3.07E+02	3.26E-02	1.17E-02	3.41E+00	3.78E-01	3.91E-01	1.08E+00	1.07E-01	3.78E-01	6.49E-02	2.03E-02	5.26E-02	7.99E-03	4.47E-02	7.63E-03	103.6
3.06	2.62	1.06E+00	b.d.	4.89E-01	5.87E+01	2.55E-02	1.51E-04	2.98E+00	1.55E-01	1.86E-01	3.82E-01	3.42E-02	1.13E-01	1.54E-02	4.80E-03	1.59E-02	2.16E-03	1.24E-02	2.25E-03	101.6
3.06	2.77	1.13E+00	b.d.	5.18E-01	6.15E+01	2.98E-02	1.47E-04	3.06E+00	1.64E-01	1.97E-01	4.08E-01	3.63E-02	1.21E-01	1.66E-02	5.10E-03	1.69E-02	2.31E-03	1.32E-02	2.33E-03	101.2
3.72	1.28	8.43E-01	b.d.	2.02E-01	1.45E+01	2.33E-02	b.d.	2.68E+00	6.92E-02	9.04E-02	1.68E-01	1.41E-02	4.64E-02	6.01E-03	1.89E-03	6.36E-03	8.54E-04	4.95E-03	8.85E-04	101.8
3.71	1.27	8.50E-01	b.d.	2.01E-01	1.46E+01	2.25E-02	8.62E-06	2.52E+00	6.97E-02	9.02E-02	1.67E-01	1.41E-02	4.58E-02	6.02E-03	1.90E-03	6.14E-03	8.49E-04	4.87E-03	8.73E-04	101.4
4.37	0.38	7.04E-01	b.d.	5.61E-02	7.43E+00	2.16E-02	b.d.	2.22E+00	1.92E-02	2.71E-02	4.80E-02	3.95E-03	1.31E-02	1.78E-03	5.59E-04	1.60E-03	2.34E-04	1.35E-03	2.49E-04	100.7
4.38	0.38	6.65E-01	b.d.	5.59E-02	7.51E+00	2.18E-02	8.62E-06	2.12E+00	1.81E-02	2.58E-02	4.55E-02	3.78E-03	1.26E-02	1.74E-03	5.53E-04	1.59E-03	2.24E-04	1.28E-03	2.43E-04	104.9
6.52	0.01	3.65E-02	b.d.	b.d.	9.45E+00	3.46E-03	6.90E-05	1.42E-01	1.19E-03	7.99E-04	2.93E-03	3.55E-04	1.62E-03	3.26E-04	9.87E-05	2.82E-04	3.56E-05	1.66E-04	3.03E-05	101.6
6.47	0.01	3.22E-02	b.d.	b.d.	6.77E+00	5.39E-03	1.29E-05	2.87E-01	6.30E-04	3.67E-04	1.41E-03	1.85E-04	9.22E-04	1.53E-04	5.26E-05	1.24E-04	1.77E-05	8.00E-05	1.82E-05	101.2
8.36	1.28	2.19E-01	b.d.	5.08E-01	2.11E+02	1.33E-02	1.64E-02	9.02E-01	1.04E-01	9.11E-02	3.21E-01	3.57E-02	1.51E-01	3.11E-02	9.65E-03	2.32E-02	3.47E-03	1.82E-02	3.10E-03	101.0
8.37	1.13	2.04E-01	b.d.	4.55E-01	1.95E+02	2.89E-03	1.47E-02	8.12E-01	9.48E-02	8.04E-02	2.95E-01	3.18E-02	1.32E-01	2.80E-02	8.69E-03	2.19E-02	3.25E-03	1.74E-02	2.72E-03	101.5
3.33	2.02	9.93E-01	b.d.	3.30E-01	3.53E+01	2.61E-02	1.72E-05	3.18E+00	1.16E-01	1.44E-01	2.80E-01	2.32E-02	7.75E-02	1.02E-02	3.19E-03	1.00E-02	1.42E-03	8.25E-03	1.49E-03	101.0
3.31	2.17	9.93E-01	b.d.	3.63E-01	3.43E+01	2.61E-02	2.15E-05	3.24E+00	1.24E-01	1.52E-01	3.00E-01	2.52E-02	8.21E-02	1.08E-02	3.32E-03	1.10E-02	1.55E-03	9.02E-03	1.62E-03	102.4
3.94	0.86	7.65E-01	b.d.	1.32E-01	1.10E+01	2.28E-02	1.72E-05	2.64E+00	4.58E-02	6.11E-02	1.11E-01	9.27E-03	2.99E-02	3.86E-03	1.23E-03	4.17E-03	5.67E-04	3.24E-03	5.94E-04	100.8
4.05	0.87	7.83E-01	b.d.	1.35E-01	1.08E+01	2.30E-02	8.62E-06	2.51E+00	4.62E-02	6.19E-02	1.12E-01	9.44E-03	3.08E-02	3.97E-03	1.26E-03	4.22E-03	5.72E-04	3.27E-03	b.d.	101.2
4.85	0.08	4.74E-01	b.d.	b.d.	1.21E+01	2.21E-02	b.d.	2.24E+00	5.03E-03	5.72E-03	9.81E-03	7.81E-04	2.41E-03	3.33E-04	1.05E-04	3.07E-04	4.21E-05	2.22E-04	4.24E-05	100.9
4.90	0.07	5.10E-01	b.d.	b.d.	1.14E+01	2.31E-02	b.d.	2.06E+00	4.61E-03	5.18E-03	8.56E-03	6.25E-04	2.09E-03	2.73E-04	9.21E-05	3.09E-04	4.32E-05	2.09E-04	3.64E-05	101.4
5.62	0.01	2.29E-01	b.d.	b.d.	8.54E+00	9.60E-03	1.68E-04	5.80E-01	6.97E-04	6.12E-04	1.73E-03	2.13E-04	8.80E-04	1.73E-04	5.92E-05	1.40E-04	1.70E-05	9.85E-05	1.82E-05	101.6
5.57	0.01	1.98E-01	b.d.	b.d.	7.25E+00	9.43E-03	5.60E-05	6.93E-01	6.75E-04	5.18E-04	1.46E-03	1.63E-04	7.42E-04	1.33E-04	5.26E-05	1.32E-04	1.79E-05	8.62E-05	1.21E-05	100.8
6.26	0.01	7.40E-02	b.d.	b.d.	1.20E+01	3.45E-03	4.31E-05	1.77E-01	8.32E-04	5.47E-04	1.99E-03	2.63E-04	1.17E-03	2.53E-04	7.24E-05	1.66E-04	2.36E-05	1.29E-04	2.43E-05	101.2
6.26	0.00	7.42E-02	b.d.	b.d.	1.11E+01	4.34E-03	0.00E+00	1.75E-01	4.50E-04	2.30E-04	8.71E-04	1.14E-04	5.89E-04	9.98E-05	3.95E-05	8.76E-05	1.18E-05	5.54E-05	1.21E-05	100.8
7.03	0.03	b.d.	b.d.	1.49E-02	1.24E+01	9.93E-04	2.24E-04	5.45E-02	3.37E-03	2.30E-03	8.38E-03	1.04E-03	4.74E-03	8.71E-04	2.70E-04	6.92E-04	8.82E-05	4.68E-04	7.88E-05	101.7
7.07	0.03	b.d.	b.d.	1.27E-02	1.34E+01	6.16E-04	1.68E-04	1.02E-01	2.78E-03	1.93E-03	7.00E-03	8.94E-04	4.20E-03	7.52E-04	2.43E-04	5.52E-04	7.63E-05	3.69E-04	6.67E-05	101.0
7.37	0.45	7.02E-02	b.d.	1.83E-01	6.07E+01	1.02E-03	5.02E-03	3.24E-01	3.69E-02	3.21E-02	1.20E-01	1.28E-02	5.35E-02	1.08E-02	3.32E-03	8.12E-03	1.23E-03	6.30E-03	1.04E-03	101.7
7.48	0.17	2.90E-02	b.d.	6.98E-02	2.18E+01	9.02E-04	1.78E-03	1.85E-01	1.42E-02	1.24E-02	4.43E-02	4.90E-03	2.03E-02	4.08E-03	1.24E-03	3.16E-03	4.53E-04	2.35E-03	3.70E-04	101.1

All values are in μmol L^{-1} soln, except pH (-log mol L^{-1}) and Soln:Soil, which is the mass ratio of suspension to soil.
b.d., below detection

Table EA-12: 350 ky Amalu Subsurface horizon

pH	DOC	Fe	Si	Al	Y	La	Ce	Pr	Nd	Sm	Eu	Gd	Tb	Dy	Ho	Er	Tm	Yb	Lu	Soln:soil
2.34	223.55	3.74E+00	4.17E+01	1.33E+03	1.15E-01	7.93E-02	1.60E-01	1.35E-02	4.45E-02	7.83E-03	2.50E-03	8.34E-03	1.64E-03	1.04E-02	1.95E-03	5.02E-03	6.33E-04	3.37E-03	4.29E-04	103.7
2.37	249.60	3.73E+00	4.12E+01	1.28E+03	1.16E-01	8.03E-02	1.61E-01	1.39E-02	4.60E-02	7.93E-03	2.60E-03	8.50E-03	1.70E-03	1.06E-02	1.98E-03	5.18E-03	6.51E-04	3.46E-03	4.46E-04	103.4
3.17	133.21	1.04E+00	2.25E+01	8.84E+02	1.56E-02	1.04E-02	1.92E-02	1.57E-03	5.08E-03	8.45E-04	2.70E-04	9.46E-04	1.85E-04	1.14E-03	2.24E-04	5.68E-04	7.10E-05	3.81E-04	4.57E-05	103.7
3.22	106.65	1.02E+00	2.26E+01	8.54E+02	1.47E-02	1.00E-02	1.86E-02	1.54E-03	5.04E-03	8.38E-04	2.76E-04	1.01E-03	1.78E-04	1.16E-03	2.24E-04	5.80E-04	7.10E-05	4.05E-04	5.14E-05	106.8
3.83	78.68	3.47E-01	7.47E+00	2.60E+02	3.75E-03	2.45E-03	4.50E-03	3.76E-04	1.25E-03	2.06E-04	7.24E-05	2.38E-04	4.15E-05	2.83E-04	5.46E-05	1.49E-04	1.78E-05	1.16E-04	1.14E-05	105.4
3.78	85.26	5.95E-01	7.74E+00	2.65E+02	4.22E-03	2.69E-03	4.95E-03	4.26E-04	1.40E-03	2.59E-04	7.90E-05	2.80E-04	4.75E-05	3.26E-04	6.06E-05	1.67E-04	2.37E-05	1.33E-04	1.71E-05	103.6
4.65	75.85	6.33E-02	4.79E+00	1.94E+00	4.72E-04	1.66E-04	4.50E-04	5.68E-05	2.43E-04	5.99E-05	1.97E-05	3.81E-05	1.18E-05	5.54E-05	1.21E-05	4.19E-05	5.92E-06	3.47E-05	5.72E-06	104.1
4.70	81.34	5.82E-02	4.67E+00	2.07E+00	4.61E-04	1.73E-04	4.85E-04	5.68E-05	2.36E-04	5.32E-05	1.97E-05	4.49E-05	1.18E-05	5.54E-05	1.21E-05	3.59E-05	5.92E-06	3.47E-05	5.72E-06	103.9
6.62	594.79	1.51E+01	2.26E+01	5.05E+01	8.73E-03	4.25E-03	1.50E-02	1.94E-03	8.62E-03	2.23E-03	6.91E-04	1.91E-03	3.16E-04	1.76E-03	3.03E-04	7.59E-04	1.01E-04	6.59E-04	8.57E-05	103.8
6.64	529.76	8.58E+00	1.55E+01	3.01E+01	6.20E-03	2.89E-03	1.05E-02	1.37E-03	5.97E-03	1.53E-03	4.61E-04	1.30E-03	2.12E-04	1.18E-03	2.00E-04	5.20E-04	7.10E-05	4.57E-04	6.29E-05	103.5
8.14	5616.52	7.35E+02	4.86E+02	2.01E+03	2.21E-01	1.10E-01	4.13E-01	4.95E-02	2.05E-01	5.72E-02	1.79E-02	4.70E-02	8.23E-03	4.72E-02	7.18E-03	1.89E-02	2.50E-03	1.57E-02	1.97E-03	103.5
7.88	8095.08	7.54E+02	5.28E+02	2.07E+03	2.25E-01	1.13E-01	4.08E-01	5.10E-02	2.11E-01	5.84E-02	1.76E-02	4.76E-02	8.22E-03	4.82E-02	7.47E-03	1.88E-02	2.52E-03	1.57E-02	2.01E-03	103.7
2.80	74.60	1.50E+00	2.91E+01	1.04E+03	3.98E-02	2.77E-02	5.35E-02	4.45E-03	1.47E-02	2.53E-03	8.16E-04	2.85E-03	5.25E-04	3.43E-03	6.49E-04	1.70E-03	2.07E-04	1.13E-03	1.43E-04	103.5
2.80	96.66	1.56E+00	2.76E+01	1.02E+03	3.94E-02	2.77E-02	5.31E-02	4.43E-03	1.45E-02	2.51E-03	8.09E-04	2.70E-03	5.39E-04	3.38E-03	6.43E-04	1.67E-03	2.13E-04	1.09E-03	1.43E-04	103.5
3.51	38.38	6.61E-01	1.60E+01	5.66E+02	8.24E-03	5.64E-03	1.04E-02	8.52E-04	2.79E-03	4.72E-04	1.51E-04	5.47E-04	1.01E-04	6.34E-04	1.21E-04	3.29E-04	4.14E-05	2.20E-04	2.86E-05	103.6
3.50	54.95	7.16E-01	1.56E+01	5.77E+02	8.58E-03	5.85E-03	1.09E-02	8.87E-04	2.92E-03	4.92E-04	1.65E-04	5.36E-04	1.01E-04	6.52E-04	1.21E-04	3.23E-04	4.14E-05	2.20E-04	2.86E-05	103.9
4.19	47.87	2.60E-01	7.12E+00	1.00E+02	2.01E-03	1.33E-03	2.46E-03	2.13E-04	7.42E-04	1.40E-04	4.61E-05	1.47E-04	2.36E-05	1.78E-04	3.03E-05	8.97E-05	1.18E-05	7.51E-05	1.14E-05	103.6
4.17	37.63	3.10E-01	7.31E+00	1.09E+02	2.01E-03	1.62E-03	2.80E-03	2.48E-04	7.97E-04	1.46E-04	5.26E-05	1.50E-04	2.98E-05	1.72E-04	3.64E-05	9.57E-05	1.18E-05	6.93E-05	1.14E-05	103.7
5.86	93.50	3.11E-01	6.53E+00	2.91E+00	1.20E-03	4.61E-04	1.43E-03	1.42E-04	4.30E-04	1.66E-04	4.61E-05	1.72E-04	3.00E-05	1.23E-04	2.43E-05	4.19E-05	5.92E-06	3.47E-05	5.72E-06	103.8
5.96	87.75	1.61E-01	5.82E+00	1.73E+00	1.19E-03	4.25E-04	1.15E-03	1.35E-04	3.81E-04	1.80E-04	3.29E-05	1.66E-04	2.39E-05	1.05E-04	2.43E-05	4.78E-05	5.92E-06	4.62E-05	5.72E-06	103.7
6.51	286.57	1.54E+00	5.03E+01	7.47E+00	2.40E-03	1.53E-03	3.93E-03	5.11E-04	2.43E-03	6.19E-04	1.58E-04	3.86E-04	6.59E-05	3.82E-04	6.06E-05	1.67E-04	2.96E-05	1.62E-04	2.29E-05	104.1
6.38	258.26	9.59E-01	5.95E+01	4.65E+00	2.29E-03	1.03E-03	3.28E-03	4.26E-04	2.02E-03	4.19E-04	1.38E-04	3.71E-04	6.02E-05	3.08E-04	6.06E-05	1.73E-04	1.78E-05	1.44E-04	1.71E-05	103.7
7.56	3555.91	3.98E+02	2.46E+02	1.03E+03	1.14E-01	5.39E-02	1.90E-01	2.41E-02	1.02E-01	2.78E-02	8.87E-03	2.49E-02	4.17E-03	2.38E-02	3.75E-03	9.54E-03	1.26E-03	7.97E-03	1.01E-03	103.6
7.57	3862.29	3.26E+02	2.69E+02	1.02E+03	1.23E-01	5.93E-02	2.19E-01	2.68E-02	1.15E-01	3.03E-02	9.74E-03	2.67E-02	4.45E-03	2.50E-02	4.01E-03	9.94E-03	1.31E-03	8.28E-03	1.06E-03	103.4
8.01	6186.00	5.51E+02	4.03E+02	1.54E+03	1.73E-01	8.59E-02	3.17E-01	3.86E-02	1.63E-01	4.45E-02	1.39E-02	3.82E-02	6.57E-03	3.76E-02	5.76E-03	1.46E-02	1.94E-03	1.21E-02	1.54E-03	103.5
7.83	5693.11	4.54E+02	3.49E+02	1.42E+03	1.56E-01	7.87E-02	2.84E-01	3.45E-02	1.50E-01	3.98E-02	1.29E-02	3.41E-02	6.00E-03	3.26E-02	5.27E-03	1.34E-02	1.71E-03	1.10E-02	1.39E-03	103.4
4.87	85.67	1.03E+00	6.28E+00	6.98E+00	9.45E-04	9.79E-04	1.55E-03	1.85E-04	8.39E-04	2.06E-04	6.58E-05	1.57E-04	2.86E-05	1.78E-04	3.03E-05	7.77E-05	1.18E-05	7.51E-05	1.14E-05	103.4
4.60	80.68	1.04E+00	6.82E+00	6.75E+00	9.90E-04	5.33E-04	1.54E-03	1.92E-04	8.18E-04	2.26E-04	6.58E-05	1.63E-04	2.87E-05	1.85E-04	3.03E-05	8.37E-05	1.18E-05	8.09E-05	1.14E-05	103.6
5.34	95.75	6.03E-02	1.13E+01	8.17E-01	3.60E-04	1.87E-04	5.21E-04	6.39E-05	3.26E-04	6.65E-05	2.63E-05	6.31E-05	1.21E-05	6.15E-05	1.21E-05	4.19E-05	5.92E-06	2.89E-05	5.72E-06	103.6
5.43	91.67	b.d.	1.23E+01	3.18E-01	4.61E-04	1.57E-02	4.28E-02	3.51E-03	9.84E-03	7.98E-05	1.97E-05	2.03E-04	1.63E-05	8.00E-05	1.21E-05	4.19E-05	5.92E-06	4.05E-05	5.72E-06	103.5
5.75	125.30	7.78E-02	1.21E+01	1.31E+00	5.40E-04	2.38E-04	1.01E-03	1.14E-04	4.71E-04	1.13E-04	3.95E-05	1.00E-04	1.82E-05	9.23E-05	1.82E-05	5.38E-05	5.92E-06	6.36E-05	5.72E-06	103.5
5.73	102.74	b.d.	1.25E+01	7.22E-01	5.51E-04	1.73E-04	9.78E-04	8.52E-05	3.81E-04	8.65E-05	2.63E-05	6.82E-05	1.20E-05	8.62E-05	1.82E-05	4.78E-05	5.92E-06	4.05E-05	5.72E-06	103.6
6.71	1125.63	5.74E+01	5.90E+01	1.91E+02	2.62E-02	1.31E-02	4.62E-02	5.92E-03	2.56E-02	6.92E-03	2.13E-03	5.84E-03	9.66E-04	5.61E-03	9.22E-04	2.29E-03	3.02E-04	1.95E-03	2.51E-04	103.9
6.84	919.16	2.97E+01	3.67E+01	9.50E+01	1.50E-02	7.58E-03	2.63E-02	3.39E-03	1.48E-02	3.86E-03	1.20E-03	3.32E-03	5.40E-04	3.10E-03	5.09E-04	1.29E-03	1.72E-04	1.10E-03	1.49E-04	104.8
7.21	2058.95	1.07E+02	1.21E+02	4.30E+02	5.20E-02	2.71E-02	9.24E-02	1.14E-02	5.03E-02	1.36E-02	4.05E-03	1.13E-02	1.87E-03	1.04E-02	1.70E-03	4.12E-03	5.56E-04	3.38E-03	4.46E-04	103.9
7.21	2170.51	1.17E+02	1.20E+02	4.53E+02	5.56E-02	2.84E-02	9.82E-02	1.23E-02	5.28E-02	1.41E-02	4.30E-03	1.19E-02	2.02E-03	1.12E-02	1.84E-03	4.40E-03	5.74E-04	3.53E-03	4.69E-04	103.8

All values are in μmol L^{-1} soln, except pH (-log mol L^{-1}) and Soln:Soil, which is the mass ratio of suspension to soil.

b.d., below detection

Table EA-13: 1,400 ky Molokai subsurface horizon

pH	DOC	Fe	Si	Al	Y	La	Ce	Pr	Nd	Sm	Eu	Gd	Tb	Dy	Ho	Er	Tm	Yb	Lu	Soln:soil
2.18	182.67	6.36E-01	9.74E+00	5.81E+02	8.58E-03	3.23E-02	6.86E-02	5.80E-03	1.89E-02	3.11E-03	9.81E-04	2.81E-03	4.37E-04	2.06E-03	2.67E-04	5.02E-04	5.33E-05	2.54E-04	2.86E-05	100.3
2.18	161.60	6.88E-01	7.40E+00	5.70E+02	8.54E-03	3.16E-02	6.75E-02	5.71E-03	1.90E-02	3.12E-03	9.87E-04	2.93E-03	4.37E-04	2.02E-03	2.55E-04	5.08E-04	4.74E-05	2.43E-04	2.86E-05	100.5
2.70	31.47	2.48E-01	4.47E+00	4.04E+02	2.98E-03	1.24E-02	2.27E-02	1.82E-03	5.87E-03	9.31E-04	3.09E-04	9.23E-04	1.30E-04	6.34E-04	7.88E-05	1.61E-04	1.18E-05	7.51E-05	5.72E-06	101.3
2.70	59.86	2.25E-01	4.46E+00	3.95E+02	2.92E-03	1.22E-02	2.22E-02	1.77E-03	5.77E-03	9.04E-04	2.83E-04	8.72E-04	1.30E-04	6.03E-04	8.49E-05	1.43E-04	1.78E-05	7.51E-05	5.72E-06	102.1
3.36	b.d.	1.39E-01	6.80E+00	2.45E+02	9.22E-04	3.74E-03	6.48E-03	5.18E-04	1.64E-03	2.66E-04	8.55E-05	2.50E-04	3.44E-05	1.72E-04	2.43E-05	4.78E-05	5.92E-06	2.31E-05	b.d.	101.2
3.33	b.d.	2.09E-01	6.16E+00	2.21E+02	9.67E-04	3.79E-03	6.64E-03	5.18E-04	1.67E-03	2.66E-04	9.21E-05	2.36E-04	3.43E-05	1.78E-04	2.43E-05	4.19E-05	5.92E-06	1.73E-05	b.d.	100.8
4.60	b.d.	7.41E-02	2.58E+00	6.05E+00	2.47E-04	4.90E-04	9.56E-04	9.94E-05	3.61E-04	7.32E-05	2.63E-05	4.43E-05	1.14E-05	4.31E-05	6.06E-06	1.79E-05	b.d.	1.16E-05	b.d.	100.0
4.62	b.d.	3.81E-02	2.47E+00	5.56E+00	1.12E-04	3.10E-04	7.28E-04	7.81E-05	2.91E-04	5.32E-05	2.63E-05	3.43E-05	5.35E-06	3.08E-05	6.06E-06	1.20E-05	b.d.	5.78E-06	b.d.	100.8
7.51	2427.77	2.56E+02	9.03E+01	3.83E+02	1.14E-02	3.00E-02	1.84E-01	9.64E-03	3.69E-02	8.60E-03	2.73E-03	6.46E-03	9.99E-04	4.66E-03	5.94E-04	1.20E-03	1.42E-04	8.44E-04	1.03E-04	101.4
8.05	2431.94	1.86E+02	7.02E+01	2.90E+02	8.86E-03	2.39E-02	1.29E-01	7.66E-03	2.85E-02	7.04E-03	2.20E-03	5.08E-03	7.93E-04	3.81E-03	4.73E-04	9.09E-04	1.07E-04	6.47E-04	8.00E-05	100.9
9.78	5907.09	6.35E+02	1.96E+02	1.02E+03	2.64E-02	6.68E-02	4.60E-01	2.16E-02	8.47E-02	2.07E-02	6.45E-03	1.56E-02	2.35E-03	1.11E-02	1.44E-03	2.71E-03	3.20E-04	1.87E-03	2.23E-04	102.2
9.62	6359.17	6.83E+02	2.16E+02	8.92E+02	2.81E-02	6.50E-02	4.81E-01	2.26E-02	8.49E-02	2.13E-02	6.73E-03	1.61E-02	2.46E-03	1.21E-02	1.49E-03	2.85E-03	3.31E-04	1.92E-03	2.23E-04	103.7
3.49	22.15	1.09E-01	5.27E+00	1.78E+02	6.97E-04	2.69E-03	4.67E-03	3.69E-04	1.18E-03	2.00E-04	6.58E-05	1.50E-04	2.27E-05	1.17E-04	1.82E-05	3.59E-05	5.92E-06	1.73E-05	b.d.	100.6
3.54	b.d.	1.17E-01	4.98E+00	1.85E+02	6.97E-04	2.73E-03	4.71E-03	3.90E-04	1.20E-03	1.93E-04	7.24E-05	1.82E-04	2.90E-05	1.23E-04	1.82E-05	2.99E-05	5.92E-06	1.16E-05	b.d.	100.4
3.93	b.d.	1.17E-01	2.62E+00	6.56E+01	3.37E-04	1.32E-03	2.48E-03	1.99E-04	6.86E-04	1.13E-04	4.61E-05	8.89E-05	1.67E-05	6.77E-05	1.21E-05	1.79E-05	b.d.	5.78E-06	b.d.	100.1
3.97	b.d.	8.99E-02	2.58E+00	6.68E+01	3.49E-04	1.38E-03	2.58E-03	2.13E-04	7.35E-04	1.26E-04	4.61E-05	8.64E-05	1.65E-05	8.00E-05	6.06E-06	2.39E-05	b.d.	5.78E-06	b.d.	100.9
5.55	b.d.	7.84E-02	2.18E+00	1.08E+00	1.35E-04	2.52E-04	8.64E-04	1.06E-04	4.16E-04	8.65E-05	2.63E-05	4.87E-05	4.86E-06	4.31E-05	6.06E-06	1.20E-05	b.d.	1.16E-05	b.d.	100.4
5.65	b.d.	1.87E-01	2.23E+00	1.06E+00	1.57E-04	3.24E-04	9.85E-04	1.14E-04	4.58E-04	1.06E-04	3.29E-05	5.43E-05	1.10E-05	4.31E-05	6.06E-06	1.20E-05	b.d.	1.16E-05	b.d.	100.3
6.15	293.48	2.88E+01	1.18E+01	6.36E+01	2.55E-03	6.53E-03	2.78E-02	1.45E-03	3.51E-03	9.91E-04	1.97E-04	1.02E-03	1.64E-04	4.80E-04	6.67E-05	1.26E-04	3.55E-05	5.78E-05	5.72E-06	100.3
6.16	283.74	2.92E+01	1.20E+01	5.86E+01	2.68E-03	6.20E-03	2.78E-02	1.37E-03	3.76E-03	8.78E-04	1.97E-04	1.01E-03	1.63E-04	5.85E-04	6.06E-05	1.32E-04	3.55E-05	5.78E-05	5.72E-06	100.2
6.70	1053.20	1.34E+02	3.25E+01	2.20E+02	5.60E-03	1.53E-02	8.96E-02	4.33E-03	1.77E-02	3.64E-03	1.18E-03	2.99E-03	4.36E-04	2.09E-03	2.49E-04	5.14E-04	6.51E-05	4.05E-04	4.57E-05	100.5
6.61	1049.87	1.25E+02	2.63E+01	1.84E+02	4.95E-03	1.34E-02	8.94E-02	4.11E-03	1.58E-02	3.64E-03	1.11E-03	2.81E-03	4.20E-04	1.98E-03	2.36E-04	4.90E-04	6.51E-05	3.29E-04	4.00E-05	100.3
6.94	1827.49	2.19E+02	4.62E+01	3.93E+02	1.07E-02	2.61E-02	1.54E-01	8.40E-03	2.95E-02	6.82E-03	2.27E-03	4.92E-03	7.59E-04	3.64E-03	4.61E-04	9.92E-04	1.30E-04	8.21E-04	9.72E-05	100.9
7.12	2041.46	2.09E+02	1.06E+01	3.14E+02	9.50E-03	2.36E-02	1.45E-01	7.43E-03	2.96E-02	6.90E-03	2.15E-03	4.93E-03	7.59E-04	3.47E-03	4.49E-04	9.09E-04	1.01E-04	6.36E-04	8.00E-05	100.5
8.42	4124.55	2.23E+02	5.81E+02	5.22E+02	1.78E-02	4.83E-02	1.79E-01	1.56E-02	6.33E-02	1.56E-02	5.03E-03	9.62E-03	1.64E-03	7.54E-03	1.05E-03	1.93E-03	2.13E-04	1.24E-03	1.43E-04	100.3
8.77	4910.50	3.54E+02	4.07E+02	5.53E+02	2.08E-02	5.32E-02	2.31E-01	1.78E-02	6.39E-02	1.68E-02	4.90E-03	1.06E-02	1.68E-03	8.73E-03	1.07E-03	1.93E-03	2.31E-04	1.25E-03	1.60E-04	102.4

All values are in μmol L^{-1} soln, except pH (-log mol L^{-1}) and Soln:Soil, which is the mass ratio of suspension to soil.

b.d., below detection

Table EA-14: 4,100 ky Kauai subsurface 2 horizon

pH	DOC	Fe	Si	Al	Y	La	Ce	Pr	Nd	Sm	Eu	Gd	Tb	Dy	Ho	Er	Tm	Yb	Lu	Soln:soil
2.03	91.50	1.17E+00	2.70E+00	6.63E+01	1.60E-02	3.02E-02	1.24E-01	1.51E-02	6.55E-02	1.54E-02	4.79E-03	1.15E-02	1.51E-03	6.98E-03	8.67E-04	1.60E-03	1.66E-04	9.71E-04	1.03E-04	102.5
2.02	97.83	1.22E+00	2.89E+00	6.68E+01	1.63E-02	3.01E-02	1.24E-01	1.54E-02	6.61E-02	1.57E-02	4.88E-03	1.20E-02	1.55E-03	7.13E-03	8.73E-04	1.65E-03	1.72E-04	9.77E-04	1.09E-04	101.7
2.48	58.45	7.45E-01	3.53E+00	6.07E+01	1.34E-02	2.47E-02	9.41E-02	1.08E-02	4.40E-02	9.80E-03	3.03E-03	8.25E-03	1.05E-03	4.92E-03	5.88E-04	1.14E-03	1.12E-04	6.24E-04	6.86E-05	102.2
2.48	58.70	7.27E-01	3.71E+00	5.77E+01	1.33E-02	2.46E-02	9.31E-02	1.07E-02	4.35E-02	9.52E-03	2.94E-03	8.13E-03	1.02E-03	4.74E-03	5.94E-04	1.11E-03	1.12E-04	6.01E-04	6.29E-05	102.6
3.01	49.45	5.50E-01	3.07E+00	5.03E+01	8.29E-03	1.62E-02	5.31E-02	5.63E-03	2.15E-02	4.36E-03	1.40E-03	3.96E-03	5.03E-04	2.41E-03	2.97E-04	5.68E-04	5.33E-05	2.83E-04	2.86E-05	102.1
3.01	40.80	3.93E-01	2.35E+00	4.84E+01	8.41E-03	1.65E-02	5.32E-02	5.67E-03	2.23E-02	4.33E-03	1.38E-03	4.00E-03	4.95E-04	2.46E-03	3.03E-04	5.68E-04	5.33E-05	2.77E-04	2.86E-05	102.3
4.55	36.22	7.17E-02	1.77E+00	2.23E+00	3.37E-04	8.21E-04	2.31E-03	1.92E-04	7.07E-04	1.26E-04	3.95E-05	1.17E-04	1.66E-05	8.00E-05	1.21E-05	1.79E-05	b.d	1.16E-05	b.d	102.8
4.52	69.10	3.75E-01	1.84E+00	1.67E+00	1.35E-04	2.81E-04	6.71E-04	6.39E-05	3.19E-04	5.99E-05	1.97E-05	6.41E-05	1.16E-05	3.69E-05	6.06E-06	1.20E-05	b.d	5.78E-06	b.d	102.5
8.78	1113.98	1.57E+02	2.77E+01	5.61E+01	7.72E-03	3.12E-02	1.20E-01	8.42E-03	3.58E-02	7.82E-03	2.28E-03	5.15E-03	8.62E-04	3.37E-03	4.37E-04	7.29E-04	8.88E-05	3.76E-04	5.72E-05	102.3
9.01	1226.38	1.76E+02	7.30E+01	5.96E+01	7.32E-03	2.83E-02	1.34E-01	7.95E-03	3.51E-02	7.38E-03	2.34E-03	4.84E-03	7.31E-04	3.11E-03	3.94E-04	7.23E-04	7.10E-05	4.57E-04	5.14E-05	102.2
10.78	2431.94	9.77E+02	2.42E+01	5.68E+02	2.25E-02	9.01E-02	4.78E-01	2.33E-02	9.29E-02	1.92E-02	5.50E-03	1.54E-02	2.01E-03	9.34E-03	1.02E-03	1.84E-03	1.89E-04	1.18E-03	1.14E-04	102.5
10.77	2429.44	8.82E+02	1.99E+01	5.16E+02	1.89E-02	8.05E-02	4.58E-01	2.07E-02	8.25E-02	1.70E-02	4.99E-03	1.42E-02	1.83E-03	8.66E-03	9.94E-04	1.73E-03	1.66E-04	1.02E-03	1.09E-04	102.6
3.35	21.31	2.62E-01	3.31E+00	3.51E+01	5.46E-03	1.12E-02	3.42E-02	3.51E-03	1.32E-02	2.54E-03	8.16E-04	2.44E-03	3.12E-04	1.51E-03	1.88E-04	3.53E-04	3.55E-05	1.56E-04	1.71E-05	102.3
3.32	14.57	4.33E-01	2.75E+00	3.58E+01	5.67E-03	1.17E-02	3.59E-02	3.65E-03	1.38E-02	2.71E-03	8.42E-04	2.50E-03	3.24E-04	1.58E-03	2.00E-04	3.59E-04	3.55E-05	1.79E-04	1.71E-05	102.7
5.50	24.81	4.68E-01	2.22E+00	2.47E-01	1.80E-04	1.30E-04	4.14E-04	4.97E-05	2.15E-04	4.66E-05	1.32E-05	2.50E-05	5.56E-06	2.46E-05	6.06E-06	5.98E-06	b.d	5.78E-06	b.d	102.3
5.58	24.06	4.02E-01	2.58E+00	3.45E-01	1.12E-04	1.58E-04	4.07E-04	2.13E-05	9.01E-05	2.66E-05	6.58E-06	2.34E-05	1.23E-05	1.23E-05	6.06E-06	5.98E-06	b.d	5.78E-06	b.d	101.6
6.43	125.88	4.44E+00	b.d.	3.53E+00	1.09E-03	2.61E-03	4.55E-03	5.04E-04	1.24E-03	4.59E-04	5.92E-05	3.86E-04	5.24E-05	6.58E-04	1.82E-05	7.77E-05	3.55E-05	2.89E-05	b.d	102.4
6.43	103.07	4.11E+00	1.23E+00	4.29E+00	1.60E-03	2.96E-03	5.65E-03	6.67E-04	1.71E-03	4.86E-04	5.92E-05	5.67E-04	6.97E-05	2.22E-04	1.82E-05	7.17E-05	4.14E-05	4.05E-05	5.72E-06	102.1
6.89	357.67	2.43E+02	1.33E+01	1.04E+02	7.95E-03	2.49E-02	6.37E-02	6.80E-03	2.74E-02	5.39E-03	1.60E-03	4.50E-03	5.85E-04	2.64E-03	3.21E-04	5.92E-04	5.33E-05	3.41E-04	2.86E-05	102.7
6.91	345.60	2.61E+02	9.99E+00	1.24E+02	9.32E-03	3.18E-02	7.22E-02	8.68E-03	3.50E-02	7.20E-03	1.99E-03	5.97E-03	8.77E-04	3.85E-03	5.40E-04	9.39E-04	8.88E-05	3.24E-04	4.00E-05	102.2
7.42	684.79	3.65E+02	2.51E+01	1.57E+02	1.09E-02	3.72E-02	1.14E-01	1.05E-02	4.04E-02	8.83E-03	2.56E-03	7.25E-03	9.26E-04	4.40E-03	5.94E-04	1.05E-03	1.01E-04	5.26E-04	6.29E-05	101.7
7.51	680.46	3.45E+02	4.45E+01	1.54E+02	1.02E-02	3.38E-02	1.00E-01	9.79E-03	4.22E-02	7.67E-03	2.63E-03	5.94E-03	7.79E-04	4.24E-03	4.85E-04	8.07E-04	7.70E-05	1.10E-03	5.72E-05	101.7
8.09	904.17	3.93E+02	2.09E+01	1.87E+02	1.07E-02	3.56E-02	1.32E-01	1.06E-02	4.57E-02	1.14E-02	2.76E-03	8.28E-03	1.01E-03	4.71E-03	4.91E-04	8.43E-04	1.18E-04	4.91E-04	6.29E-05	101.8
8.32	955.79	4.07E+02	2.80E+01	1.78E+02	9.86E-03	3.46E-02	1.52E-01	9.59E-03	3.94E-02	7.82E-03	2.64E-03	7.11E-03	9.47E-04	3.88E-03	4.73E-04	9.03E-04	1.01E-04	4.57E-04	5.72E-05	102.7
10.12	1939.89	7.85E+02	2.58E+01	4.02E+02	1.76E-02	6.04E-02	3.42E-01	1.57E-02	6.35E-02	1.51E-02	4.40E-03	1.15E-02	1.40E-03	6.68E-03	7.46E-04	1.29E-03	1.60E-04	7.22E-04	9.14E-05	102.3
10.16	2025.64	9.06E+02	3.00E+01	4.25E+02	1.65E-02	5.95E-02	3.77E-01	1.67E-02	6.86E-02	1.36E-02	4.30E-03	1.09E-02	1.55E-03	6.47E-03	8.06E-04	1.45E-03	1.60E-04	8.44E-04	1.09E-04	101.9
3.72	57.28	3.21E-01	2.14E+00	2.42E+01	3.57E-03	7.98E-03	2.34E-02	2.31E-03	8.72E-03	1.66E-03	5.33E-04	1.44E-03	2.11E-04	1.01E-03	1.27E-04	2.33E-04	2.37E-05	1.16E-04	1.14E-05	100.9
3.87	23.23	1.10E-01	2.08E+00	2.05E+01	2.88E-03	6.68E-03	1.90E-02	1.85E-03	6.97E-03	1.34E-03	4.41E-04	1.16E-03	1.67E-04	8.12E-04	9.70E-05	1.85E-04	1.78E-05	8.67E-05	1.14E-05	100.0

All values are in μmol L^{-1} soln, except pH (-log mol L^{-1}) and Soln:Soil, which is the mass ratio of suspension to soil.
b.d., below detection